

The Texas Medical Center Library

DigitalCommons@TMC

The University of Texas MD Anderson Cancer
Center UTHealth Graduate School of
Biomedical Sciences Dissertations and Theses
(Open Access)

The University of Texas MD Anderson Cancer
Center UTHealth Graduate School of
Biomedical Sciences

12-2011

Quantitative comparison of late effects following photon versus proton external-beam radiation therapies: Toward an evidence-based approach to selecting a treatment modality

Rui Zhang

Follow this and additional works at: https://digitalcommons.library.tmc.edu/utgsbs_dissertations

 Part of the [Other Physics Commons](#)

Recommended Citation

Zhang, Rui, "Quantitative comparison of late effects following photon versus proton external-beam radiation therapies: Toward an evidence-based approach to selecting a treatment modality" (2011). *The University of Texas MD Anderson Cancer Center UTHealth Graduate School of Biomedical Sciences Dissertations and Theses (Open Access)*. 187.

https://digitalcommons.library.tmc.edu/utgsbs_dissertations/187

This Dissertation (PhD) is brought to you for free and open access by the The University of Texas MD Anderson Cancer Center UTHealth Graduate School of Biomedical Sciences at DigitalCommons@TMC. It has been accepted for inclusion in The University of Texas MD Anderson Cancer Center UTHealth Graduate School of Biomedical Sciences Dissertations and Theses (Open Access) by an authorized administrator of DigitalCommons@TMC. For more information, please contact digitalcommons@library.tmc.edu.

The
TMC LIBRARY
Health Sciences Resource Center

Quantitative comparison of late effects following photon *versus* proton external-beam radiation therapies: Toward an evidence-based approach to selecting a treatment modality

by

Rui Zhang, M.S.

APPROVED, THESIS COMMITTEE:

Wayne Newhauser, Ph.D.
Supervisory Professor

Rebecca Howell, Ph.D.

Dragan Mirkovic, Ph.D.

Anita Mahajan, M.D.

Carol Etzel, Ph.D.

APPROVED:

Dean, The University of Texas at Houston
Graduate school of Biomedical Sciences

**QUANTITATIVE COMPARISON OF LATE EFFECTS FOLLOWING PHOTON
VERSUS PROTON EXTERNAL-BEAM RADIATION THERAPIES: TOWARD
AN EVIDENCE-BASED APPROACH TO SELECTING A TREATMENT
MODALITY**

A
DISSERTATION

Presented to the Faculty of
The University of Texas
Health Science Center at Houston
and
The University of Texas
M.D. Anderson Cancer Center
Graduate School of Biomedical Sciences
in Partial Fulfillment

of the Requirements

For the Degree of
DOCTOR OF PHILOSOPHY

by

Rui Zhang, M.S.

Houston, Texas

December, 2011

ABSTRACT

Radiation therapy has been used as an effective treatment for malignancies in pediatric patients. However, in many cases, the side effects of radiation diminish these patients' quality of life. In order to develop strategies to minimize radiogenic complications, one must first quantitatively estimate pediatric patients' relative risk for radiogenic late effects, which has not become feasible till recently because of the calculational complexity. The goals of this work were to calculate the dose delivered to tissues and organs in pediatric patients during contemporary photon and proton radiotherapies; to estimate the corresponding risk of radiogenic second cancer and cardiac toxicity based on the calculated doses and on dose-risk models from the literature; to test for the statistical significance of the difference between predicted risks after photon *versus* proton radiotherapies; and to provide a prototype of an evidence-based approach to selecting treatment modalities for pediatric patients, taking second cancer and cardiac toxicity into account. The results showed that proton therapy confers a lower predicted risk of radiogenic second cancer, and lower risks of radiogenic cardiac toxicities, compared to photon therapy. An uncertainty analysis revealed that the qualitative findings of this study are insensitive to changes in a wide variety of host and treatment related factors.

ACKNOWLEDGEMENTS

Many people have contributed to this work. First, I owed my committees who helped me shape the whole project and guided the direction of the research. Thanks to my Advisory Committee (Drs. Wayne Newhauser, Dragan Mirkovic, Mary Martel, Carol Etzel and Shiao Woo), Examination Committee (Drs. George Starkschall, Dragan Mirkovic, Carol Etzel and Uwe Titt), Supervisory Committee (Drs. Wayne Newhauser, Rebecca Howell, Dragan Mirkovic, Carol Etzel and Anita Mahajan). In particular, thanks to Dr. Wayne Newhauser, for his mentorship and active supervision during my research and graduate studies, the contributions to the development of my scientific knowledge and teaching me how to be a good scientist.

Special thanks to Dr. Rebecca Howell for her numerous contributions to this project, including photon treatment planning, contouring, photon stray dose measurement and helpful suggestions. Thanks to Dr. Anita Mahajan, for her help with contouring, reviewing each treatment plan and helpful discussions. Thanks to Dr. Dragan Mirkovic for his contributions to dose and risk calculations, and his support with maintenance of the treatment planning system. Thanks to Dr. Carol Etzel for help with statistical analysis and helpful discussions.

For helpful scientific discussions, I am grateful to Drs. Phillip Taddei, Mary Martel, Shiao Woo, George Starkschall, and Uwe Titt. I am also grateful to Dr. George Coutrakon for serving on my defense committee.

Thanks to Annelise Giebeler, one of my group members, for her contributions to the proton treatment planning. And I also need to thank other members of our group: Dr.

Angélica Pérez-Andújar, Kenny Homann, Laura Rechner, John Eley and Tim Jones for many helpful discussions.

Finally, I need to acknowledge the financial support from Sowell-Huggins Cancer Answer Scholarship, President Research Scholarship and 1 year stipend from University of Texas Graduate School of Biomedical Sciences, and the National Cancer Institute Grant (award 1R01CA131463-01A1).

TABLE OF CONTENTS

ABSTRACT	III
ACKNOWLEDGEMENTS	IV
1. INTRODUCTION AND BACKGROUND	1
1.1 MEDULLOBLASTOMA	1
1.2 RADIOGENIC SECOND CANCER	2
1.3 RADIOGENIC CARDIAC TOXICITY	5
1.4 COMPARATIVE STUDIES BETWEEN DIFFERENT TREATMENT MODALITIES	7
1.5 STATEMENT OF THE PROBLEM	10
1.6 HYPOTHESIS AND SPECIFIC AIMS	11
2. METHODS AND MATERIALS	14
2.1 PATIENT SELECTION	14
2.2 ORGANS AT RISK	15
2.3 TREATMENT PLANNING	16
2.3.1 <i>Proton treatment plans</i>	16
2.3.2 <i>Photon treatment plans</i>	17
2.3.3 <i>Evaluation volume</i>	18
2.4 THERAPEUTIC AND STRAY RADIATION DOSE RECONSTRUCTIONS	18
2.4.1 <i>Stray dose reconstructions for proton therapy</i>	18

2.4.2	<i>Stray dose reconstructions for photon therapy</i>	21
2.5	CALCULATION OF RISK OF SECOND CANCER.....	24
2.6	CALCULATION OF RISK OF CARDIAC TOXICITY	26
2.7	UNCERTAINTY ANALYSIS	29
3	RESULTS	33
3.1	THERAPEUTIC AND STRAY RADIATION DOSES RECONSTRUCTIONS	33
3.1.1	<i>Evaluation volume coverage for photon versus proton treatment plans</i> ...	33
3.1.2	<i>Dose reconstruction for photon therapy</i>	34
3.1.3	<i>Dose reconstruction for proton therapy</i>	37
3.2	PREDICTED RISK OF RADIOGENIC SECOND CANCER	48
3.3	PREDICTED RISK OF CARDIAC TOXICITY	51
3.4	SENSITIVITY OF PREDICTED RISK OF SECOND CANCER TO MODELING ASSUMPTIONS	
	62	
3.5	SENSITIVITY OF PREDICTED RISK OF CARDIAC TOXICITY TO MODELING	
	ASSUMPTIONS.....	67
4	DISCUSSION	74
4.1	OUTCOMES OF SPECIFIC AIM ONE	74
4.2	OUTCOMES OF SPECIFIC AIM TWO	75
4.3	OUTCOMES OF SPECIFIC AIM THREE	76
4.4	COHERENCE WITH EXISTING LITERATURE	78
4.5	IMPLICATIONS AND SIGNIFICANCE OF THE FINDINGS	86
4.6	STRENGTHS OF THIS STUDY	87
4.7	LIMITATIONS OF THIS STUDY.....	89

4.8 FUTURE WORK	92
5. CONCLUSION	94
BIBLIOGRAPHY	95
LIST OF PUBLICATIONS DURING PHD PERIOD	113
VITA.....	114

List of Figures

Figure 2-1. Proton therapy treatment apparatus and the voxelized phantom oriented for the superior spinal proton field. The beam delivery system includes a vacuum window (A), a beam profile monitor (B), a range modulator wheel (C), a second scatter (D), a range shifter assembly (E), backup and primary monitors (F), the snout (G), the range compensator (I), treatment couch (I) and the patient (J).....	20
Figure 2-2 The commercial anthropomorphic phantom used for stray photon dose measurement	22
Figure 2-3 Sagittal slice of absorbed dose distribution for the photon plan for a 4-year-old boy. The heart was included in the 5% isodose surface (yellow).....	23
Figure 3-1 Sagittal slice of the photon absorbed dose distribution for a 4-year-old boy from all photon CSI fields.....	34
Figure 3-2 Values of stray radiation absorbed dose equivalent per therapeutic absorbed dose (H/D) as a function of distance from field edge (x). Measured data were taken from Howell <i>et al</i> (2011).The dashed lines are 95% confidence interval of fitting result (Newhauser 2011, personal communication).	36
Figure 3-3 Sagittal slice of the proton absorbed dose distribution for a 4-year-old boy from all proton CSI fields.	37
Figure 3-4 Sagittal slice of the stray neutron equivalent dose (from external and internal neutrons from all fields) distribution generated during proton CSI for a 4-year-old boy.	39
Figure 3-5 Stray neutron equivalent dose H_T to the whole heart and sub-structures from proton therapy as a function of patient age at exposure, e.....	41

Figure 3-6 Comparison of stray equivalent dose per therapeutic absorbed dose, H/D , as a function of distance from field edge, x , between photon and proton CSI. Measured photon stray dose data were taken from Howell <i>et al</i> (2011). Stray equivalent dose data from proton CSI were from this study.	42
Figure 3-7 Cumulative DVHs from the treatment plans for a 4-year-old boy (patient No. 2) Proton and photon DVHs are indicated by dashed and solid lines, respectively, for various organs (This figure was from Howell, personal communication).	43
Figure 3-8 Absorbed dose, D , to the whole heart and sub-structures for proton and photon CSI plans as a function of patient's age at exposure, e	44
Figure 3-9 Dose (therapeutic dose + stray dose) ratio (proton/photon) for the heart sub-structures as a function of patient age at exposure, e	47
Figure 3-10 The population-average dose ratio values. The error bars represent the standard deviation for each group of data, <i>e.g.</i> , whole heart, pericardium and myocardium.	47
Figure 3-11 Equivalent Dose (D) to the thyroid for both proton and photon plans, as a function of patient's age at exposure, e	48
Figure 3-12 Axial (left) and sagittal (right) slices of absorbed dose distribution from the photon plan (top) and the proton plan (bottom) for a 4-year-old boy receiving CSI.	52
Figure 3-13 Differential DVHs of heart sub-structures from (a) proton (b) and photon CSI treatment plans (therapeutic + stray radiation doses) for a 4-year-old boy.	53
Figure 3-14 Predicted $RNTCP$ values for a population of patients as a function of patient's age at exposure.	58

Figure 3-15 Predicted <i>RNTCP</i> values <i>versus</i> age at exposure, <i>e</i> , by sex for a sample of patients (n=18) for which proton and photon CSI treatment plans were prepared.....	59
Figure 3-16 <i>RNTCP</i> VS mean organ dose ratio ($D_{\text{proton}}/D_{\text{photon}}$) for heart sub-structures for a population of pediatric patients.....	61
Figure 3-17 The population-average <i>RNTCP</i> values. The error bars represent the standard deviation of <i>RNTCP</i> values for each group of data, <i>e.g.</i> , whole heart, pericardium and myocardium.	62
Figure 3-18 Sensitivity of the <i>RLAR</i> values to changes in the maximum radiation weighting factor for neutrons.....	65
Figure 3-19 Excess relative risk as a function of equivalent dose, <i>H</i> . (LEXP = linear-exponential; LPLA = linear-plateau) used in this work to estimate excess relative risk (ERR) in the thyroid. The numbers in the legend refer to the location of the approximate point beyond which risk decreases or plateaus.	66
Figure 3-20 Surfaces of predicted <i>RNTCP</i> values for heart sub-structures as functions of different <i>NTCP</i> parameters. (Upper) The surfaces displayed were calculated for <i>m</i> values of 0.1, 0.3, 0.5 and 1 (pericardium), γ values of 0.1, 0.5, 1 and 2 (myocardium and whole heart). (Lower)The surfaces displayed were calculated for <i>n</i> values of 0.1, 0.3, 0.5 and 1 (pericardium), <i>s</i> values of 0.1, 0.5 and 1 (myocardium and whole heart). Color interpolated to facilitate visualization.....	68
Figure 3-21 Sensitivity of the predicted <i>RNTCP</i> values to changes in the neutron radiation weighting factor (w_R) for the (a) pericardium, (b) myocardium and (c) whole heart.....	71

Figure 3-22 Heat sub-structures contouring: (a) baseline contouring (b) revised

contouring. 72

Figure 4-1 Cumulative second cancer incidence from CCSS study (Meadows *et al*

2009, with permission) and from this study..... 84

List of Tables

Table 1-1 Spectrum of radiogenic cardiovascular disease, end points, biologic models used to analyze dose-response relationship and selected references.	7
Table 2-1 Proton beam specifications of the CSI fields.	24
Table 2-2 <i>NTCP</i> model parameters for cardiac toxicity from the literature.	29
Table 3-1 Comparison of target coverage and the maximum dose in the target between photon and proton CSI (Howell <i>et al</i> 2011).....	34
Table 3-2 Minimum, maximum and mean absorbed dose from therapeutic radiation to different heart sub-structures resulting from photon therapy for the population of pediatric patients.	35
Table 3-3 Minimum, maximum and mean absorbed doses from therapeutic radiation to different heart structures resulting from proton therapy for the population of pediatric patients.	38
Table 3-4 Mean stray neutron equivalent dose (H) in the whole heart and sub-structures of each patient from proton CSI.....	40
Table 3-5 The mean, standard deviation (SD), SD of the mean, median, minimum, and maximum equivalent dose (sum of therapeutic dose and stray dose) to the whole heart of the sample patients.....	45
Table 3-6 The mean, standard deviation (SD), SD of the mean, median, minimum, and maximum of equivalent dose (sum of therapeutic dose and stray dose) to the pericardium of the sample patients.	45

Table 3-7 The mean, standard deviation (SD), SD of the mean, median, minimum, and maximum of equivalent dose (sum of therapeutic dose and stray dose) to the myocardium of the sample patients.	46
Table 3-8 Mean organ equivalent doses from proton and photon CSI plans for a 4-year-old boy. For proton CSI, both therapeutic and stray doses were listed, and a summation of them was also listed. For photon CSI, the combined dose from both therapeutic and stray doses was listed.	49
Table 3-9 Baseline calculations of relative risk of radiogenic second cancer for a 4-year-old boy in each organ (RR_T), and ratio of relative risk ($RRR = RR_{\text{proton}}/RR_{\text{photon}}$) following photon and proton therapies at 15, 30, 45, 60, 75 and 95 years after treatment.	49
Table 3-10 Mean organ equivalent dose to heart sub-structures from proton and photon plans for a 4-year-old boy receiving CSI.	52
Table 3-11 <i>NTCP</i> values for heart sub-structures and relative <i>NTCP</i> ($RNTCP$) values based on existing model parameters.	54
Table 3-12 Predicted <i>NTCP</i> values for the whole heart, pericardium and myocardium following proton and photon therapies for a population of pediatric patients ($n = 18$). $RNTCP = NTCP_{\text{proton}}/NTCP_{\text{photon}}$	54
Table 3-13 The mean, standard deviation (SD), SD of the mean, median, minimum, maximum of <i>NTCP</i> values for the whole heart of the sample of patients.	55
Table 3-14 The mean, standard deviation (SD), SD of the mean, median, minimum, maximum of <i>NTCP</i> values for the pericardium of the sample of patients.	56

Table 3-15 The mean, standard deviation (SD), SD of the mean, median, minimum, maximum of $NTCP$ values for the myocardium of the sample of patients.....	56
Table 3-16 Predicted relative risk (15 years after exposure) in each tissue (LAR_T) and the ratio of LAR_{proton} to LAR_{photon} ($RLAR$) for various scaling factors of the radiation weighting factor ($\overline{w_R}$) for neutrons.	63
Table 3-17 The predicted RR and RRR values in thyroid for various dose-risk models plotted in Figure 3-19. The dose-risk models include: linear non-threshold (LNT); linear-exponential (LEXP); linear-plateau (LPLAT). The numbers in the parenthesis indicate the dose at which the model rolls off the risk due to the cell sterilization effect.	67
Table 3-18 $NTCP$ and $RNTCP$ values of cardiac toxicity for a 4-year-old boy and a 14-year-old boy using combinations of $NTCP$ model parameters.	69
Table 3-19 Predicted $NTCP$ and $RNTCP$ values of cardiac toxicity for a 4-year-old boy and a 14-year-old boy based on modified contours.	73
Table 4-1 Comparison of lifetime risk (prescribed dose 23.4 Gy) of second cancer incidence and ratio of the lifetime risk between proton CSI and conventional photon CSI (CRT) from different studies.	78
Table 4-2 Risk coefficients for lifetime second cancer incidence from ICRP Publication 60 (ICRP 1991) and BEIR VII (NRC, 2006).....	80
Table 4-3 Comparison of stray organ doses from proton CSI between different studies.	82
Table 4-4 Mean therapeutic absorbed dose to the heart (averaged for different cases, 5 cases in Mu <i>et al</i> (2005), and 18 in current work) from photon and proton CSI.....	85

1. INTRODUCTION AND BACKGROUND

In this chapter, a brief overview of medulloblastoma (MB) disease is provided (Section 1.1), followed by the description of radiogenic late effects for MB patients including second cancer (Section 1.2) and cardiac toxicity (Section 1.3). The comparative studies between different radiation therapy modalities are discussed (Section 1.4). The central problem statement of this work is given (Section 1.5) and finally the hypothesis and specific aims are introduced (Section 1.6).

1.1 MEDULLOBLASTOMA

Medulloblastoma (MB), one of the most common pediatric tumors of the central nervous system, accounts for approximately 25% of all pediatric brain tumors. It is a malignant tumor that begins in the lower part of the brain (posterior fossa) and can spread to the spine or other parts of the body. There are more than 500 cases diagnosed annually in the United States (CBTRUS 2002). The median age of the patient at presentation is 6-7 years, and the number of male patients is slightly larger than the number of female patients (1.2/1). The current standard of care is a combination of craniospinal irradiation (CSI) and chemotherapy (Freeman *et al* 2002). Usually the MB patients are categorized into different risk groups: average risk group and high risk group. For average risk group, the survival rates are considered satisfactory and the late effects are of concern; for high risk group, both late toxicity and poor survival are of concern (Fossati *et al* 2009).

The 5-year survival rate of MB patients has improved significantly over the past decades (Polednak and Flannery 1995, David *et al* 1997, Miralbell *et al* 1997a, Miralbell *et al* 2002, St Clair *et al* 2004, Fossati *et al* 2009, Smith *et al* 2010).

This increased survival is primarily attributed to the use of postoperative radiation therapy (del Charco *et al* 1998). Radiation therapy typically uses megavoltage external beam photon therapy (conventional therapy) to treat the entire craniospinal axis. However, with conventional photon radiation, large amounts of normal tissues outside the target receive substantial radiation doses. These doses are thought to cause radiogenic late effects that can diminish the lifespan and quality of life of MB survivors. The late effects may occur months, years, or even decades after irradiation and may include second cancer, cardiac toxicity, pneumonitis, thyroiditis, cognitive deficiency, reduction in fertility and bone growth, etc. (Choux *et al* 1983, Hoppe-Hirsch *et al* 1990, Kiltie *et al* 1997, Mulhern *et al* 1998, Fossati *et al* 2009).

1.2 RADIOGENIC SECOND CANCER

Cancer is one of the most significant health care problems in the United States. It is the leading cause of death for men and women younger than 85. An estimate total of 1,529,560 new cancer cases and 569,490 deaths from cancer occurred in the United States in 2010 (Jemal *et al* 2010). Approximately, 1 in 4 deaths is due to cancer in the United States, and more than half of the cancer patients will receive some form of radiation treatment for their diseases (Dyk 1999).

With increasing long term survival rates of the pediatric cancer patients (Hewitt 2003, Jemal *et al* 2008), avoiding potentially fatal complications, such as radiogenic second cancers, is increasingly important (Newhauser and Durante 2011). Radiogenic second cancer is usually fatal and can seriously reduce patients' quality of life. For some types of cancers and in some pediatric cancers, second cancers can cause more deaths than the primary cancers (Tubiana 2009). However, the potential incidence of second cancer has long been underestimated, and one of the major reasons is the short follow-up time and patient survival times were shorter than the latency period for second cancer (Tubiana 2009). Second cancers account for 6~10% of all cancers and are the fourth or fifth most common cancer in the USA (Neugut 1999).

Data from the Surveillance, Epidemiology, and End Results (SEER) registries demonstrated that childhood cancer survivors are at around 6-fold increased risk of second cancers compared to the general population, and the risk continues to increase with attained age (Inskip and Curtis 2007). The Childhood Cancer Survivor Study (CCSS) (Robison *et al* 2002), which has the largest cohort of long-term childhood cancer survivors, reported the 30-year cumulative incidence of second malignant neoplasms was 9.3%, and that of nonmelanoma skin cancer was 6.9%. Risk of second cancers remains elevated for more than 20 years of follow-up for all primary childhood cancers (Meadows *et al* 2009). The overall cumulative mortality for those patients is 18.1% at 30 years from diagnosis (Armstrong *et al* 2009). Importantly, the rate of mortality attributable to recurrence or progression of primary disease is decreasing, while the rate of mortality attributable to second cancers, cardiac death, and pulmonary death is increasing (Armstrong *et al* 2009).

There are many risk factors associated with second cancers. It has been found that second cancers are more likely to occur in patients diagnosed with primary cancer at a young age, received high-dose radiation therapy and certain chemotherapeutic agents, and in those with a known genetic predisposition to cancer (Bhatia and Sklar 2002). Ionizing radiation is one of the most important treatment-related risk factors.

The radiation therapy practitioners continually seek out treatment modalities that can improve dose conformality to reduce acute toxicity and late effects from radiation. One such modality is proton therapy, which delivers a more conformal dose distribution and less integral dose to patients than photon therapy (Miralbell *et al* 1997b, Lin *et al* 2000, Miralbell *et al* 2002, Kirsch and Tarbell 2004, St Clair *et al* 2004, Yuh *et al* 2004, MacDonald *et al* 2008) because of its physical characteristics. Stray dose exists for both photon and proton therapy, but is of greater concern for proton therapy because the main component of stray dose from proton therapy is secondary neutrons (Agosteo *et al* 1998, Yan *et al* 2002, Hall 2006, Zacharatou Jarlskog and Paganetti 2008, Fontenot *et al* 2009, Newhauser *et al* 2009, Taddei *et al* 2009, Taddei *et al* 2010b). The main reason for the concern regarding secondary neutrons is that the relative biological effectiveness (RBE) for carcinogenesis is not well known and some authors have opined that the dose from neutrons may negate the advantage of proton therapy (Hall 2006, 2007). While those stray radiation doses are typically very low compared to the primary radiation dose, they are not negligible and will increase patients' risks of radiogenic late effects (Suit *et al* 2007, Tubiana 2009, Newhauser and Durante 2011).

1.3 RADIOGENIC CARDIAC TOXICITY

Radiation induced cardiac toxicity, one of the focuses of this work, is of great concern because it can be physically and psychologically devastating to patients that survive their first cancer. The Life Span Study (LSS) of Japanese atomic bomb survivors reported that the mortality from myocardial infarction 40 years after irradiation was significantly increased in the survivors who had received the acute dose of 1~2 Gy (Preston *et al* 2003), and there is emerging evidence of risks of cardiovascular disease at low radiation dose in those survivors although the dose response relation for the risk is not well defined (Little 2009). The CCS found that the risk of cardiovascular disease was substantial higher in cancer survivors than the general population (Oeffinger *et al* 2006, Mertens *et al* 2008, Armstrong *et al* 2009, Lipshultz and Adams 2010), and cardiovascular events are the leading non-malignant cause of death among cancer survivors (Mulrooney *et al* 2009). The American Society of Clinical Oncology also reported the estimated aggregate incidence of radiogenic cardiac disease for cancer survivors at 10% to 30% by 5 to 10 years after treatment, respectively (Carver *et al* 2007). Radiation therapy was more strongly associated with the development of cardiovascular disease risk factors than was chemotherapy (Meacham *et al* 2010), and cardiovascular disease risk increases with time since radiation therapy (Mertens *et al* 2001, Adams *et al* 2007, Heidenreich *et al* 2007). Coronary vascular disease was found to be associated with higher radiation dose for Hodgkin's disease survivors (Hull *et al* 2003). Aleman *et al* (2003) reported that the leading noncancer mortality in radiation treated Hodgkin's disease patients is cardiovascular death. Jakacki *et al* (1993) found that CSI patients are at risk for

significant cardiac dysfunction and the asymmetric impairment of heart development, where asymmetric distribution of radiation may be the cause. Gurney *et al* (2003) reported that pediatric survivors who received radiation therapy and chemotherapy for brain tumors are at increased risk for cardiovascular late effects.

The major structures of interest in the heart include the pericardium, myocardium, valves, conduction system, and coronary arteries (Stewart *et al* 1995, Adams *et al* 2003). These structures are thought to be at greatest risk radiation induced damage.

Table 1-1 lists the most common radiogenic cardiac diseases and end points, biologic models used to analyze dose-response relationship and selected references. In order to calculate the risk of cardiac toxicity for various sub-structures of the heart, detailed dose distributions of the different heart sub-structures are required because the different parts of the heart have different biological functions.

Table 1-1 Spectrum of radiogenic cardiovascular disease, end points, biologic models used to analyze dose-response relationship and selected references.

Structure	End-points	Dose-response model	Selected references
Whole heart	Ischemic heart disease, Cardiac mortality	Lyman model, Relative seriality model	Gagliardi <i>et al</i> 1998, 2001, 2010, Eriksson <i>et al</i> 2000, Carr <i>et al</i> 2005
Myocardium	Restrictive cardiomyopathy, Angina pectoris, Pancarditis, Myocardial infarction, Myocardial ischemia	Relative seriality model	Gagliardi <i>et al</i> 1998, 2001, 2010, Adams <i>et al</i> 2003
Pericardium	Pericarditis, Pericardial effusion, Pericardial constriction	Lyman model, Relative seriality model	Martel <i>et al</i> 1998, Adams <i>et al</i> 2003, Burman <i>et al</i> 1991, Kallman <i>et al</i> 1992
Valves	Valvular stenosis, Incompetent valve	N/A	Adams <i>et al</i> 2003
Coronary Arteries	Atherosclerosis	N/A	Adams <i>et al</i> 2003, Carr <i>et al</i> 2005

1.4 COMPARATIVE STUDIES BETWEEN DIFFERENT TREATMENT MODALITIES

Until recently, there was limited knowledge involving accurate organ doses associated with stray radiation from advanced-technology radiation therapy. The prediction of doses of stray radiation is computationally complex, expensive, and has only recently become available for proton therapy (Jiang *et al* 2005, Koch and

Newhauser 2005, Zacharatou Jarlskog and Paganetti 2008, Zhang *et al* 2008, Fontenot *et al* 2009, Newhauser *et al* 2009, Taddei *et al* 2009, Taddei *et al* 2010b). There is also limited knowledge of models to convert dose to risk of radiogenic late effects for patients following advanced forms of radiation therapy. Most of the current dose-risk coefficients assumed linear-no threshold (LNT) model, which was based on Atomic Bomb survivors data and is valid for low dose (0~2.5 Sv). However, at higher dose, the cell killing mechanism may suppress the risk from high dose. Different dose-risk curves, like linear-exponential model and linear-plateau model, were proposed by different studies (Brenner *et al* 2000, Schneider *et al* 2005, Sigurdson *et al* 2005, Ronckers *et al* 2006b, Schneider *et al* 2008, Fontenot *et al* 2009). Additionally, comparative risk assessments may vary strongly with the treatment site and other factors like treatment and host factors, methodology used in the dose reconstruction and risk predictions. For these reasons, comparative studies of treatment planning and risks of radiogenic late effects are limited in number and scope, and there is a vital need for multidisciplinary inquiry into dose reconstruction and risk assessment (Newhauser 2010).

St Clair *et al* (2004) reported a treatment planning comparison between conventional photon, modulated photon and proton therapy for a pediatric patient with MB. They found that proton therapy provided substantially superior normal-tissue sparing compared to photon therapy and they inferred that the long-term toxicity such as cardiac dysfunction could be improved based on the dose sparing. Other similar treatment planning studies that compared dose sparing between proton and other radiation therapy techniques (Miralbell *et al* 1997a, Miralbell *et al* 1997b, Lin *et al*

2000, Tarbell *et al* 2000, Lee *et al* 2005, Cochran *et al* 2008) confirmed that proton therapy provides superior sparing of normal tissues than other techniques.

Miralbell *et al* (2002) calculated the risk of second cancer after photon and proton radiation therapies for a 3-year-old boy with MB, and concluded that proton therapy can substantially reduce the second cancer risk. However, that study only considered spinal radiation treatment fields and did not include the cranial treatment fields. In addition, the doses reported by Miralbell *et al* (2002) study were entirely based on treatment planning system calculations that did not include stray radiation for proton therapy and underestimated stray radiation for photon therapy. Mu *et al* (2005a) investigated different spinal irradiation techniques, and they recommended intensity modulated proton therapy (IMPT) for medulloblastoma patients instead of conventional photon therapy, IMRT or intensity modulated electron therapy. Again, they did not take stray radiation doses into account when they calculated risks. Newhauser *et al* (2009) expanded upon the work from Miralbell *et al* (2002) by supplementing the therapeutic proton therapy doses with stray doses and calculating the predicted incidence of second cancer after CSI. They reported that proton therapies carried a substantially lower predicted risk than photon therapies. However, the predicted risks reported by Newhauser *et al* did not take into account the underestimation of stray dose predicted by photon treatment planning systems.

In all those previous CSI studies, the risk of late effects were either not calculated (St Clair *et al* 2004), or were calculated based on age, sex non-specific risk coefficients from ICRP report (Miralbell *et al* 2002, Mu *et al* 2005b, Newhauser *et al* 2009), which were designed for radiation protection purpose. In addition, these studies

had limited consideration of organ doses from stray radiation. Specifically, for proton therapy, stray radiation was either not included (Miralbell *et al* 2002, Mu *et al* 2005b) or estimated by dose inside a small spherical receptor put in the organs of a computational phantom (Newhauser *et al* 2009). Similarly, for photon therapy stray radiation was underestimated because commercial treatment planning systems were used to determine organ doses and these systems are known to underestimate stray dose (Howell *et al* 2010).

Compared to the literature on second cancer following proton radiation therapy, reports on other late effects are sparse (Fuss *et al* 2000, Kaser-Hotz *et al* 2002, Mu *et al* 2005a, Brodin *et al* 2011). This lack of information is an obstacle to making evidence-based clinical decisions on choosing a radiotherapy modality. In recent decades, Gagliardi and colleagues (Gagliardi *et al* 1996, Gagliardi *et al* 1998, Eriksson *et al* 2000, Gagliardi *et al* 2001, Gagliardi *et al* 2010) used normal tissue complication probability (*NTCP*) model to calculate radiogenic cardiac toxicity for breast cancer and Hodgkin's disease patients. However, there is still a complete lack of predicted risk values for cardiac toxicity following proton or photon CSI.

1.5 STATEMENT OF THE PROBLEM

Radiation therapy has been used as an effective treatment for malignancies in pediatric patients. However, in many cases, the side effects of radiation diminish these patients' quality of life. In order to develop strategies to minimize predicted radiation complications, one must first be able to accurately estimate pediatric patients' relative

risk for radiogenic late effects, which has not become feasible till recently because of the calculational complexity.

There is still limited knowledge of accurate organ doses and incidence of radiogenic late effects. In the case of proton therapy, the dosimetry of whole body exposure to neutrons is physically complex and computationally challenging, and detailed models that convert dose to effect have only recently become available. Although dosimetric data and risk models are available, there is incomplete knowledge in the literature of estimated radiogenic secondary cancer and cardiac toxicity for pediatric patients who receive advanced forms of radiation therapy. The current gaps in knowledge are obstacles to realize an evidence-based approach to clinical decision making, *i.e.*, selecting treatment modalities for pediatric patients with the lowest achievable predicted risk of late effects.

The goals of this work are to estimate dose delivered to tissues and organs in pediatric patients receiving contemporary proton and photon radiotherapies; to calculate the risk of radiation induced second cancer and cardiac toxicity; to test the statistical significance of the difference in the predicted risk of radiation induced late effects after proton *versus* photon therapies; and to prototype a tool to enable an evidence-based approach for selecting treatment modalities for pediatric patients quantitatively, taking second cancer and cardiac toxicity into account.

1.6 HYPOTHESIS AND SPECIFIC AIMS

We proposed to test the following hypothesis: A population of survivors of childhood cancer of the central nervous system (CNS) who receive proton CSI are at

lower predicted risk of incidence of radiogenic second cancer and cardiac toxicity than those who receive photon CSI, and the differences in risk of second cancers and cardiac toxicity after photon *versus* proton CSI are significant.

To test this hypothesis, we estimated the risk of second cancer for one pediatric patient and risk of cardiac toxicity for a population (n=18) of pediatric CNS patients undergoing proton therapy *versus* photon therapies. To do so, we performed the following specific aims:

Specific Aim 1: Predict the ratio of relative risk (*RRR*) and ratio of lifetime attributable risk (*RLAR*) values (defined in section 2.5) of radiogenic second cancer for one pediatric CNS patient treated with proton *vs.* photon therapies according to the prevailing standards of care at our institution.

One pediatric patient was chosen for this aim. A proton plan and a photon plan were created using a commercial treatment planning system (TPS). Detailed therapeutic dose and stray dose distributions were reconstructed using the TPS, Monte Carlo simulations and measurements. Risk models from the literature were used to calculate risk of secondary cancer based on therapeutic and stray radiation doses.

Specific Aim 2: Predict the values of ratio of normal tissue complication probability (*RNTCP*) (defined in section 2.6) of radiogenic cardiac toxicity in a population of pediatric CNS patients treated with proton therapy *vs.* photon therapy using the current standards of care.

Patients (n=18) of different ages, sexes, sizes, and treatment conditions were included in this aim. Photon and proton treatment plans were created for each patient, and detailed dose reconstructions were performed for each treatment plan. Normal tissue complication probability (*NTCP*) models from the literature were to estimate the risk of developing cardiac toxicity.

Specific Aim 3: Estimate the uncertainty in the calculated *RRR*, *RLAR* and *RNTCP* values (proton vs. photon therapies), taking into account dosimetric uncertainties, uncertainties in dose-response model parameters, uncertainty in the mean neutron radiation weighting factors and host-specific factors such as patient sex, size, age at exposure and attained age, and treatment related factors.

We tested for significance by assessing the difference between the median of *RNTCP* values and unity at the 95% significance level. Rigorous error propagation was carried out for uncertainties that are comparatively well known, and sensitivity tests were carried out for other variables with uncertainties that are less well known.

2. METHODS AND MATERIALS

This chapter describes the methods by which the hypothesis was tested. The selection of the population of patients used in this project is described in section 2.1. The organs of interest for second cancer and cardiac toxicity risks assessments are described in section 2.2. The treatment planning techniques for both proton and photon therapies are given in Section 2.3. Section 2.4 describes the method used to estimate therapeutic and stray radiation doses for proton and photon treatments. Sections 2.5 and 2.6 describe the methods used to calculate risk of second cancers and cardiac toxicities. Lastly, the uncertainty analysis is discussed in Section 2.7.

2.1 Patient selection

Patients treated with radiation therapy at The University of Texas MD Anderson Cancer Center during 2007 to 2009 were included in this study using the consecutive sampling method. Inclusion criteria included: patients of age between 2 and 18 at the time of treatment, treated with proton therapy in supine position, and with CT images available. Exclusion criteria included: Patients treated with photon therapy, CT image of patient acquired in prone position, and age younger than 2 or older than 18. The reason to choose patients treated with proton therapy is because proton therapy treatment plans are much more susceptible to range errors associated with CT HU calibration and patient setup errors. Therefore it was much easier to recreate photon plans in a proton treatment planning system than to recreate proton plans in a photon treatment planning system. Eighteen MB patients were included: $N = 10$ for patients in group 1, ($2 \leq \text{age} \leq 10$), $N = 8$ for patients in group 2, ($10 < \text{age} \leq 18$). The patients in our sample include patients with different ages, sexes, sizes,

statures and treatment techniques that are representative of the MB pediatric population at our institution.

2.2 Organs at risk

The organs of interest for second cancer study in specific aim 1 included stomach, colon, lungs, bladder, thyroid, liver, gonads and remainder (*i.e.*, all other tissues/organs for which organ-specific risk coefficients were not explicitly provided in the BEIR VII report). Skin and bone marrow were not included in this study for simplicity. These organs were delineated on the planning CT images of each patient.

For the cardiac toxicity study in specific aim 2, the major structures of interest in the heart included the pericardium, myocardium, valves, conduction system, and coronary arteries (Stewart *et al* 1995, Adams *et al* 2003). These structures were thought to be at greatest risk for damage induced by irradiation. Table 1-1 lists the structures, end points, dose-response models, and selected references. Because the different parts of the heart have different biological functions, in order to calculate the risk of cardiac toxicity for various sub-structures of the heart, the detailed dose distributions throughout the entire organ were reconstructed.

The heart was contoured in detail because of the complexity and different radiation sensitivities of the heart sub-structures: the external surface of the heart was contoured in every CT slice, from the inferior border of the right pulmonary artery to the apex of the heart; the pericardium was defined as a 2-mm shell inside the external heart surface contours; the myocardium had an external contour identical to the internal contour of pericardium, and thickness of the myocardium varied from 1 cm to 2 cm, with the wall thickness of the left part being twice that of the right part.

2.3 Treatment planning

Both proton and photon treatment plans were created using a commercial TPS (Eclipse version 8.9, Varian Medical Systems, Palo Alto, CA). For all the patients, multiple radiation therapy fields were designed to treat the entire craniospinal axis. The final plans for each patient were approved by a board certified radiation oncologist. More details about the proton and photon radiotherapy treatment plans can be found in sections 2.3.1-2 below and in Howell *et al* (2011).

2.3.1 Proton treatment plans

The proton treatment plans were designed to treat the patient using the passively scattered proton beam line at our institution (Arjomandy *et al* 2009). The treatment planning system was previously configured and tested for clinical use (Newhauser *et al* 2007b). The patients were treated in the supine position and the CT scans were obtained from the top of the head to the thigh or lower. An age-specific target volume was defined for each patient. For patients < 15 years of age, the target volume included the brain, spinal canal, and the entire vertebral body (to prevent bone growth deformity due to non-uniform dose distribution in the vertebral body). For patients ≥ 15 years of age, the target volume included the only the brain and spinal canal (with 2-3 mm margin anteriorly). The proton treatment plan was designed to deliver CSI of 23.4 Gy (RBE) to the target volume (including brain and spinal canal) (i.e., $21.3 \text{ Gy} \times 1.1 \text{ RBE}$) with 1.8 Gy (RBE)/fraction. The boost fields were not considered in this study for simplicity, and because the contributions of boost fields to stray doses were previously found to be negligible (Taddei *et al* 2009). The proton treatment plans included right and left posterior oblique cranial fields (gantry angle of 255° and 105°) and one to three posterior-anterior spinal fields (gantry angle of 180°)

depending on the length of the spine. Patient-specific devices included a range compensator and field-defining collimator. The standard of care for proton treatments at our institution included one to three junction shifts, which were generally one to two cm apart, to reduce the hot and cold spots at the field junctions. In this project, however, the junction shifts were eliminated because the hot and cold spots were dosimetrically irrelevant to second cancer and cardiotoxicity risks. Also, the treatment plans were used as the basis for stray radiation dose calculations and it was not feasible to repeat these stray dose calculations multiple times because of junction shifts. The treatment plans were initially calculated with junction shifts and then we removed the junction shifts and reoptimized the plans to achieve approximately the same uniformity as the plans with shifts (Giebel, personal communication).

2.3.2 Photon treatment plans

The photon treatment plans typical contained the following fields: two opposed lateral cranial fields (gantry angles of 270° and 90°), and one or two posterior-anterior spinal fields (gantry angle of 180°) depending on the length of the spine. All photon fields were 6 MV. The plans were designed to deliver 23.4 Gy to the cerebrospinal fluid volume (including brain and spinal canal) with 1.8 Gy/fraction. The plans included junction shifts after 9 Gy and 16.2 Gy. At our institution, an intensity modulated field-in-field (FIF) technique was used to reduce dose heterogeneity in the field matching areas (Yom *et al* 2007): the FIF technique uses multiple lower-weighted reduction fields, which contain blocked segments strategically placed within primary cranial spinal fields to reduce the highest dose areas and to force greater homogeneity in the target volume (Howell *et al* 2011).

2.3.3 Evaluation volume

Evaluation volumes were created to provide to compare dose distributions from proton and photon treatment plans. The evaluation volume included the entire CSF volume (including the brain and spinal canal through S2). This was done because the proton plans used an age specific 3-dimensional target volume and the photon plans did not have an explicit 3-dimensional target volume (they were simply designed to cover the CSF volume).

2.4 Therapeutic and stray radiation dose reconstructions

The therapeutic doses in proton and photon therapies were taken from the dose-volume histograms (DVH) calculated by the TPS. Organs whose risk coefficients were not explicitly provided in the BEIR VII report were included in “remainder”, and the dose to it was estimated as the mean dose for all the other organs (excluding skin and bone marrow).

Because the TPS did not calculate stray radiation doses accurately for photon and proton therapies, we used supplemental methods. Sections 2.4.1 and 2.4.2 describe the techniques used to determine the stray radiation doses during proton and photon therapies, respectively.

2.4.1 Stray dose reconstructions for proton therapy

Previous publications indicated that the patient can be exposed to whole body neutron dose about several hundred mSv during proton CSI proton (Newhauser *et al* 2009, Taddei *et al* 2009). Each patient requires a unique treatment technique and the impact of inter-patient variations in treatment technique is not known. Therefore the stray neutron doses were reconstructed for each patient included in this study.

The stray dose associated with the proton treatment was estimated by Monte Carlo transport calculations using the Monte Carlo N-Particle (MCNPX) code (version 2.6, Los Alamos National Laboratory) (Hendricks *et al* 2006). Its suitability for simulating radiation dose has been well established (Fontenot *et al* 2005, Herault *et al* 2005, Koch and Newhauser 2005, Newhauser *et al* 2005, Polf and Newhauser 2005, Polf *et al* 2005, Tayama *et al* 2006, Fontenot *et al* 2007, Herault *et al* 2007, Newhauser *et al* 2007a, Newhauser *et al* 2007c, Zheng *et al* 2007, Koch *et al* 2008, Moyers *et al* 2008, Titt *et al* 2008, Zheng *et al* 2008, Bednarz *et al* 2009, Fontenot *et al* 2009, Newhauser *et al* 2009, Athar *et al* 2010, Bednarz *et al* 2010, Taddei *et al* 2010a, Taddei *et al* 2010b, Zhang *et al* 2010, Mowlavi *et al* 2011). The treatment plan for each patient was imported into an in-house Monte Carlo Proton Radiotherapy Treatment Planning (MCP RTP) code system (Newhauser *et al* 2007b, Newhauser *et al* 2008) and the code system models the proton beam delivery system (Newhauser *et al* 2007b) and the patient (Figure 2-1). The voxelized patient phantom was created based on the CT images of the patient as described in Newhauser *et al* (2007a) and Taddei *et al* (2009). The three-dimensional CT image matrix was segmented into $4 \times 4 \times 5 \text{ mm}^3$ voxels because of a memory constraint in the Monte Carlo system. The matrix of Hounsfield Unit values in these voxels was then converted into a corresponding matrix of material composition indices and a matrix of mass density values. The elemental material compositions of tissues were taken from Woodard and White (1986). The material list was read as a text file by the MCNPX input file using the READ card in MCNPX.

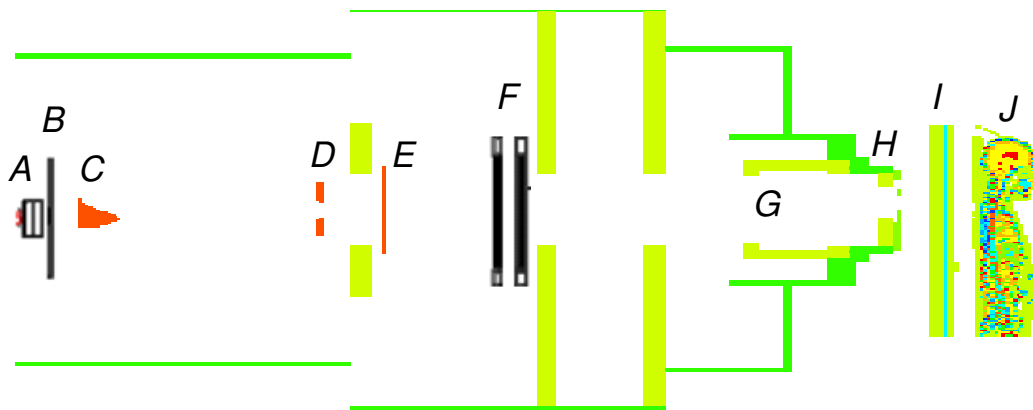


Figure 2-1. Proton therapy treatment apparatus and the voxelized phantom oriented for the superior spinal proton field. The beam delivery system includes a vacuum window (A), a beam profile monitor (B), a range modulator wheel (C), a second scatterer (D), a range shifter assembly (E), backup and primary monitors (F), the snout (G), the range compensator (I), treatment couch (I) and the patient (J).

Stray neutrons were generated both in the treatment unit (external neutrons) and in the patient (internal neutrons). Separate simulations were performed to predict the dose from external and internal neutrons, and total neutron dose was the summation of them. Details of the simulation methods were described previously (Newhauser *et al* 2009, Taddei *et al* 2009).

For each patient, we tracked 5×10^8 source particles for each cranial field stray neutron dose simulation and 1×10^9 source particles for each spinal field stray neutron dose simulation. As mentioned above, the external and internal neutron simulations were separated. Statistical uncertainties in doses were reported at the 68% confidence interval by MCNPX. The simulations were run in parallel on a 1072-CPU cluster with 2.6-GHz, 64-bit processors and the average total computation time for one patient simulation was approximately 4×10^4 cpu-hours.

The equivalent dose in each organ, H_T , was calculated by multiplying the organ dose by the mean radiation weight factor, $\overline{w_R}$. The $\overline{w_R}$ values were taken as 1.1

for therapeutic proton and 1 for photon beams, respectively. For stray neutrons, $\overline{w_R}$ values were taken from a study by Newhauser *et al* (2009), in which the mean neutron radiation weighting factors were estimated based on organ-specific simulations of neutron spectral fluence. They simulated neutron spectral fluence within the organs of an anthropomorphic computational phantom receiving CSI, and they calculated $\overline{w_R}$ values based on ICRP Publication 92 recommendations (ICRP 2003). The mean $\overline{w_R}$ values averaged over all organs were 7.75 for the cranial fields, 8.09 for the superior spinal field and 8.17 for the inferior spinal field. These values were applied to the corresponding fields in this study, and the average $\overline{w_R}$ values (8.13) between superior and inferior spinal field was used for middle spinal field in this study.

2.4.2 Stray dose reconstructions for photon therapy

Stray dose in photon therapy was obtained from the TPS or thermoluminescent dosimeter (TLD) measurements in a realistic anthropomorphic phantom.



Figure 2-2 The commercial anthropomorphic phantom used for stray photon dose measurement

Howell *et al* (2010a, 2010b) recently reported a methodology for determining radiation doses for organs either in-field, out-of-field or partially in-field: for in-field organs (the entire organs were within the 5% isodose line), the organ doses were obtained from TPS directly; for out-of-field organs (no part of the organ received more than 5% of the prescribed dose), the mean doses from TLD measurements in phantom were used; for partially in-field organs, a combination of TPS dose result and TLD measurement was used.

An anthropomorphic phantom (ATOM, CIRS, Inc., Norfolk, VA) was used for stray dose measurement (Figure 2.2). The measurement was performed by Howell *et al* (personal communication). The phantom was transected longitudinally in 2.5 cm slices and included a grid of holes that held TLD capsules. A CT scan of the phantom was acquired and then imported into the TPS. A 6 MV FIF photon treatment plan was

developed to irradiate the entire cranial and spinal region of the phantom; the treatment plan was consistent with the planning methodology used for the patient treatment plans (described in section 2.3). Measurement locations were defined throughout the phantom at various distances from the field edge. Further details of photon stray dose measurement were reported by Howell *et al* (2011).

For the cardiac toxicity study, all heart sub-structures in all patients were within the 5% isodose surface (Figure 2-3). Recent work by Howell *et al* found that doses reported by the TPS used in this work were accurate to the level of the 5% of the prescribed dose. Therefore, the dose reported by the TPS for the heart (and substructures of the heart) was used for risk calculations. The photon stray dose to thyroid was also obtained from TPS directly because the thyroid was included in the 5% isodose surface for all patients considered.

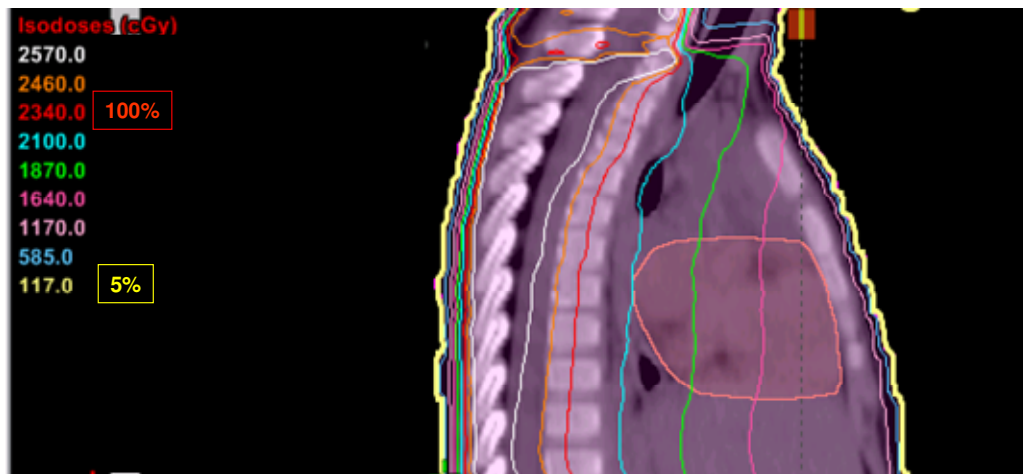


Figure 2-3 Sagittal slice of absorbed dose distribution for the photon plan for a 4-year-old boy. The heart was included in the 5% isodose surface (yellow).

For organs other than the heart and thyroid, they were first categorized as in-field, out-of-field, or partially in-field organs, and then the methodology of Howell *et al* (2010) was used to calculate organ doses.

2.5 Calculation of risk of second cancer

As stated in specific aim 1, the ratio of relative risk (*RRR*) value of radiogenic second cancer was calculated for one pediatric CNS patient treated with proton vs. photon therapies. A 4-year-old boy diagnosed with medulloblastoma was chosen for this purpose to facilitate comparison with previous studies from Miralbell *et al* (2002) and Newhauser *et al* (2009). The proton treatment technique for this patient is listed in Table 2-1.

Table 2-1 Proton beam specifications of the CSI fields.

	A	B	C	D
Target	Cranium	Cranium	Upper spine	Lower spine
Proton energy at nozzle entrance (MeV)	180	180	160	160
Range in patient (cm H ₂ O)	16	15.7	10.9	10.7
SOBP width (cm H ₂ O)	16	16	5	6
Gantry angle (degree)	255	105	180	180
Air gap (cm)	10.8	11.3	115	11.8
Aperture thickness (cm)	6	6	4	4
Prox margin around CTV (cm)	0.3	0.3	0.3	0.4
Distal margin around CTV (cm)	0.8	0.8	-0.2	0

The models contained in the report of the committee on the Biological Effects of Ionizing Radiation (BEIR VII) (NRC 2006) was used to calculate risk of radiogenic second cancer based on radiation doses determined in section 2.4 of this work.

The risk of developing a radiogenic cancer depends on many host and treatment factors, including the amount of radiation, age at exposure, attained age, and sex. Allowing for adjustments of the models based on these factors, the BEIR-VII committee provided organ-specific linear-no-threshold (LNT) risk models suitable for the estimation of excess relative risk (*ERR*) at low-dose and low-dose rate exposures.

For each organ or tissue, T, ERR_T was defined as:

$$ERR_T = RR_T - 1, \quad (2-1)$$

where RR_T is relative risk for the organ or tissue T and was defined as the ratio of disease incidence rates in exposed and unexposed groups.

The BEIR-VII committee recommended the following equation to calculate ERR_T :

$$ERR_T = \beta_s H_T \exp(\gamma e^*) \left(\frac{a}{60} \right)^\eta, \quad (2-2)$$

where H_T is the equivalent dose in Sv and is the sum of doses from multiple therapeutic fields and stray radiation doses generated from each therapeutic field to a certain organ, e is age at exposure in years, e^* is $(e - 30) / 10$ for $e < 30$ and zero for $e > 30$, and a is attained age in years, β_s is the sex-specific, organ-specific instantaneous ERR/Sv value, γ is the per-decade increase in age at exposure over the range 0–30 years, and η is the exponent of attained age ($\eta = 0$ for thyroid because the model for thyroid in the BEIR VII report is not dependent on attained age). Values for β_s , γ , and η were taken from Table 12-2 of BEIR VII. Using these data and equation (2-2), we estimated risk of second cancer at various times since exposure, *e.g.*, at 15, 30, 45, 60, 75 and 95 years after radiotherapy. Equation (2-2) was based on the LNT model. However, other effects may come into play at high radiation dose such as cell sterilization effect. These will be discussed in the uncertainty analysis section 2.7.

The BEIR VII report defined Excess Absolute Risk (EAR) as the difference between the cancer incidence rates of the exposed and unexposed groups. BEIR VII report also defined Lifetime Attributable Risk (LAR) as the probability that an irradiated patient will develop a radiation-induced second cancer during his or her lifetime (living to 100 years) exposed to certain equivalent dose H_T at age e , and it recommended that LAR should be estimated using both relative and absolute risk

transport models. The LAR coefficients of cancer incidence were provided in Table 12D-1 in the BEIR VII report, which were used to calculate cumulative lifetime risk of second cancer incidence. For simplicity, EAR coefficients were used to calculate the cumulative risk of radiogenic second cancer incidence of this patient living to certain years and was exposed at 4 years (age at exposure for this patient).

For each modality, the total LAR was calculated as

$$LAR_{modality} = \left(\sum_T LAR_T \right)_{modality}, \quad (2-3)$$

where the sum is over all the organs or tissues. And to compare the risks between proton and photon therapies, the ratio of lifetime attributable risk ($RLAR$) was defined as

$$RLAR = LAR_{proton} / LAR_{photon} \quad (2-4)$$

2.6 Calculation of risk of cardiac toxicity

There is growing interest in developing models that predict the risks of late effects based on the radiation dose (Gagliardi *et al* 1998, Eriksson *et al* 2000, Gagliardi *et al* 2001, Merchant *et al* 2002, Blanco *et al* 2005, Chapet *et al* 2005, Krasin *et al* 2005, Yorke *et al* 2005, Merchant *et al* 2006, Kong *et al* 2007, Merchant *et al* 2008). However, as yet, such late-effect calculations have not been performed routinely in the radiation treatment planning process for a variety of reasons: normal tissue complication rates among patients were low (Moiseenko *et al* 2000, Schultheiss 2001, Yorke 2001); patient survival times for patients with some first cancers were historically shorter than the latency period for late cardiac toxicity; the importance to minimize radiation late effects was not as fully appreciated; and adequately detailed dose response models were not available; until recently, the

computation of accurate doses to organs and tissues of the whole-body was not feasible for advanced-technology radiotherapies.

Based on a comprehensive literature search (listed in Table 1-1), the relative seriality (RS) model (Kallman *et al* 1992) and Lyman model (Lyman 1985) were used to calculate the Normal Tissue Complication Probability (*NTCP*) of radiogenic cardiac toxicity. These methods are briefly reviewed for the convenience of the reader.

The RS model is based on the Poisson model of cell survival. The probability of cell death when irradiating a tissue to a dose D is

$$P(D) = 2^{-\exp\{e\gamma(1-D/D_{50})\}}, \quad (2-5)$$

where γ is the maximum relative slope of the dose-response curve, D_{50} is the dose that will result in 50% complication probability. The cumulative complication probability due to an inhomogeneous irradiation is given by

$$NTCP = \left\{ 1 - \prod_{i=1}^n [1 - P(D_i)^s]^{V_i/V} \right\}^{1/s}, \quad (2-6)$$

where s is the relative seriality which describes the hybrid serial/parallel architecture of the organ, ($s = 0$ indicates parallel organization while $s = 1$ indicates serial organization), n is the number of sub-volumes in the dose-calculation volume, D_i is the dose in each sub-volume and V_i is the volume of each sub-volume in the differential DVH, and V is the total volume of the organ.

The Lyman model assumes is that the probability of complication is a normal distribution as the function of dose for the uniformly partial radiated volume V . The cumulative complication probability is given by

$$NTCP = \frac{1}{\sqrt{2\pi}} \int_{-\infty}^t e^{-t'^2/2} dt' \quad (2-7)$$

$$t = (D - TD_{50}(V))/(m \cdot TD_{50}(V)) \quad (2-8)$$

$$TD_{50}(V) = TD_{50}(1)/V^n \quad (2-9)$$

where $TD_{50}(V)$ is the tolerance dose that would result in 50% complication probability for the partial volume V , and $TD_{50}(1)$ is the tolerance dose that would result in 50% complication probability for the full organ, n indicates the volume effect (n close to 1 means there exists strong volume effect), and m is inversely proportional to the slope of dose-response curve.

The *NTCP* models give a quantitative prediction of organ response to radiation based on a dose distribution. They calculate the cumulative risk of normal tissue complications. The *NTCP* models used in this work were not age or sex specific, which is a limitation that will be discussed in section 4.7.

To compare *NTCP* values between photon and proton plans, the ratio of *NTCP* values (*RNTCP*) was defined as

$$RNTCP = NTCP_{\text{proton}} / NTCP_{\text{photon}} \quad (2-10)$$

For each patient DVHs for heart sub-structures were exported from TPS to calculate the corresponding *NTCP* values. Each step in the differential DVHs was corrected to 2 Gy(RBE)/fraction schedule by using the linear quadratic model (Steel 2002). The α/β ratio of 3 was chosen for the late effects in the heart (Eriksson *et al* 2000).

Table 2-2 lists *NTCP* model parameter sets used to model cardiac toxicity from the literature. These studies include models for patients treated for Hodgkin's disease (Eriksson *et al* 2000), breast cancer (Gagliardi *et al* 1996, Eriksson *et al* 2000, Gagliardi *et al* 2001), esophageal cancer (Martel *et al* 1998) and historical data which were mostly based on patients with Hodgkin's disease and breast cancer (Burman *et al* 1991, Kallman *et al* 1992). The literature contained no reports containing detailed

dosimetry and clinical outcomes data on cardiac toxicity for CSI patients.

Consequently, *NTCP* model parameters specifically for CSI patients are not available.

The model parameters listed in Table 2-2 were initially used for cardiac toxicity calculations for one pediatric patient. Based on calculation results for this first patient, shown in Table 3-11 in section 3.3, the following *NTCP* parameters were used for the baseline cardiac toxicity calculations for the entire sample: pericardium: $D_{50} = 50.6$ Gy, $n = 0.64$, $m = 0.13$; myocardium, $D_{50} = 52.2$ Gy, $\gamma = 1.25$, $s = 0.87$; for whole heart the average of three sets of parameters in Table 2-2 were used: $D_{50} = 62$ Gy, $\gamma = 1.06$, $s = 1$. Sensitivity tests were performed to quantify the impact of using different sets of *NTCP* model parameters for cardiac toxicity predictions.

Table 2-2 *NTCP* model parameters for cardiac toxicity from the literature.

Parameters		Pericardium			Myocardium	Whole heart		
		Burman <i>et al</i> (1991), Hodgkin's disease + breast cancer	Martel <i>et al</i> (1998), esophagus patients	Kallman <i>et al</i> (1992), Hodgkin's disease + breast cancer	Gagliardi <i>et al</i> (2001), breast cancer	Gagliardi <i>et al</i> (2001), breast cancer	Eriksson <i>et al</i> (2000), Hodgkin's disease + breast cancer	Eriksson <i>et al</i> (2000), Hodgkin's disease
Lyman Model	D_{50}	48	50.6	-	-	-	-	-
	n	0.35	0.636	-	-	-	-	-
	m	0.1	0.13	-	-	-	-	-
RS Model	D_{50}	-	-	49.2	52.2	52.3	63.3	70.3
	γ	-	-	3	1.25	1.28	0.93	0.96
	s	-	-	0.2	0.87	1	1	1

2.7 Uncertainty analysis

The baseline calculations of second cancer risk were based on the LNT model, which is mostly based on low dose data (<2.5 Sv) from atomic bomb survivors (NRC 2006). However, at higher doses, the cell sterilization mechanism may be important (Sigurdson *et al* 2005, Ronckers *et al* 2006a, Bhatti *et al* 2010) and other possible

non-linear dose-response relationships, *e.g.* linear-plateau relation and linear-exponential relationship may be more accurate (Hall and Wu 2003, Schneider and Kaser-Hotz 2005). Fontenot *et al* (2010) recently estimated the uncertainties in risk calculations following photon and proton radiotherapies for prostate cancer based on rigorous error propagation (eq. 2-9, based on Fontenot *et al* (2010) and was modified for Ratio of Lifetime Attributable Risk (*RLAR*) analysis. $RLAR = LAR_{\text{proton}} / LAR_{\text{photon}}$) and sensitivity tests. They concluded the baseline calculations of risks showed only a small sensitivity to cell sterilization effects. The relative uncertainty in *RLAR* is given by

$$\left(\frac{\sigma_{RLAR}}{RLAR} \right)^2 = \left(\frac{\sum_T LAR_1^2 \left(\frac{\sigma_{D_T^1}}{D_T^1} \right)^2 + LAR_2^2 \left(\frac{\sigma_{D_T^2}}{D_T^2} \right)^2}{\left(\sum_T LAR_T \right)^2} \right)_h + \left(\frac{\sum_T LAR_1^2 \left(\frac{\sigma_{D_T^1}}{D_T^1} \right)^2 + LAR_2^2 \left(\frac{\sigma_{D_T^2}}{D_T^2} \right)^2}{\left(\sum_T LAR_T \right)^2} \right)_p \quad (2-9)$$

where $\left(\frac{\sigma_{D_T^1}}{D_T^1} \right)$ is the relative uncertainty in the therapeutic dose, and $\left(\frac{\sigma_{D_T^2}}{D_T^2} \right)$ is the

relative uncertainty in the stray dose. The subscript *h* denotes proton therapy, and subscript *p* denotes photon therapy. A similar uncertainty analysis was also applied to the calculated risk second cancer in thyroid for one patient in this study, because the dose-risk relationship for thyroid is apparently not linear (Sigurdson *et al* 2005, Ronckers *et al* 2006a, Bhatti *et al* 2010)

As discussed in section 2.6, *NTCP* model parameters specifically for cardiac toxicity for CSI pediatric patients were not available. Considering the potentially large unknown uncertainties in the *NTCP* model parameters, we used different set of parameters to calculate *NTCP* for each heart sub-structure for one patient. More specifically, each *NTCP* parameter was varied over its plausible range (for Lyman

model, $10 \leq D_{50} \leq 100$ Gy, $0.1 \leq n \leq 1$, $0.1 \leq m \leq 1$; for RS model, $10 \leq D_{50} \leq 100$ Gy, $0.1 \leq \gamma \leq 3$, $0.1 \leq s \leq 1$) to test the sensitivity of *RNTCP* to changes in each parameter. In the sensitivity test, the intervals of *NTCP* parameters were chosen to include any parameter values in the literature, so they covered the baseline parameters and the calculation results based on those parameters bounded the real cardiac toxicity risk calculation for CSI patients.

There are large uncertainties in the value of the mean radiation weighting factor values for neutrons. The ICRP Publication 92 (2003) recommended a maximum neutron radiation weighting factor of 20. A recent reanalysis of atomic bomb survivors data deduced that the 95% confidence interval of neutron RBE was 25~400 (Kellerer *et al* 2006). Newhauser *et al* (2009) pointed out that patient's second cancer risk from passively scattered proton therapy will be lower than conformal photon therapy for CSI even if the neutron $\overline{w_R}$ values were increased by a factor of 35. Fontenot *et al* (2010) also concluded that proton therapy conferred lower predicted risks than photon therapy for prostate cancer as long as neutron $\overline{w_R}$ values were less than 100 (scaled by a factor of 5). In this study, the sensitivity test quantified the impact of uncertainty in the $\overline{w_R}$ values by using different scaling factors in both second cancer and cardiac toxicity calculations.

Contouring of heart sub-structures is challenging and may introduce large uncertainties. Imaging methods for the current standards of care for external beam radiation therapy at our institution did not clearly show those sub-structures, and it is hard to differentiate the heart border from the liver and diaphragm. The heart also moves with respiratory and cardiac cycles. The definition of the heart sub-structure is not standardized and the dosimetric impact of the uncertainty in heart contours is not well understood. For those reasons, we varied the thickness of different heart-

substructures to see how sensitive the baseline risk predictions would be to the uncertainties in heart contouring.

3. RESULTS

This chapter describes the results of dose reconstruction for both proton and photon therapies (section 3.1), followed by calculations of risks of second cancer (section 3.2) and cardiac toxicities (section 3.3). The sensitivities of the baseline risk calculations to changes in the key variables were analyzed for second cancer in section 3.4 and cardiac toxicity in section 3.5.

3.1 Therapeutic and stray radiation doses reconstructions

The tables and figures below summarize the therapeutic absorbed dose and stray radiation dose to heart sub-structures from photon and proton CSI.

3.1.1 Evaluation volume coverage for photon versus proton treatment plans

Photon and proton CSI both provided equivalent coverage of the crainospinal axis. This was evaluated by comparing the population-averaged percent volume receiving the prescription dose of 23.4 Gy (RBE) ($V_{23.4}$) for the evaluation volumes for photon and proton CSI. A paired t-test indicated no significant difference in the V_{100} for the two modalities. The maximum dose (D_{\max}) in the evaluation volume was greater for photon than for proton therapy ($p < 0.01$). These results are summarized in Table 3-1 (Howell *et al* 2011).

Table 3-1 Comparison of target coverage and the maximum dose in the target between photon and proton CSI (Howell, personal communication).

Parameter	Photons (Gy(RBE))		Protons (Gy(RBE))		t-test p-value	Level of significance
	Mean	SD	Mean	SD		
$V_{23.4}$	99.36	1.04	99.23	0.88	6.96E-01	NS*
D_{\max}	28.13	15.21	26.05	7.87	1.60 E-05	<0.01

* Not significant.

3.1.2 Dose reconstruction for photon therapy

Figure 3-1 shows the absorbed dose distribution in a representative pediatric patient (patient no. 2, a 4-year-old boy) from therapeutic photon treatment fields. The treatment plan provided adequate coverage of the target: cerebrospinal fluid volume (including brain and spinal canal). However, the exit dose to other parts of the patient body is also high.

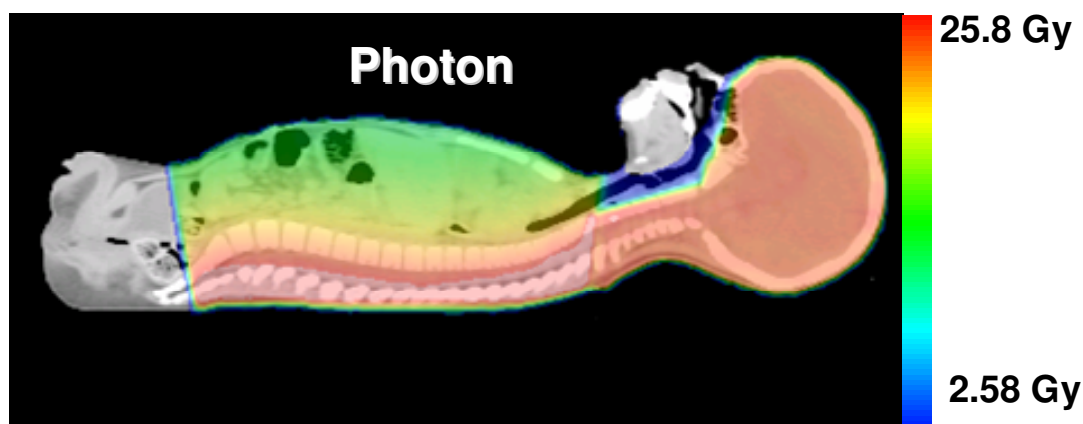


Figure 3-1 Sagittal slice of the photon absorbed dose distribution for a 4-year-old boy from all photon CSI fields.

Table 3-2 lists the absorbed doses (minimum, mean and maximum) to the whole heart and sub-structures from photon therapy for each pediatric patient. For heart sub-structures, the stray photon doses in photon plans were included in the dose exported from TPS in this table, as discussed in section 2.4.2.

Table 3-2 Minimum, maximum and mean absorbed dose from therapeutic radiation to different heart sub-structures resulting from photon therapy for the population of pediatric patients.

Patient index	Patient Age (y)	Patient Sex	Photon absorbed dose (cGy)								
			Whole heart			Pericardium			Myocardium		
			min	max	mean	min	max	mean	min	max	mean
1	2	F	123.7	2163	1425	123.7	2165	1295	131.4	2138	1405
2	4	M	85.7	2112	1231	86.4	2110	1059	90	2090	1172
3	6	F	65.6	2013	893	65.6	2013	887	67.9	1991	868
4	8	F	89.2	2144	1150	89.6	2144	1089	89.6	2144	1018
5	10	F	62.7	2065	1090	60.9	2017	931	62.8	1998	950
6	3	M	108.7	2104	1341	108.6	2095	1261	115.7	2077	1294
7	4	M	81.7	2077	1077	82.7	2068	1053	86.4	2052	1008
8	6	M	65.3	2097	1027	65.4	2096	1036	68.6	2055	964
9	7.6	M	86.4	2953	1256	87.3	2953	1199	91	2918	1191
10	9.4	M	57.6	2012	969	57.6	2012	913	60.2	1980	915
11	12	F	98.2	2032	1166	98.8	2028	1081	102	2008	1089
12	13	F	69.5	2084	1052	69.4	2085	993	72.6	2053	989
13	16	F	48.4	2001	779	48.5	1998	768	51.6	1976	728
14	12	M	76.9	1924	872	77.4	1924	812	79.8	1879	800
15	13	M	96.9	2703	1146	97.6	2709	1108	100.6	2437	1072
16	14	M	67.1	2294	916	51.7	2134	764	52.9	2103	764
17	15	M	51.2	1901	634	51.2	1901	664	54.2	1866	626
18	16	M	57.3	1888	640	57.3	1889	656	59.6	1795	608

Figure 3-2 plots the measured photon stray dose in terms of equivalent dose per therapeutic dose (mSv/Gy) as a function of distance from field edge (cm) (Howell 2011, personal communication), where field edge was defined as the 50% isodose line according to ICRU recommendation (ICRU 1993). Data from the measurement were fit

with a double-Gaussian curve as a function of distance from field edge (Newhauser 2011, personal communication).:

$$H = a[ce^{-\frac{(x-\bar{x}_1)^2}{2\sigma_1^2}} + (1-c)e^{-\frac{(x-\bar{x}_2)^2}{2\sigma_2^2}}] \quad (3-1)$$

where H is the stray equivalent dose (cSv/Gy). The values a , c , \bar{x}_1 , \bar{x}_2 , σ_1 , σ_2 are fitted parameters, and the best fit result is:

$$H = 159.80 \cdot e^{-\frac{(x+3.32)^2}{2(3.37)^2}} + 116.13 \cdot e^{-\frac{(x+2.55)^2}{2(9.66)^2}} \quad (3-2)$$

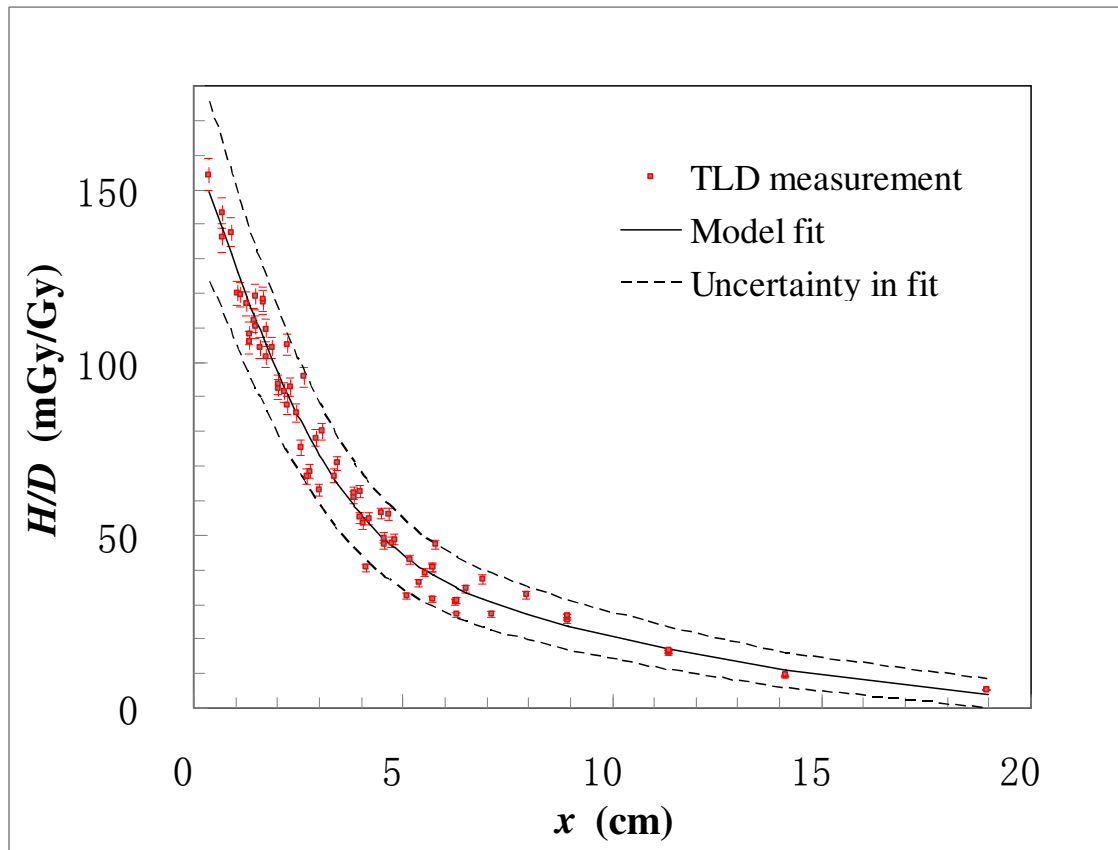


Figure 3-2 Values of stray radiation absorbed dose equivalent per therapeutic absorbed dose (H/D) as a function of distance from field edge (x). Measured data were taken from Howell *et al* (personal communication). The dashed lines are 95% confidence interval of fitting result (Newhauser 2011, personal communication).

3.1.3 Dose reconstruction for proton therapy

Figure 3-3 shows the proton therapeutic absorbed dose distribution for a representative pediatric patient. The treatment plan provided adequate coverage of the age-specific treatment target.

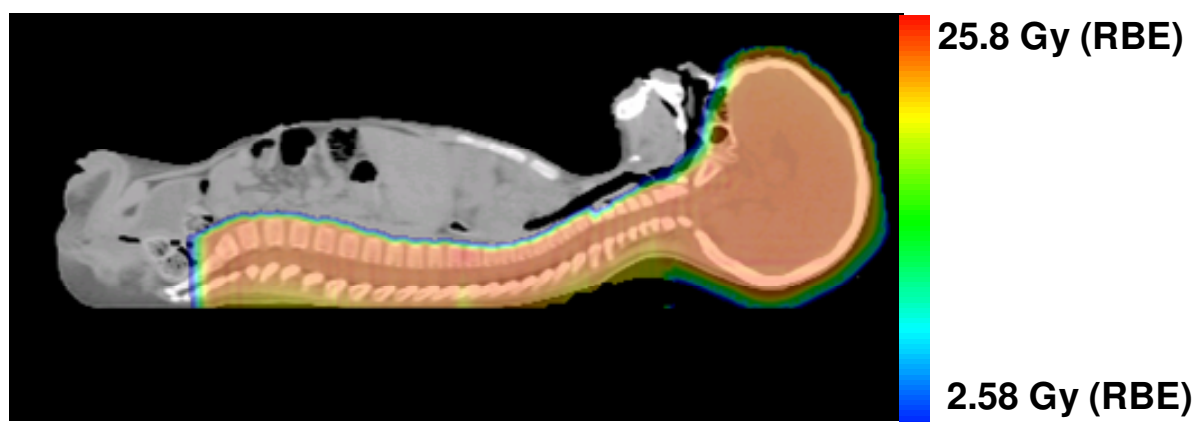


Figure 3-3 Sagittal slice of the proton absorbed dose distribution for a 4-year-old boy from all proton CSI fields.

Table 3-3 lists the therapeutic absorbed dose statistics (minimum, mean, and maximum) to the whole heart and sub-structures resulting from proton therapy for the population of pediatric patients. Note very low doses to the heart from proton CSI for patient index 13, 15, 17, 18 (ages are 16, 13, 15, 16). The proton target volume only included spinal axis for patients older than 15, whereas for all other patients the proton target volume was more anterior because it was designed to cover the entire vertebral body. Patient no. 15, who is a 13-year-old boy, also did not have his whole vertebral body covered because of his large stature.

Table 3-3 Minimum, maximum and mean absorbed doses from therapeutic radiation to different heart structures resulting from proton therapy for the population of pediatric patients.

Patient index	Patient Age (y)	Patient Sex	Proton therapeutic dose (cGy (RBE))								
			Whole heart			Pericardium			Myocardium		
			min	max	mean	min	max	mean	min	max	mean
1	2	F	0	1157	3.9	0	1127	13.2	0	434	1.2
2	4	M	0	3001	21.1	0	2949	60.6	0	2419	13.5
3	6	F	0	1995	12.5	0	1987	30.9	0	1784	8.8
4	8	F	0	2240	32.5	0	2238	85.3	0	2241	44.4
5	10	F	0	2127	39.4	0	2126	95.7	0	1961	30.8
6	3	M	0	1740	61.6	0	1714	109.5	0	1651	51.7
7	4	M	0	2047	32.1	0	2047	74.9	0	1978	24.3
8	6	M	0	1597	8.7	0	1560	21.4	0	1303	5.9
9	7.6	M	0	1873	31.1	0	1873	84.6	0	1596	21.9
10	9.4	M	0	953	4.9	0	953	15.5	0	665	3
11	12	F	0	1916	15.4	0	1874	43.2	0	1226	10.9
12	13	F	0	2184	14.4	0	2184	44.4	0	1982	8.8
13	16	F	0	249	0.2	0	237	0.6	0	76	0.2
14	12	M	0	1621	16.6	0	1620	41	0	1375	15.9
15	13	M	0	0	0.1	0	0	0.1	0	0	0.1
16	14	M	0	2520	39.7	0	2520	126.3	0	2501	34.1
17	15	M	0	259	0.3	0	259	1.1	0	123	0.2
18	16	M	0	0	0.1	0	0	0.1	0	0	0.1

Figure 3-4 shows the stray neutron equivalent dose distribution to a pediatric patient from proton CSI. Although the stray neutron equivalent dose is much lower in magnitude compared to the therapeutic proton dose, it penetrated the whole body of the patient and was not negligible.

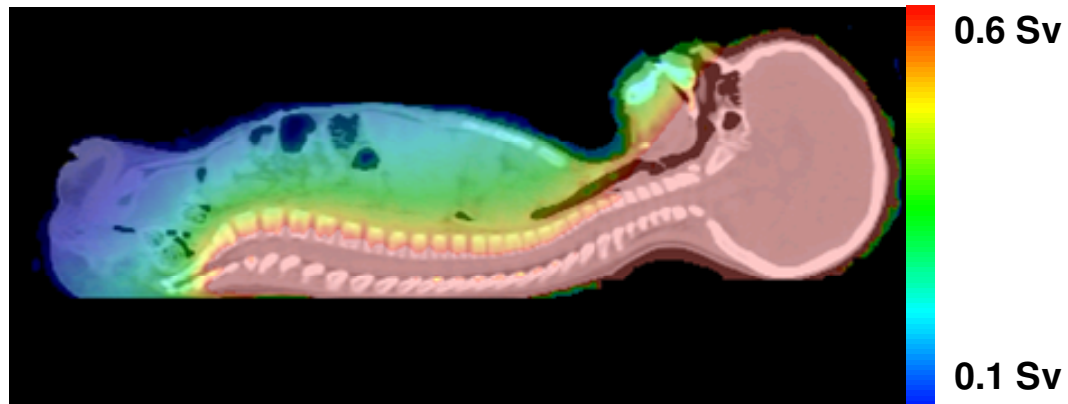


Figure 3-4 Sagittal slice of the stray neutron equivalent dose (from external and internal neutrons from all fields) distribution generated during proton CSI for a 4-year-old boy.

Table 3-4 lists mean stray neutron dose to the whole heart and sub-structures from proton therapy, and Figure 3-5 shows the stray neutron dose to heart sub-structures as a function of patient's age. The stray neutron dose to older patients were slightly higher than those to younger patients, and there were strong and significant correlation between stray neutron dose and patients' age at exposure (whole heart, correlation coefficient $r = 0.55$, $p = 0.018$, pericardium, $r = 0.57$, $p = 0.014$, myocardium, $r = 0.56$, $p = 0.016$). The possible reason for higher stray equivalent neutron doses to older patients was that older patients have longer spine, so more spinal fields (typically 3) were used for older patients *versus* 1 or 2 spinal fields used for younger patients.

Table 3-4 Mean stray neutron equivalent dose (H) in the whole heart and sub-structures of each patient from proton CSI.

Patient Index	Patient Age (y)	Patient Sex	H (mSv)		
			Whole heart	Pericardium	Myocardium
1	2	F	235.5	238.1	234.8
2	4	M	259.9	261.0	259.7
3	6	F	244.6	249.8	244.0
4	8	F	206.4	244.4	217.7
5	10	F	298.3	304.2	297.7
6	3	M	231.6	233.4	231.3
7	4	M	242.3	245.5	240.9
8	6	M	276.8	281.5	275.3
9	7.6	M	228.7	252.9	225.9
10	9.4	M	262.7	265.9	261.7
11	12	F	254.7	259.2	254.0
12	13	F	401.6	415.1	397.1
13	16	F	262.8	267.4	262.8
14	12	M	375.2	387.9	375.0
15	13	M	238.9	241.2	239.6
16	14	M	376.8	386.1	374.6
17	15	M	289.9	297.3	288.9
18	16	M	324.9	336.9	323.8

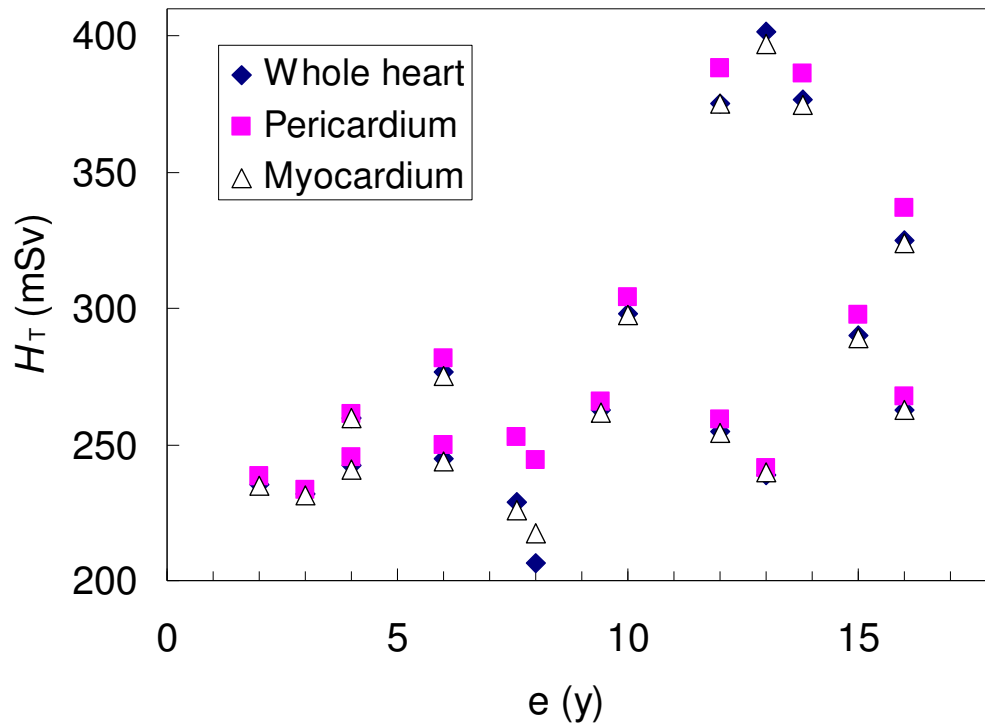


Figure 3-5 Stray neutron equivalent dose H_T to the whole heart and sub-structures from proton therapy as a function of patient age at exposure, e .

We compared the stray neutron dose generated by proton CSI to those from photon dose in photon CSI (Figure 3-6). Close to the field edge, the stray neutron dose from proton CSI is much lower than the stray photon dose from photon CSI. Further away from field edge, the difference between stray neutron dose and stray photon dose became smaller. This difference in stray dose from proton *versus* photon CSI was indistinguishable beyond 14 cm distance.

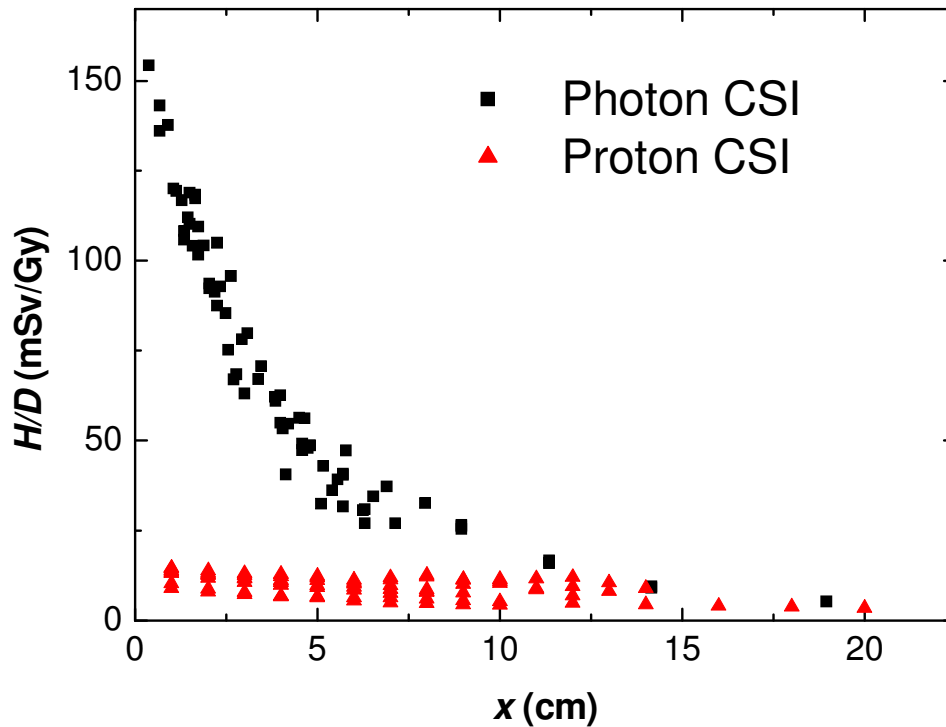


Figure 3-6 Comparison of stray equivalent dose per therapeutic absorbed dose, H/D , as a function of distance from field edge, x , between photon and proton CSI. Measured photon stray dose data were taken from Howell *et al* (in preparation). Stray equivalent dose data from proton CSI were from this study.

Overall, the proton treatment plans provided a significant reduction in exit dose to normal tissues distal to the target compared to the photon plans (see Figure 3-1 and Figure 3-3). Figure 3-7 plots DVHs for therapeutic dose from photon and proton CSI plans (Howell *et al* 2011). Both plans provided good coverage to the treatment target, and the superior normal tissue sparing of the proton treatment plan is evident in this figure.

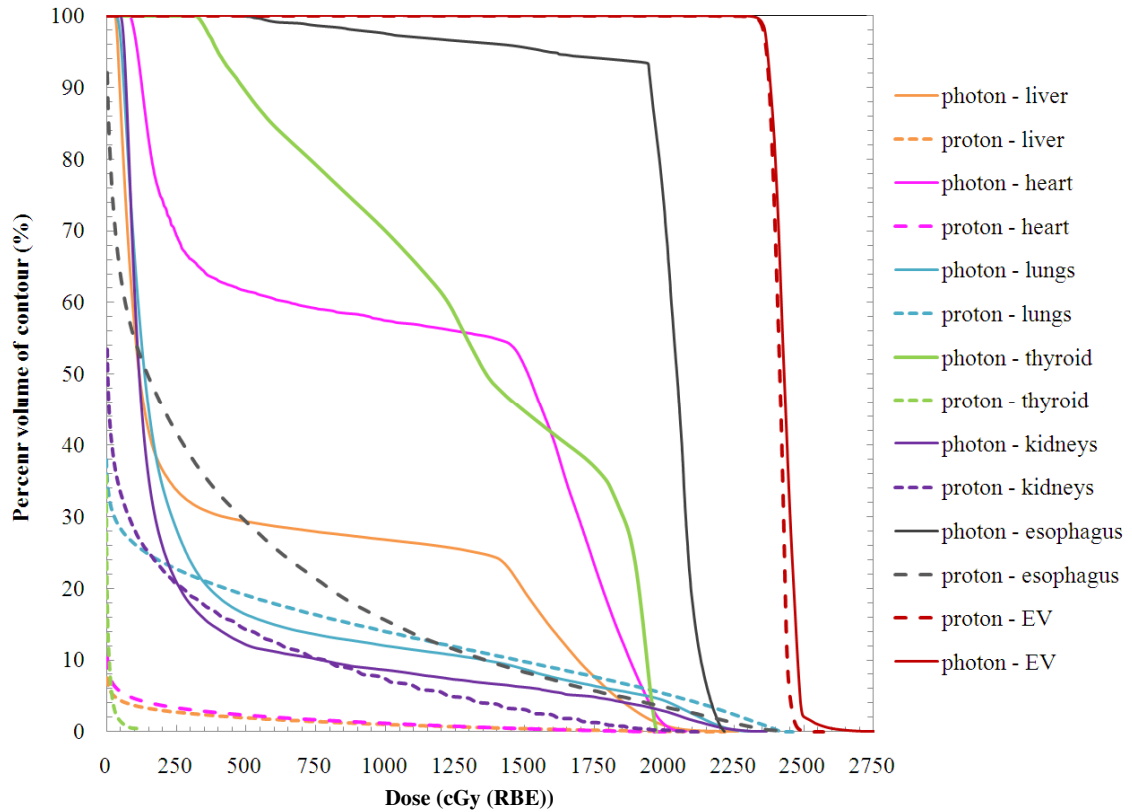


Figure 3-7 Cumulative DVHs from the treatment plans for a 4-year-old boy (patient No. 2) Proton and photon DVHs are indicated by dashed and solid lines, respectively, for various organs (This figure was from Howell, personal communication).

The dose to the heart (Figure 3-8) from both proton and photon CSI plans are shown here as an illustrative comparison. This figure clearly demonstrates that photon CSI resulted in much higher doses to the heart compared to proton CSI.

The mean therapeutic doses to whole heart, pericardium, and myocardium for this population of patients received proton CSI were 185.9, 471.3 and 153.2 mGy (RBE); and were 10370, 9760 and 9700 mGy from photon CSI.

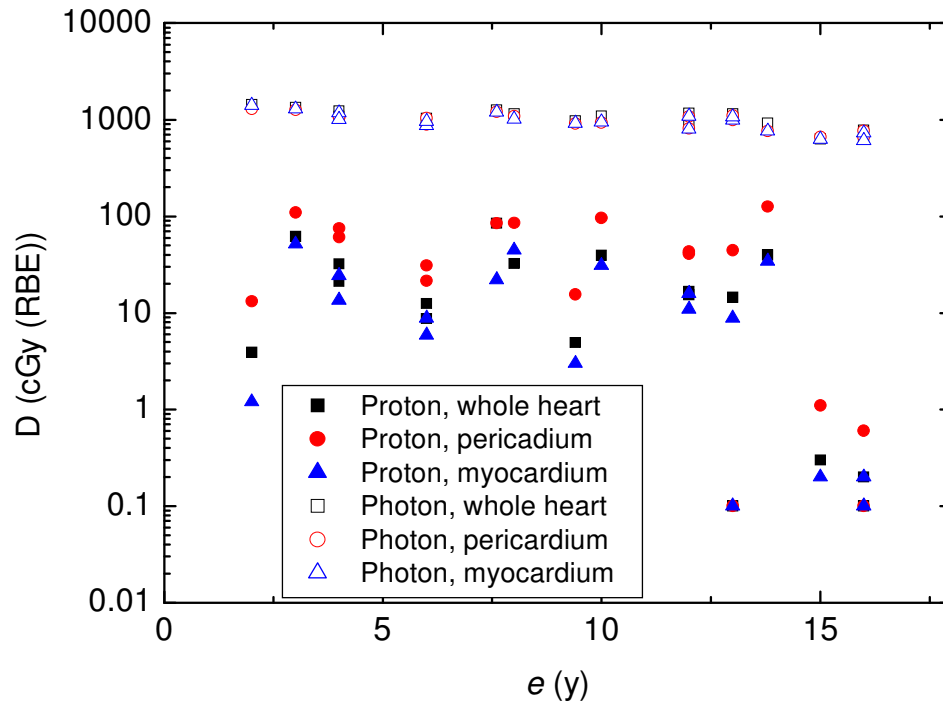


Figure 3-8 Absorbed dose, D , to the whole heart and sub-structures for proton and photon CSI plans as a function of patient's age at exposure, e .

The equivalent total dose (sum of therapeutic dose and stray dose) ratio between proton CSI and photon CSI was plotted in Figure 3-9, and there was no correlation between dose ratio and patient age (whole heart, $r = 0.18$; pericardium, $r = 0.009$; myocardium, $r = 0.28$). Table 3-5, Table 3-6 and Table 3-7 list the mean, standard deviation (SD), SD of the mean, median, minimum, and maximum of dose (sum of therapeutic absorbed dose and stray equivalent dose) to the whole heart, pericardium and myocardium of the sample patients.

Table 3-5 The mean, standard deviation (SD), SD of the mean, median, minimum, and maximum equivalent dose (sum of therapeutic dose and stray dose) to the whole heart of the sample patients.

Statistical	Whole heart		
Parameter	D_{proton} (cGy)(RBE)	D_{photon} (cGy)	$D_{\text{proton}}/D_{\text{photon}}$
Mean	4.64E+01	1.04E+03	4.56E-02
Standard Deviation	1.79E+01	2.21E+02	1.61E-02
Median	4.40E+01	1.06E+03	4.46E-02
SD of the mean	4.23E+00	5.21E+01	3.80E-03
Minimum	2.40E+01	6.34E+02	1.93E-02
Maximum	8.48E+01	1.42E+03	8.44E-02
n	18	18	18

Table 3-6 The mean, standard deviation (SD), SD of the mean, median, minimum, and maximum of equivalent dose (sum of therapeutic dose and stray dose) to the pericardium of the sample patients.

Statistical	Pericardium		
Parameter	D_{proton} (cGy)(RBE)	D_{photon} (cGy)	$D_{\text{proton}}/D_{\text{photon}}$
Mean	7.58E+01	9.76E+02	7.86E-02
Standard Deviation	4.16E+01	1.91E+02	4.60E-02
Median	7.45E+01	1.01E+03	7.29E-02
SD of the mean	9.80E+00	4.50E+01	1.08E-02
Minimum	2.42E+01	6.56E+02	2.19E-02

Maximum	1.65E+02	1.29E+03	2.16E-01
n	18	18	18

Table 3-7 The mean, standard deviation (SD), SD of the mean, median, minimum, and maximum of equivalent dose (sum of therapeutic dose and stray dose) to the myocardium of the sample patients.

Statistical	Myocardium		
Parameter	D_{proton} (cGy)(RBE)	D_{photon} (cGy)	$D_{\text{proton}}/D_{\text{photon}}$
Mean	4.31E+01	9.70E+02	4.61E-02
Standard Deviation	1.64E+01	2.18E+02	1.85E-02
Median	3.79E+01	9.76E+02	4.24E-02
SD of the mean	3.86E+00	5.13E+01	4.36E-03
Minimum	2.41E+01	6.08E+02	1.76E-02
Maximum	7.48E+01	1.40E+03	9.37E-02
n	18	18	18

The mean equivalent dose ratio values were 0.0456, 0.0786 and 0.0461 for whole heart, pericardium and myocardium, respectively. A t test was performed to determine if the mean of the total dose ratio values were significantly less than 1, and the test results revealed that the proton CSI delivered significantly lower dose to whole heart, pericardium and myocardium than did photon CSI (Figure 3-10).

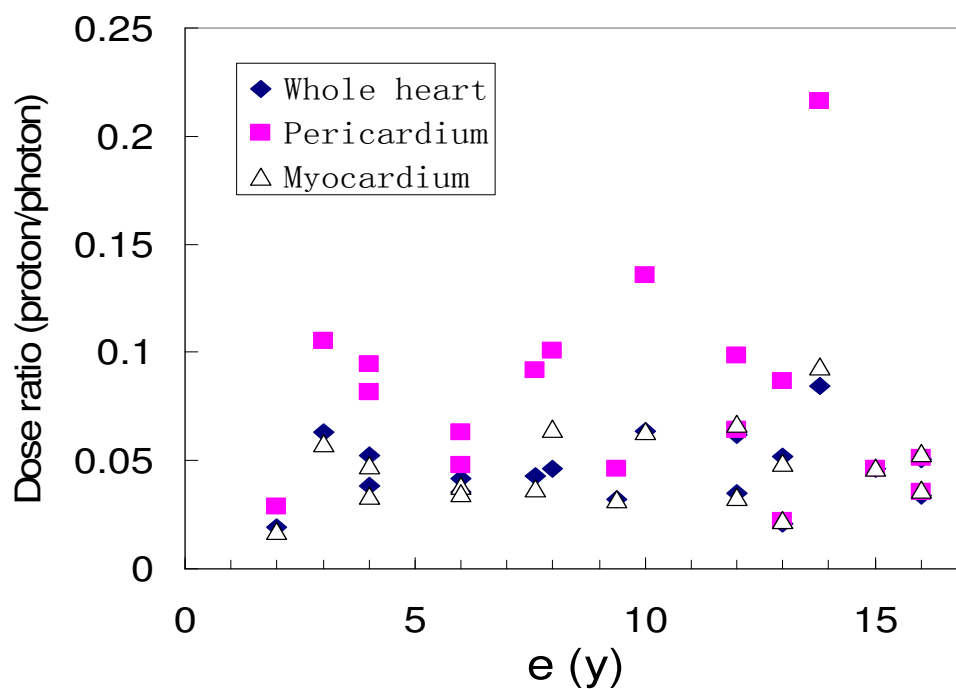


Figure 3-9 Dose (therapeutic dose + stray dose) ratio (proton/photon) for the heart substructures as a function of patient age at exposure, e .

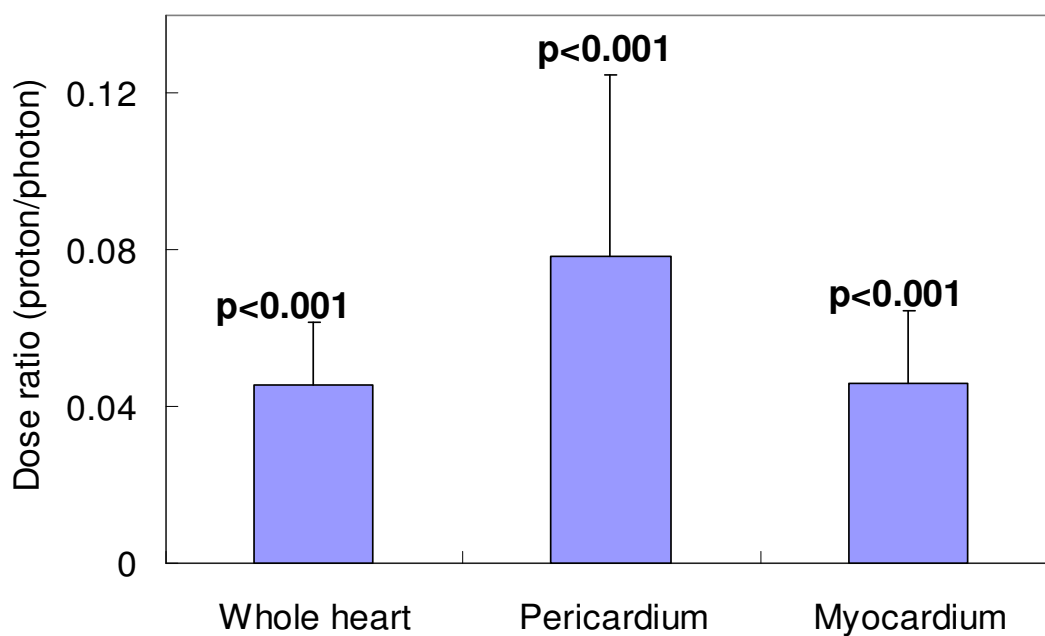


Figure 3-10 The population-average dose ratio values. The error bars represent the standard deviation for each group of data, *e.g.*, whole heart, pericardium and myocardium.

The equivalent dose to the thyroid (Figure 3-11) from both proton and photon CSI plans are also shown here. It is readily apparent that the photon therapy delivered much higher doses to the thyroid compared to proton therapy.

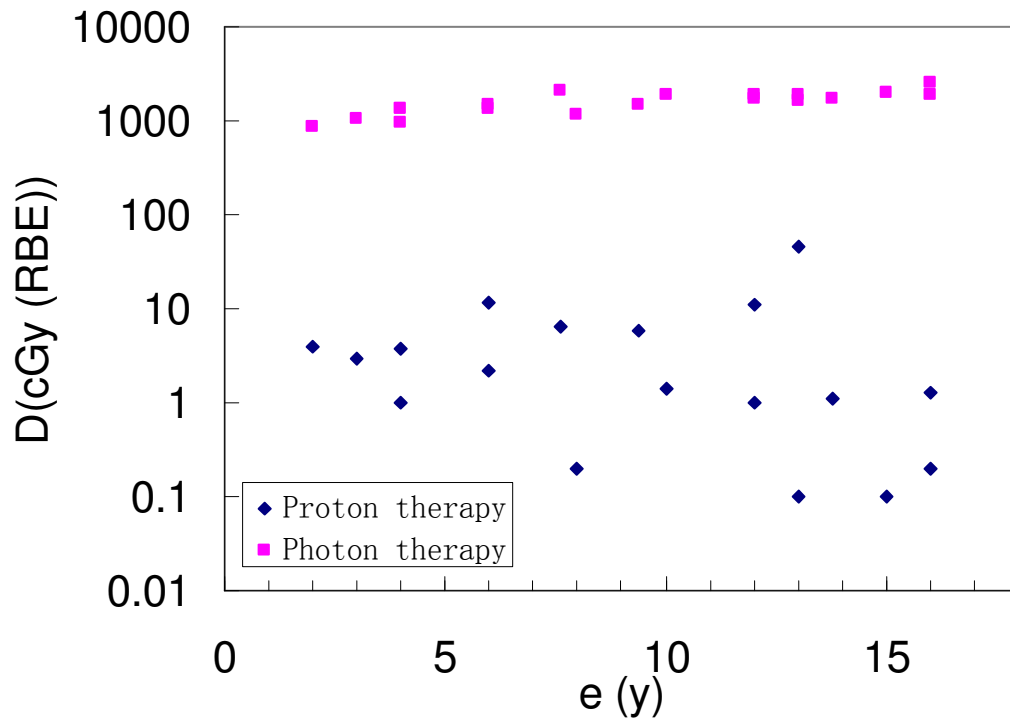


Figure 3-11 Equivalent Dose (D) to the thyroid for both proton and photon plans, as a function of patient's age at exposure, e .

3.2 Predicted risk of radiogenic second cancer

A 4-year-old boy was chosen for risk calculations of radiogenic second cancers to facilitate comparison with previous investigations by Miralbell *et al* (2002) and Newhauser *et al* (2009). Table 3-8 lists mean organ equivalent doses from proton and photon radiation treatment plans for a 4-year-old boy (patient index no. 2). For proton

CSI, therapeutic and stray equivalent doses are listed, and total equivalent doses are also listed. For photon CSI, the total equivalent dose values are listed. The equivalent dose to the remainder, which includes any organ for which risk coefficients were not explicitly provided by the BEIR VII report, was estimated as the mean equivalent dose for the other organs listed in Table 3-8.

Table 3-8 Mean organ equivalent doses from proton and photon CSI plans for a 4-year-old boy. For proton CSI, both therapeutic and stray doses were listed, and a summation of them was also listed. For photon CSI, the combined dose from both therapeutic and stray doses was listed.

Organs	$H_{T, \text{Proton}}$ (mSv)			$H_{T, \text{Photon}}$ (mSv)	$H_{T, \text{Proton, total}} / H_{T, \text{Photon, total}}$
	Therapeutic	Stray	Total	Total	
Gonads	1	159	160	1662	0.096
Colon	165	209	374	6415	0.058
Lungs	248	329	577	4413	0.131
Stomach	673	289	962	4076	0.236
Bladder	5	170	175	3127	0.056
Liver	171	249	420	5493	0.076
Thyroid	6	383	389	10854	0.036
Remainder	181	255	437	5149	0.085

The therapeutic and stray doses in Table 3-8 were used to estimate organ-specific radiogenic second cancer risks for this boy. Specifically, the baseline values of relative risk are listed in Table 3-9, and they were calculated by using a linear non-threshold (LNT) dose-risk model from the BEIR VII report (NRC 2006) and the neutron radiation weighting factors based on data from Newhauser *et al* (2009).

Table 3-9 Baseline calculations of relative risk of radiogenic second cancer for a 4-year-old boy in each organ (RR_T), and ratio of relative risk ($RRR = RR_{\text{proton}}/RR_{\text{photon}}$) following photon and proton therapies at 15, 30, 45, 60, 75 and 95 years after treatment.

	15 years			30 years			45 years		
Organs	RR_T Proton	RR_T Photon	$RR_{proton}/$ RR_{photon}	RR_T Proton	RR_T Photon	$RR_{proton}/$ RR_{photon}	RR_T Proton	RR_T Photon	$RR_{proton}/$ RR_{photon}
Stomach	3.204	10.340	0.310	1.976	5.136	0.385	1.585	3.479	0.456
Colon	3.571	45.101	0.079	2.138	20.527	0.104	1.682	12.706	0.132
Liver	2.467	20.181	0.122	1.649	9.493	0.174	1.389	6.092	0.228
Lung	3.015	16.410	0.184	1.892	7.823	0.242	1.535	5.090	0.302
Prostate	1.210	3.176	0.381	1.093	1.964	0.557	1.056	1.578	0.669
Bladder	1.955	18.061	0.108	1.423	8.554	0.166	1.253	5.529	0.227
Thyroid	2.784	50.782	0.055	2.784	50.782	0.055	2.784	50.782	0.055
Other	7.440	76.878	0.096	2.263	15.876	0.142	1.454	6.347	0.229

	60 years			75 years			95 years		
Organs	RR_T Proton	RR_T Photon	$RR_{proton}/$ RR_{photon}	RR_T Proton	RR_T Photon	$RR_{proton}/$ RR_{photon}	RR_T Proton	RR_T Photon	$RR_{proton}/$ RR_{photon}
Stomach	1.403	2.706	0.518	1.300	2.270	0.573	1.219	1.926	0.633
Colon	1.470	9.055	0.162	1.350	6.998	0.193	1.255	5.373	0.234
Liver	1.268	4.503	0.282	1.199	3.609	0.332	1.145	2.902	0.395
Lung	1.368	3.814	0.359	1.274	3.096	0.412	1.200	2.528	0.475
Prostate	1.038	1.397	0.743	1.028	1.296	0.794	1.021	1.216	0.840
Bladder	1.174	4.116	0.285	1.130	3.320	0.340	1.095	2.692	0.407
Thyroid	2.784	50.782	0.055	2.784	50.782	0.055	2.784	50.782	0.055
Other	1.215	3.531	0.344	1.119	2.404	0.466	1.063	1.746	0.609

The calculated *RRR* values were always much less than 1 at 15, 30, 45 and 60 years after exposure. The *RRR* values increased with attained age. All predicted baseline *RRR* values were less than 1, indicating a lower risk of second cancer following proton CSI compared to photon CSI.

LAR coefficients were used to calculate the cumulative risk of radiogenic second cancer incidence of this patient at an attained age of 100 years (exposed at 4 years). The cumulative lifetime risk of second cancer following proton CSI was estimated at 7.7%, while the risk following photon CSI was 92.0%. The ratio of risks from proton and photon therapies is 0.083 (95% confidence interval is 0.081-0.085). The cumulative lifetime risk of second cancer incidence following proton therapy is 4.5% from therapeutic radiation and 6.1% from stray radiation. (Due to the

methodology used to calculate photon absorbed dose, it was not possible to separate therapeutic dose from stray dose in photon CSI).

3.3 Predicted risk of cardiac toxicity

Figure 3-12 shows the therapeutic dose distributions to the heart from photon and proton treatment plans for a 4-year-old boy (patient index No.2). Obviously, the primary proton beams provided much lower dose to the heart. Taking the secondary neutron dose from proton therapy into account, the mean organ doses to the whole heart and sub-structures were listed in Table 3-10. Again, the proton therapy plan provided much lower mean radiation dose to the heart.

DVHs for heart sub-structures for this patient were exported from TPS and Figure 3-13 shows differential DVHs for photon and proton plans. For the photon plans, the DVHs were obtained from TPS directly; for the proton plans, the DVHs for primary dose were obtained from TPS, then a mean neutron equivalent dose was added uniformly to the primary DVH assuming the secondary neutron dose is uniformly distributed. Again, the photon plan delivered higher dose to the heart sub-structures compared to the proton plan.

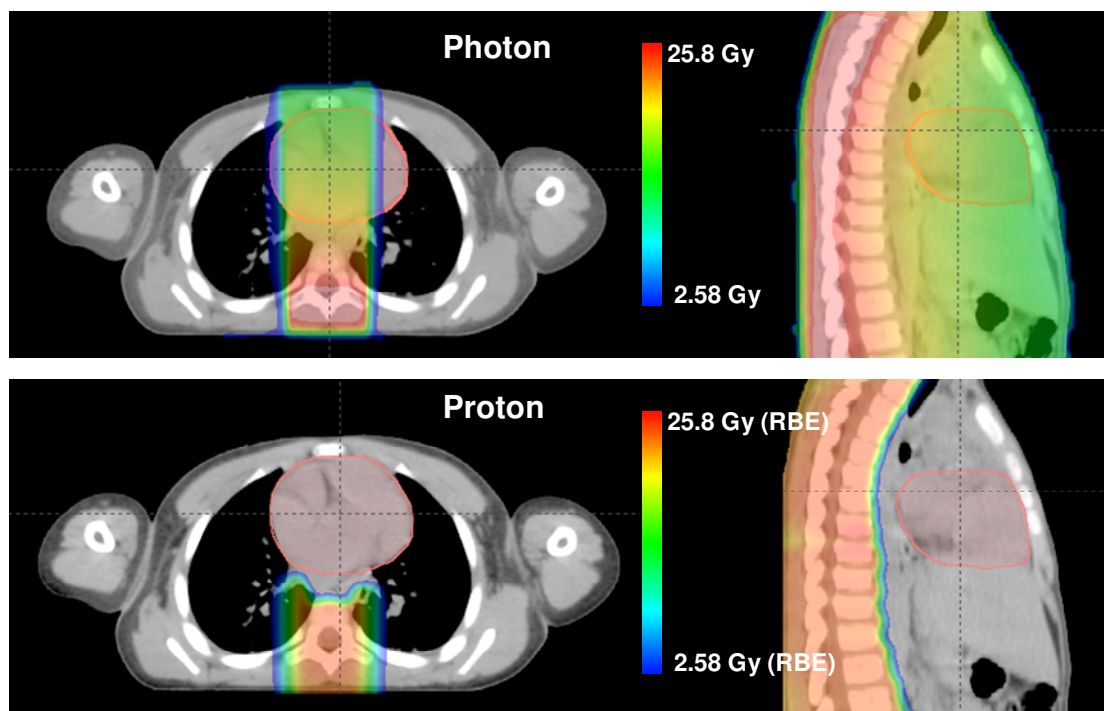


Figure 3-12 Axial (left) and sagittal (right) slices of absorbed dose distribution from the photon plan (top) and the proton plan (bottom) for a 4-year-old boy receiving CSI.

Table 3-10 Mean organ equivalent dose to heart sub-structures from proton and photon plans for a 4-year-old boy receiving CSI.

Organ	Proton therapy dose			Photon H_T (Sv)	Dose ratio (proton/photon)
	D_T (Gy (RBE))	H_T (Sv)	Total (Sv)		
Pericardium	0.61	0.26	0.87	10.59	0.08
Myocardium	0.14	0.26	0.40	11.72	0.03
Whole heart	0.21	0.26	0.47	12.31	0.04

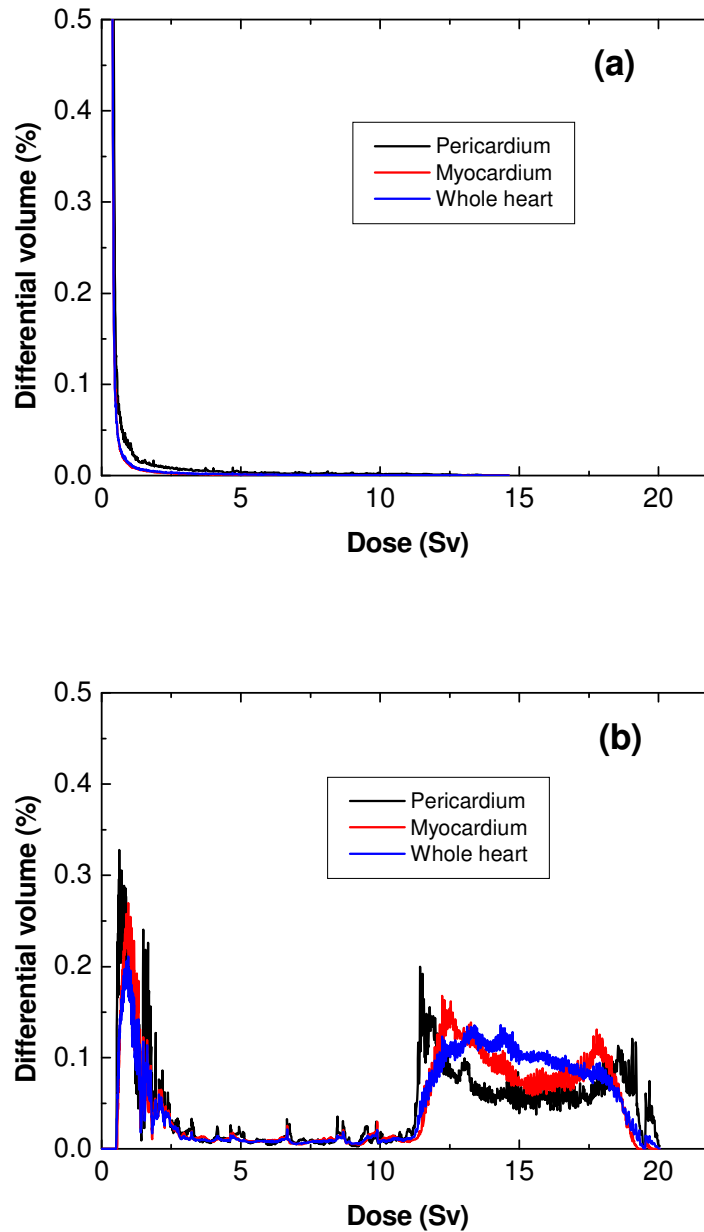


Figure 3-13 Differential DVHs of heart sub-structures from (a) proton (b) and photon CSI treatment plans (therapeutic + stray radiation doses) for a 4-year-old boy.

Table 3-11 lists the calculated *NTCP* values of the whole heart and its sub-structures for this patient based on DVHs from photon and proton plans and baseline *NTCP* model parameters listed in Table 2-2. The predicted *RNTCP* values were always

much less than one regardless of the parameter sets used, which suggests that proton CSI would deliver a much lower risk of cardiac toxicity compared to photon therapy.

Table 3-11 *NTCP* values for heart sub-structures and relative *NTCP* (*RNTCP*) values based on existing model parameters.

	D_{50} (Gy)	n	m	γ	s	$NTCP_{\text{Proton}}$ (%)	$NTCP_{\text{Photon}}$ (%)	$RNTCP$
Pericardium	48	0.35	0.1	-	-	0	4.66×10^{-12}	0
Pericardium	50.6	0.64	0.13	-	-	2.98×10^{-12}	4.67×10^{-8}	6.38×10^{-5}
Pericardium	49.2	-	-	3	0.2	0	0	N/A
Myocardium	52.2	-	-	1.25	0.87	9.63×10^{-7}	0.032	3.01×10^{-5}
Whole heart	52.3	-	-	1.28	1	2.00×10^{-5}	0.025	8.00×10^{-4}
Whole heart	63.3	-	-	0.93	1	0.022	0.58	0.0383
Whole heart	70.3	-	-	0.96	1	0.00107	0.31	0.0345

Predicted *NTCP* values for the population of patients are listed in Table 3-12, where the following *NTCP* parameters were used: pericardium, $D_{50} = 50.6$ Gy, $n = 0.64$ and $m = 0.13$; myocardium, $D_{50} = 52.2$ Gy, $\gamma = 1.25$ and $s = 0.87$; for the whole heart the average of 3 sets of parameters were used: $D_{50} = 62$ Gy, $\gamma = 1.06$ and $s = 1$.

Table 3-12 Predicted *NTCP* values for the whole heart, pericardium and myocardium following proton and photon therapies for a population of pediatric patients ($n = 18$). $RNTCP = NTCP_{\text{proton}}/NTCP_{\text{photon}}$.

Index	Age	Sex	Proton <i>NTCP</i> (%)			Photon <i>NTCP</i> (%)			<i>RNTCP</i>		
			Whole heart	Pericardium	Myocardium	Whole heart	Pericardium	Myocardium	Whole heart	Pericardium	Myocardium
1	2	F	5.06E-04	1.19E-12	1.39E-07	2.04E-01	2.74E-07	4.80E-02	2.48E-03	4.34E-06	2.90E-06
2	4	M	7.82E-04	2.96E-12	7.64E-07	1.52E-01	4.67E-08	3.17E-02	5.14E-03	6.34E-05	2.41E-05
3	6	F	9.09E-04	2.15E-12	5.49E-06	8.55E-02	1.28E-08	1.44E-02	1.06E-02	1.68E-04	3.81E-04
4	8	F	1.90E-03	5.63E-12	1.85E-04	1.36E-01	3.46E-08	2.72E-02	1.40E-02	1.63E-04	6.80E-03
5	10	F	2.00E-03	6.36E-12	3.11E-05	1.13E-01	1.75E-08	1.67E-02	1.77E-02	3.63E-04	1.86E-03
6	3	M	1.90E-02	6.22E-12	2.94E-05	1.88E-01	2.40E-07	4.20E-02	1.01E-01	2.59E-05	7.00E-04

7	4	M	2.00E-03	5.10E-12	3.91E-05	1.26E-01	5.32E-08	2.36E-02	1.59E-02	9.59E-05	1.66E-03
8	6	M	5.98E-04	1.60E-12	4.23E-07	1.22E-01	5.15E-08	2.25E-02	4.90E-03	3.11E-05	1.88E-05
9	8	M	1.02E-03	4.47E-12	2.78E-06	4.28E-01	4.38E-07	2.33E-01	2.38E-03	1.02E-05	1.19E-05
10	10	M	5.13E-04	1.27E-12	1.52E-07	9.60E-02	1.57E-08	1.63E-02	5.34E-03	8.09E-05	9.33E-06
11	12	F	6.53E-04	2.20E-12	3.11E-07	1.24E-01	5.17E-08	2.20E-02	5.27E-03	4.26E-05	1.41E-05
12	13	F	1.20E-03	3.23E-12	7.88E-06	1.21E-01	3.26E-08	2.30E-02	9.92E-03	9.91E-05	3.43E-04
13	16	F	4.97E-04	1.01E-12	1.43E-07	6.01E-02	4.32E-09	8.50E-03	8.27E-03	2.34E-04	1.68E-05
14	12	M	7.21E-04	2.42E-12	1.31E-06	5.27E-02	4.39E-09	5.67E-03	1.37E-02	5.51E-04	2.31E-04
15	13	M	4.06E-04	9.33E-13	1.11E-07	1.40E-01	1.05E-07	2.76E-02	2.90E-03	8.89E-06	4.02E-06
16	14	M	6.87E-03	1.69E-11	7.52E-04	1.11E-01	5.19E-09	1.38E-02	6.19E-02	3.26E-03	5.45E-02
17	15	M	5.05E-04	1.05E-12	1.48E-07	3.79E-02	1.51E-09	4.40E-03	1.33E-02	6.95E-04	3.36E-05
18	16	M	4.37E-04	1.04E-12	1.28E-07	2.67E-02	1.02E-09	2.24E-03	1.64E-02	1.02E-03	5.71E-05

Table 3-13, Table 3-14 and Table 3-15 list the mean, standard deviation (SD), SD of the mean, median, minimum, maximum of predicted *NTCP* values for the whole heart, pericardium and myocardium, respectively, of the sample of patients.

Table 3-13 The mean, standard deviation (SD), SD of the mean, median, minimum, maximum of *NTCP* values for the whole heart of the sample of patients.

Statistical Parameter	Whole heart		
	$NTCP_{\text{proton}}$ (%)	$NTCP_{\text{photon}}$ (%)	$RNTCP$
Mean	2.25E-03	1.29E-01	1.73E-02
Standard Deviation	4.44E-03	8.82E-02	2.48E-02
Median	7.52E-04	1.22E-01	1.03E-02
SD of the mean	1.05E-03	2.08E-02	5.85E-03
Minimum	4.06E-04	2.67E-02	2.38E-03
Maximum	1.90E-02	4.28E-01	1.01E-01
n	18	18	18

Table 3-14 The mean, standard deviation (SD), SD of the mean, median, minimum, maximum of *NTCP* values for the pericardium of the sample of patients.

Statistical	Pericardium		
Parameter	<i>NTCP</i> _{proton} (%)	<i>NTCP</i> _{photon} (%)	<i>RNTCP</i>
Mean	3.65E-12	7.72E-08	3.84E-04
Standard Deviation	3.81E-12	1.19E-07	7.69E-04
Median	2.31E-12	3.36E-08	9.75E-05
SD of the mean	8.98E-13	2.81E-08	1.81E-04
Minimum	9.33E-13	1.02E-09	4.34E-06
Maximum	1.69E-11	4.38E-07	3.26E-03
n	18	18	18

Table 3-15 The mean, standard deviation (SD), SD of the mean, median, minimum, maximum of *NTCP* values for the myocardium of the sample of patients.

Statistical	Myocardium		
Parameter	<i>NTCP</i> _{proton} (%)	<i>NTCP</i> _{photon} (%)	<i>RNTCP</i>
Mean	5.87E-05	3.24E-02	3.70E-03
Standard Deviation	1.78E-04	5.15E-02	1.28E-02
Median	1.04E-06	2.23E-02	4.54E-05
SD of the mean	4.21E-05	1.21E-02	3.01E-03
Minimum	1.11E-07	2.24E-03	2.90E-06
Maximum	7.52E-04	2.33E-01	5.45E-02

n	18	18	18
---	----	----	----

Figure 3-14 shows the *RNTCP* values for the population of patients as a function of age at exposure. Figure 3-15 plots the predicted *RNTCP* values for males and females separately to check if there is any sex-dependency. The *RNTCP* values were much less than one, regardless of patient's age and sex. There was no significant association between predicated *RNTCP* values and age at exposure (whole heart, correlation coefficient $r = 0.14$, $p = 0.59$, pericardium, $r = 0.43$, $p = 0.07$, myocardium, $r = 0.21$, $p = 0.40$), and the *RNTCP* values were independent of sex (t test for equal means: whole heart, $p = 0.34$, pericardium, $p = 0.41$, myocardium, $p = 0.55$; Wilcoxon rank sum test for equal medians: whole heart, $p = 0.86$, pericardium, $p = 0.66$, myocardium, $p = 0.60$).

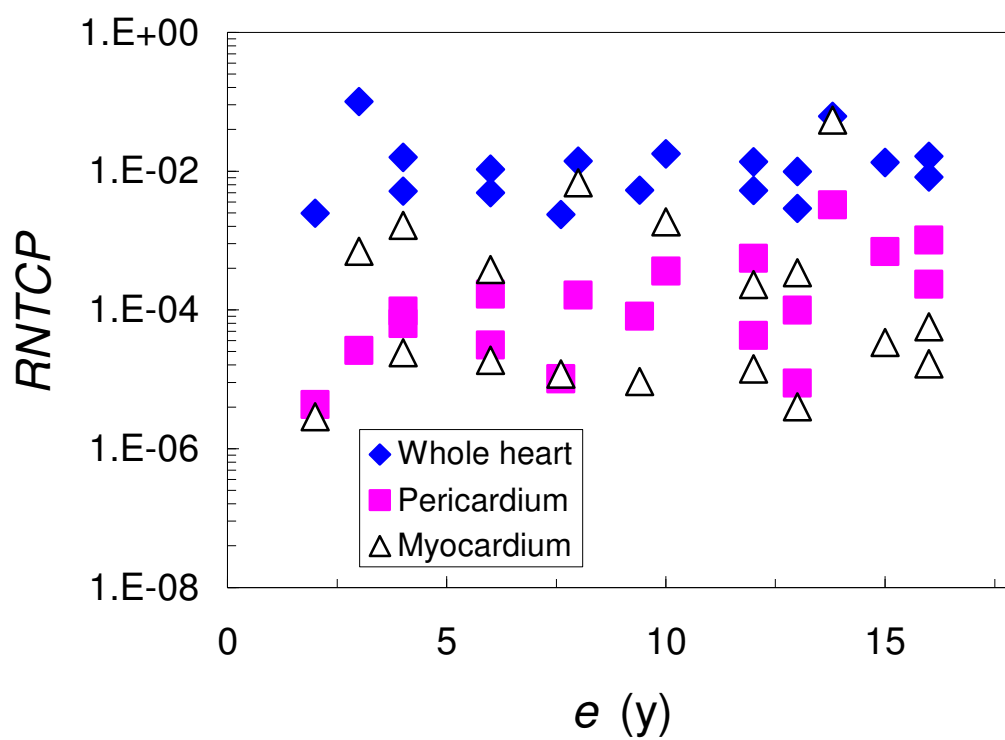


Figure 3-14 Predicted $RNTCP$ values for a population of patients as a function of patient's age at exposure.

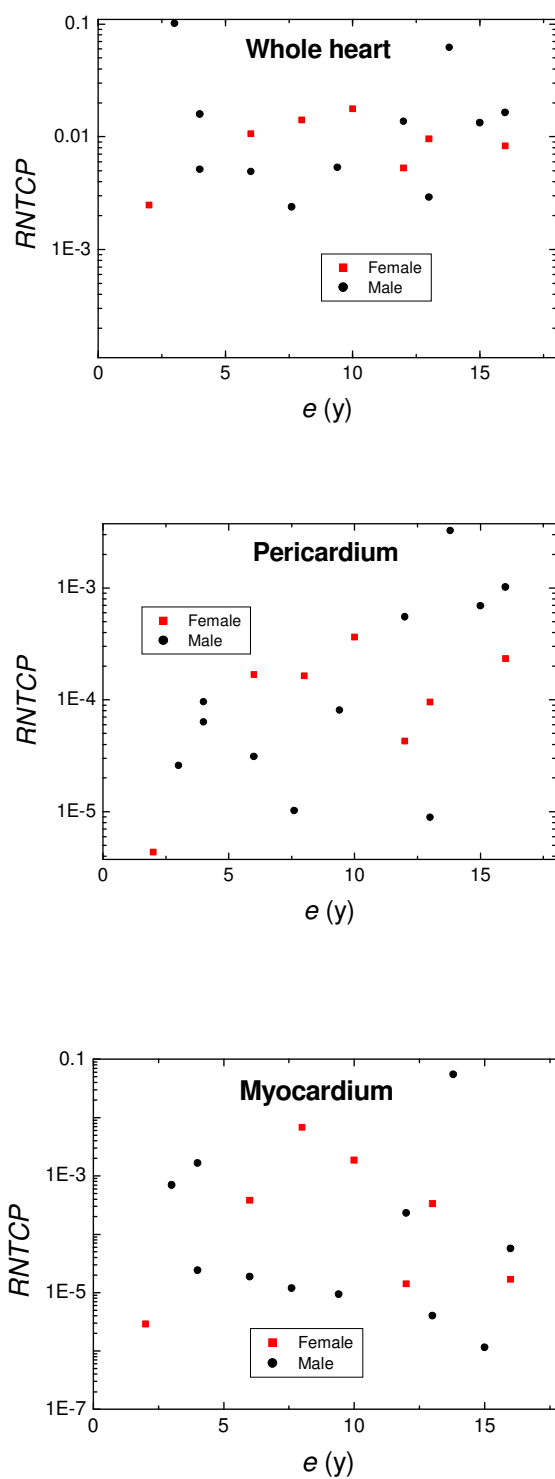


Figure 3-15 Predicted $RNTCP$ values *versus* age at exposure, e , by sex for a sample of patients ($n=18$) for which proton and photon CSI treatment plans were prepared.

There are strong and significant correlations between the organ dose ratio and *RNTCP* values (Figure 3-16) (whole heart, correlation coefficient $r = 0.66$, $p = 0.003$, pericardium, $r = 0.69$, $p = 0.001$, myocardium, $r = 0.69$, $p = 0.002$), which indicates the radiation dose to the heart is the governing factor for risk of cardiac toxicities.

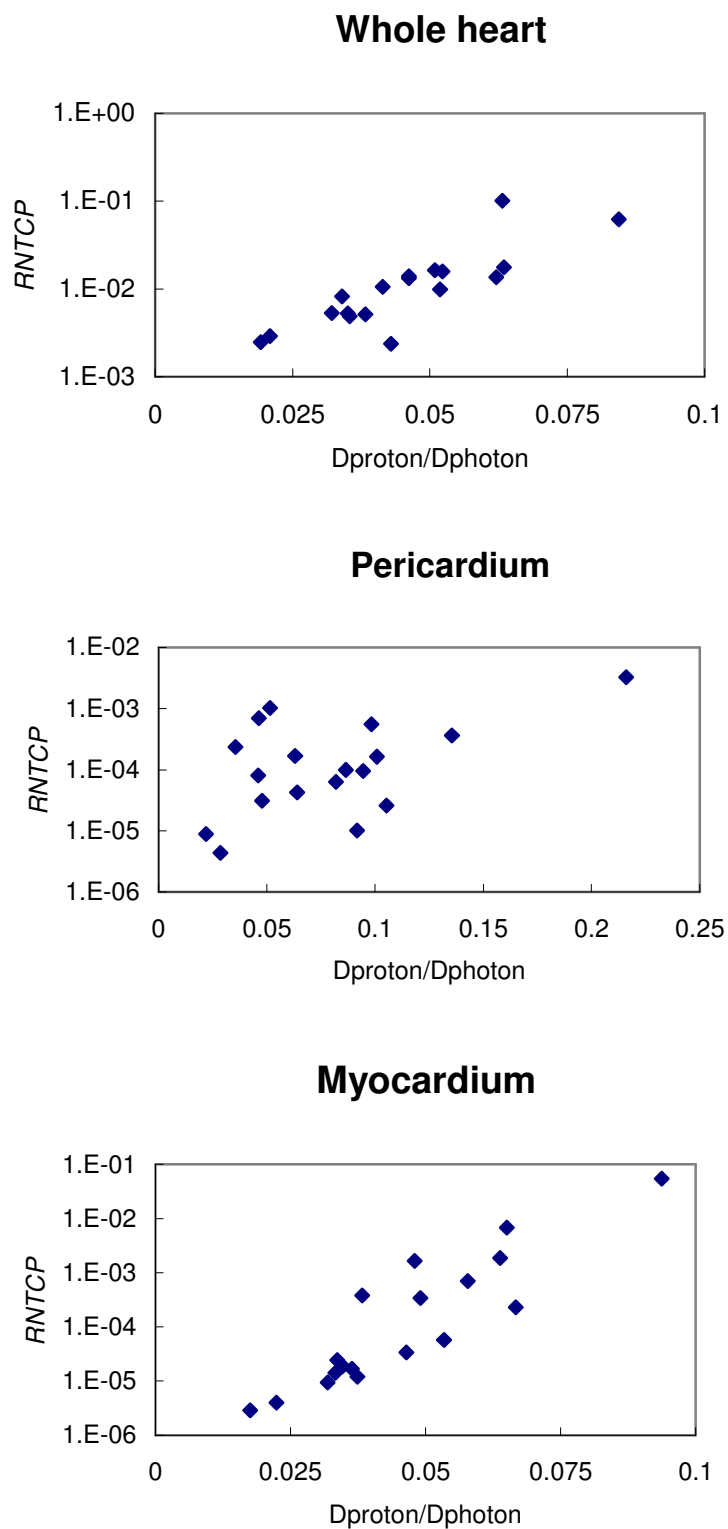


Figure 3-16 RNTCP VS mean organ dose ratio ($D_{\text{proton}}/D_{\text{photon}}$) for heart sub-structures for a population of pediatric patients.

The averaged predicted *RNTCP* values were 1.66×10^{-2} , 3.46×10^{-4} and 3.70×10^{-3} for whole heart, pericardium and myocardium, respectively (Figure 3-17). The t test and sign test were performed to determine if the mean and the median of the *RNTCP* values were significantly less than 1. The *RNTCP* values were shown to be statistically significantly less than 1 for the whole heart, myocardium and pericardium.

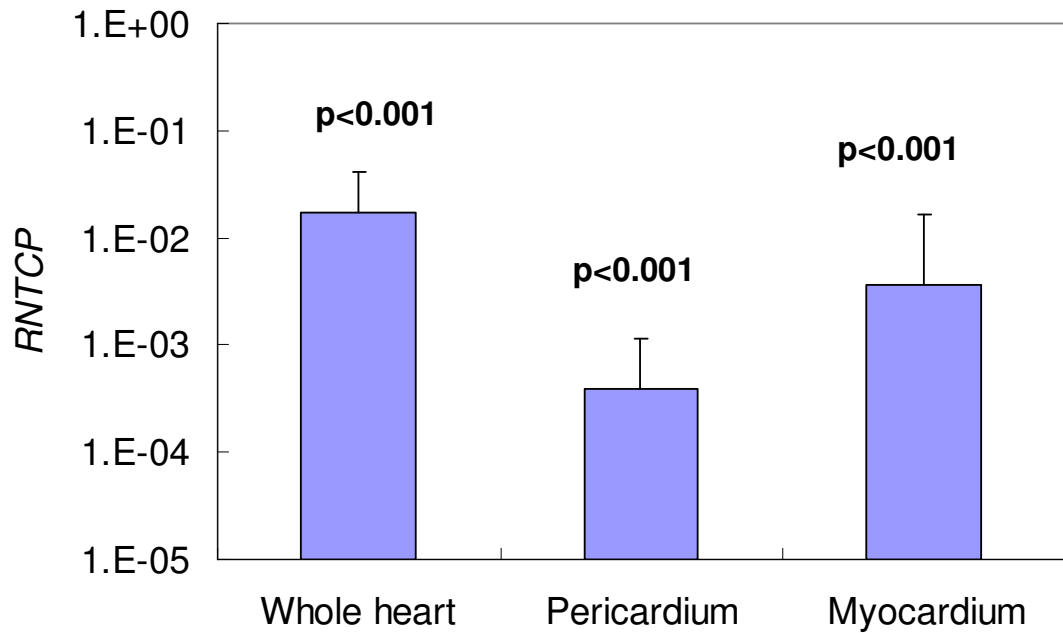


Figure 3-17 The population-average *RNTCP* values. The error bars represent the standard deviation of *RNTCP* values for each group of data, *e.g.*, whole heart, pericardium and myocardium.

3.4 Sensitivity of predicted risk of second cancer to modeling assumptions

The baseline risks of radiogenic second cancer were calculated based on the assumptions embodied in the LNT models from the BEIR VII report and mean radiation weighting factors for neutrons, $\overline{w_R}$, based on recommendations of ICRP

Publication 92. Because of the large uncertainties associated with those methods, sensitivity tests were performed to examine how sensitive the final risk values were to those aspects of dose and risk modeling

Table 3-16 lists the lifetime risks in each tissue (LAR_T), sum of LAR_T values over all tissues ($LAR_{modality}$) and the ratio of LAR_{proton} to LAR_{photon} ($RLAR$) for various scaling factors (0.5, 2, 5, 10, 20, 25) of the mean neutron radiation weighting factor ($\overline{w_R}$). As the mean neutron radiation weighting factor increased, the LAR values for proton therapy increased, and the final $RLAR$ values also increased because it increased the stray neutron equivalent dose from proton therapy. The total dose in photon therapy remained the same because there was no neutron dose generated in 6 MV photon beams.

Table 3-16 Predicted relative risk (15 years after exposure) in each tissue (LAR_T) and the ratio of LAR_{proton} to LAR_{photon} ($RLAR$) for various scaling factors of the radiation weighting factor ($\overline{w_R}$) for neutrons.

Organs	LAR_T (%)							
	Nominal $\overline{w_R}$		$\overline{w_R}/2$		$\overline{w_R} * 2$		$\overline{w_R} * 5$	
	Proton	Photon	Proton	Photon	Proton	Photon	Proton	Photon
Stomach	0.65	2.73	0.55	2.73	0.84	2.73	1.42	2.73
Colon	1.10	18.92	0.80	18.92	1.72	18.92	3.57	18.92
Liver	0.22	2.87	0.16	2.87	0.35	2.87	0.74	2.87
Lung	1.57	12.00	1.12	12.00	2.46	12.00	5.15	12.00
Prostate	0.13	1.38	0.067	1.38	0.27	1.38	0.66	1.38
Bladder	0.32	5.72	0.17	5.72	0.63	5.72	1.57	5.72
Thyroid	0.33	9.12	0.17	9.12	0.65	9.12	1.61	9.12
Other	3.33	39.23	2.36	39.23	5.27	39.23	11.11	39.23
$RLAR$	0.083		0.058		0.13		0.28	

Organs	LAR_T					
	$\overline{w_R} * 10$		$\overline{w_R} * 20$		$\overline{w_R} * 25$	
	Proton	Photon	Proton	Photon	Proton	Photon

Stomach	2.39	2.73	4.32	2.73	5.29	2.73
Colon	6.65	18.92	12.82	18.92	15.90	18.92
Liver	1.39	2.87	2.69	2.87	3.34	2.87
Lung	9.62	12.00	18.57	12.00	23.05	12.00
Prostate	1.32	1.38	2.64	1.38	3.30	1.38
Bladder	3.12	5.72	6.23	5.72	7.79	5.72
Thyroid	3.22	9.12	6.44	9.12	8.05	9.12
Other	20.85	39.23	40.31	39.23	50.04	39.23
<i>RLAR</i>	0.53		1.02		1.27	

The relationship between predicted *RLAR* values and the maximum weighting factor for neutrons is shown in Figure 3-18, revealing that the maximum neutron weighting factor would have to be more than 20 times larger (corresponding to a maximum w_R value of more than 400) than the values in ICRP Publication 92 in order for the risk of radiogenic second cancer following proton CSI to exceed that following photon CSI. The ICRP Publication 92 (2003) recommended the maximum neutron radiation weighting factor was 20. A recent reanalysis of atomic bomb survivors data deduced that the 95% confidence interval of neutron RBE was 25~400 (Kellerer *et al* 2006). This indicates that proton CSI reduced the predicted risk of second cancer compared to photon CSI for this pediatric patient, regardless of the change of the neutron dose in a possible range (5~400).

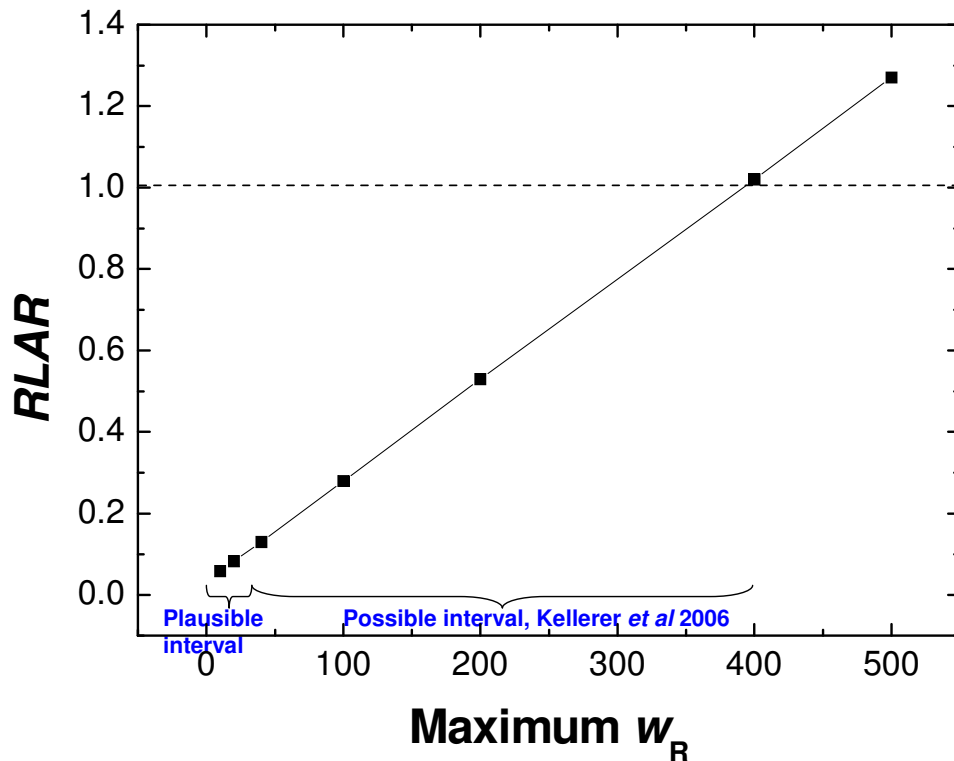


Figure 3-18 Sensitivity of the *RLAR* values to changes in the maximum radiation weighting factor for neutrons.

Evidence from CCSS strongly suggests that the dose-risk relationship for thyroid is not linear due to cell killing mechanism (Sigurdson *et al* 2005, Ronckers *et al* 2006, Bhatti *et al* 2010). Therefore the sensitivity of the baseline risk calculation, which utilized an LNT model, for thyroid to change in dose-risk model was examined using linear-exponential models, linear-plateau models with different inflection points (Figure 3-19), as discussed in section 2.7. Neutron radiation weighting factors were based on ICRP Publication 92 recommended $w_R(E)$ function and Monte Carlo simulated energy-dependent neutron fluence $\Phi(E)$ (Newhauser *et al* 2009) were used in the calculations. Because the exit dose to thyroid in proton plan for this patient (a 4-year-old boy, patient

index no. 2) was less than 1.1 Gy (RBE) and the LNT model is recommended for the dose range 0~2.5 Sv, the different dose-risk models were only tested for photon plan, where the thyroid (exist) dose was much larger than 2.5 Sv.

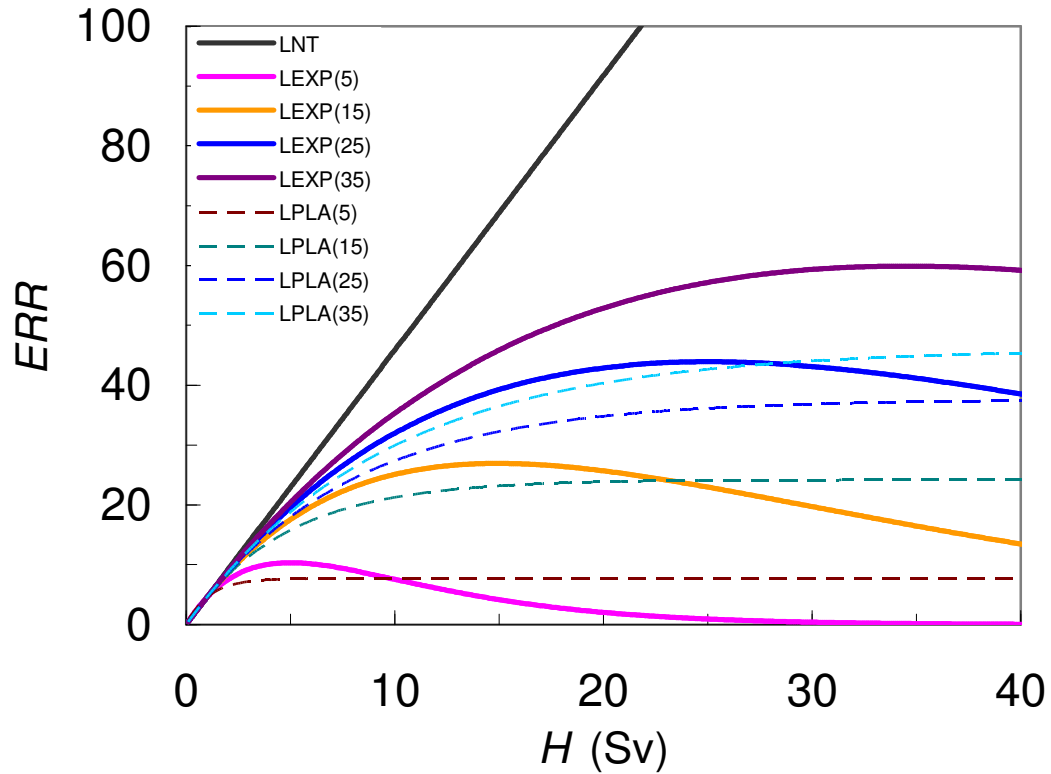


Figure 3-19 Excess relative risk as a function of equivalent dose, H . (LEXP = linear-exponential; LPLA = linear-plateau) used in this work to estimate excess relative risk (ERR) in the thyroid. The numbers in the legend refer to the location of the approximate point beyond which risk decreases or plateaus.

Table 3-17 lists the predicted RR and RRR values for each of the thyroid risk models studied. The RR values in photon CSI showed substantial sensitivity to the selected risk model. Dose-risk models with the low dose roll-off points suppressed the risk from high doses, thus reducing the RR value from photon CSI, while increasing the RRR value since the RR value from proton CSI was not changed (sensitivity tests were only used for photon CSI). However, the predicted RRR values were still less than 1,

ranging from 0.055 to 0.36, suggesting that proton CSI confers lower risk of second cancer of the thyroid compared to that from photon CSI for this pediatric patient, regardless of the cell sterilization effect showing in alternative dose-risk models, *e.g.*, linear-plateau model and linear-exponential model.

Table 3-17 The predicted *RR* and *RRR* values in thyroid for various dose-risk models plotted in Figure 3-19. The dose-risk models include: linear non-threshold (LNT); linear-exponential (LEXP); linear-plateau (LPLAT). The numbers in the parenthesis indicate the dose at which the model rolls off the risk due to the cell sterilization effect.

Dose Risk Model	<i>RR</i>		
	Proton	Photon	<i>RRR</i>
LNT	2.78	50.81	0.055
LEXP (5)	2.78	7.65	0.36
LEXP (15)	2.78	22.79	0.12
LEXP (25)	2.78	30.89	0.09
LEXP (35)	2.78	35.24	0.079
LPLAT (5)	2.78	8.63	0.32
LPLAT (15)	2.78	20.31	0.14
LPLAT (25)	2.78	26.33	0.11
LPLAT (35)	2.78	29.10	0.096

3.5 Sensitivity of predicted risk of cardiac toxicity to modeling assumptions

The baseline risks of radiogenic cardiac toxicity were calculated using *NTCP* models, model parameters from the literature, and nominal neutron radiation weighting factors from ICRP Publication 92. However, there are large unknown uncertainties associated with those aspects of the risk calculations. Sensitivity tests were performed to explore how sensitive the final *RNTCP* values were to those uncertainties.

Figure 3-20 plots $RNTCP$ for the whole heart, myocardium and pericardium using various $NTCP$ model parameters. The Lyman model was tested for the pericardium, while RS model was tested for the myocardium and the whole heart. For the pericardium, the $RNTCP$ values were not sensitive to changes in n values, while the $RNTCP$ values were more sensitive to changes in D_{50} values and very sensitive to changes in m values (as m increased from 0.1 to 1, the $RNTCP$ increased substantially). For the myocardium and the whole heart, the $RNTCP$ values were not sensitive to changes in D_{50} and s values, while the $RNTCP$ values were very sensitive to changes in γ values (as γ increased from 0.1 to 2, the $RNTCP$ decreased substantially).

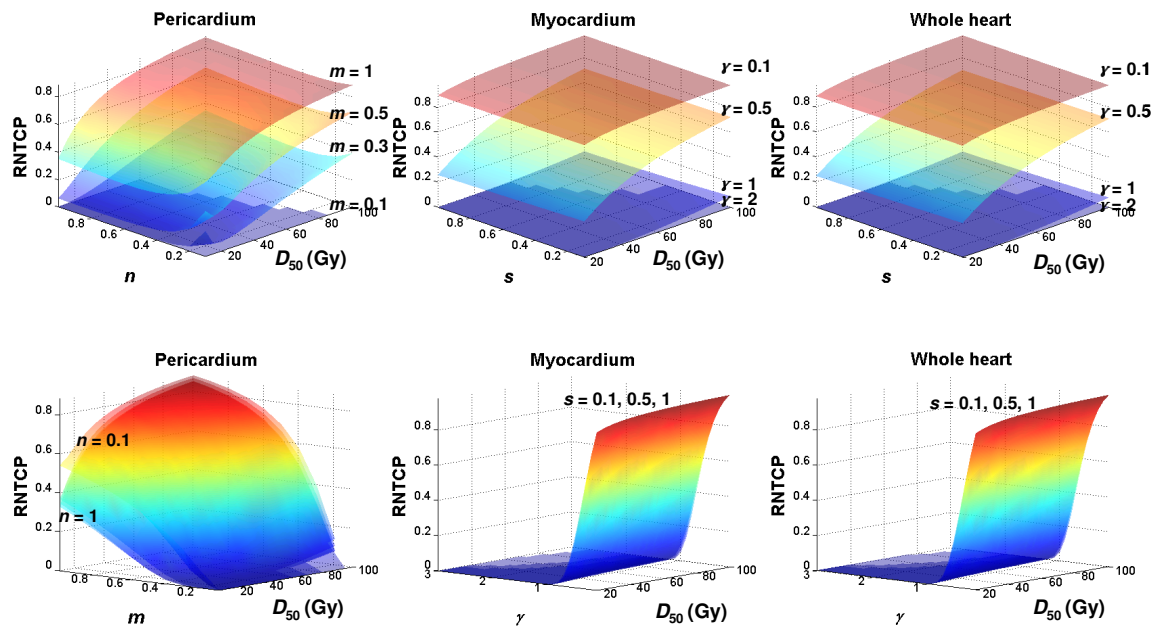


Figure 3-20 Surfaces of predicted $RNTCP$ values for heart sub-structures as functions of different $NTCP$ parameters. (Upper) The surfaces displayed were calculated for m values of 0.1, 0.3, 0.5 and 1 (pericardium), γ values of 0.1, 0.5, 1 and 2 (myocardium and whole heart). (Lower) The surfaces displayed were calculated for n values of 0.1, 0.3, 0.5 and 1 (pericardium), s values of 0.1, 0.5 and 1 (myocardium and whole heart). Color interpolated to facilitate visualization.

Based on the results plotted Figure 3-20, the following combinations were selected to estimate the minimum and maximum *RNTCP* values for the pericardium (min: $D_{50} = 10$ Gy, $n = 1$, $m = 0.05$, max: $D_{50} = 90$ Gy, $n = 0.12$, $m = 0.5$), the myocardium (min: $D_{50} = 10$ Gy, $\gamma = 3$, $s = 0.1$, max: $D_{50} = 90$ Gy, $\gamma = 0.1$, $s = 1$), and the whole heart (min: $D_{50} = 10$ Gy, $\gamma = 3$, $s = 0.1$, max: $D_{50} = 90$ Gy, $\gamma = 0.1$, $s = 1$). The intervals for the *NTCP* model parameters were set large enough to include all published values from the literature. The *NTCP* calculations were done for two patients (a 4-year-old boy, patient index no. 2 and a 14-year-old boy, patient index no. 16), and the results were listed in Table 3-18. The *RNTCP* values were always less than 1. Considering the expansive interval of *NTCP* model parameters which include the large underlying uncertainties associated with *NTCP* models, and the substantial differences in the dose distributions from proton vs. photon CSI, the results of this work strongly suggest that proton CSI carries a significantly lower risk of cardiac toxicity compared to photon CSI.

Table 3-18 *NTCP* and *RNTCP* values of cardiac toxicity for a 4-year-old boy and a 14-year-old boy using combinations of *NTCP* model parameters.

Patient index	Age at exposure (y)	Structure	<i>RNTCP</i>		
			Min	Baseline	Max
2	4	Pericardium	0	6.34E-05	0.70
		Myocardium	9.58×10^{-27}	2.41E-05	0.98
		Whole heart	1.99×10^{-19}	5.14×10^{-3}	0.97
16	14	Pericardium	0	3.26×10^{-3}	0.99
		Myocardium	2.58E-05	5.45×10^{-2}	0.99
		Whole heart	1.03×10^{-10}	6.19×10^{-2}	0.98

The relationship between *RNTCP* values and the neutron w_R scaling factor is plotted in Figure 3-21, revealing that the *RNTCP* values were always much less than 1

for plausible values (5~40) (BEIR VII, 2006) of the radiation weighting factor for neutrons. This suggests that proton CSI confers a lower risk of cardiac toxicity compared to photon CSI, regardless of the change of the max radiation weighting factor for neutrons in a plausible range.

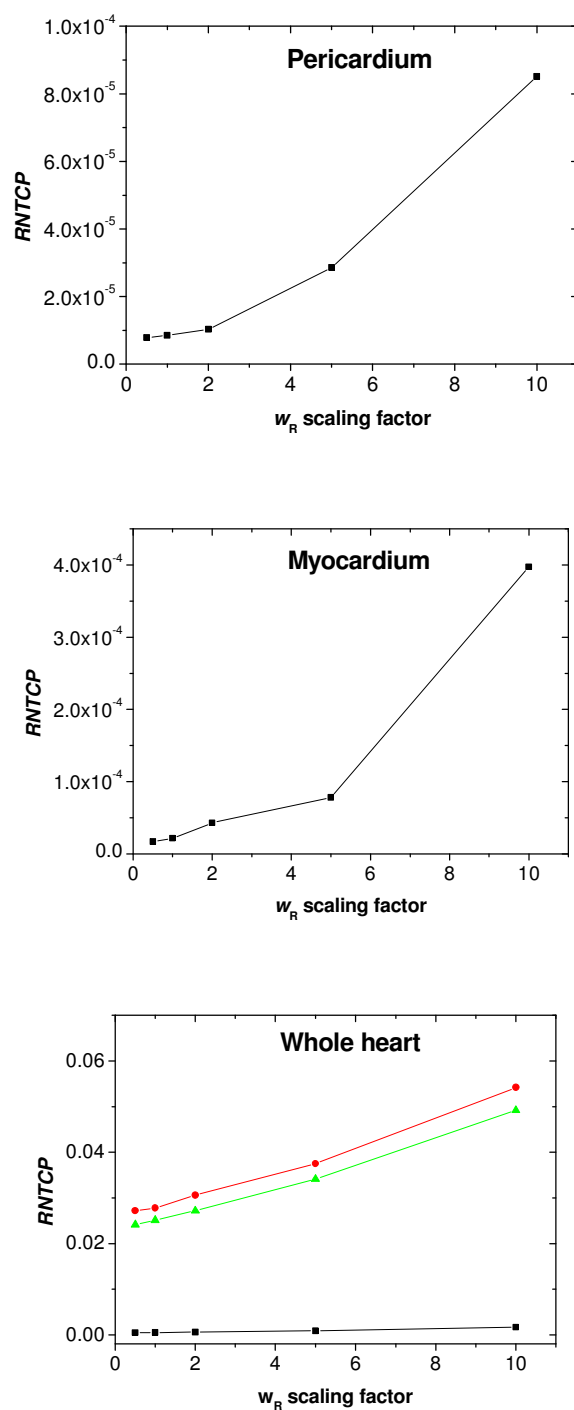


Figure 3-21 Sensitivity of the predicted $RNTCP$ values to changes in the neutron radiation weighting factor (w_R) for the (a) pericardium, (b) myocardium and (c) whole heart.

The contouring of the heart sub-structures involves large uncertainties. The methods for radiographic identification and delineation of the heart sub-structures is not standardized and challenging, and the knowledge of the uncertainty in the contouring is incomplete (Gagliardi *et al* 2010). Various methods for the heart sub-structures have been reported (Martel *et al* 1998, Gagliardi *et al* 2001, Wei *et al* 2008).

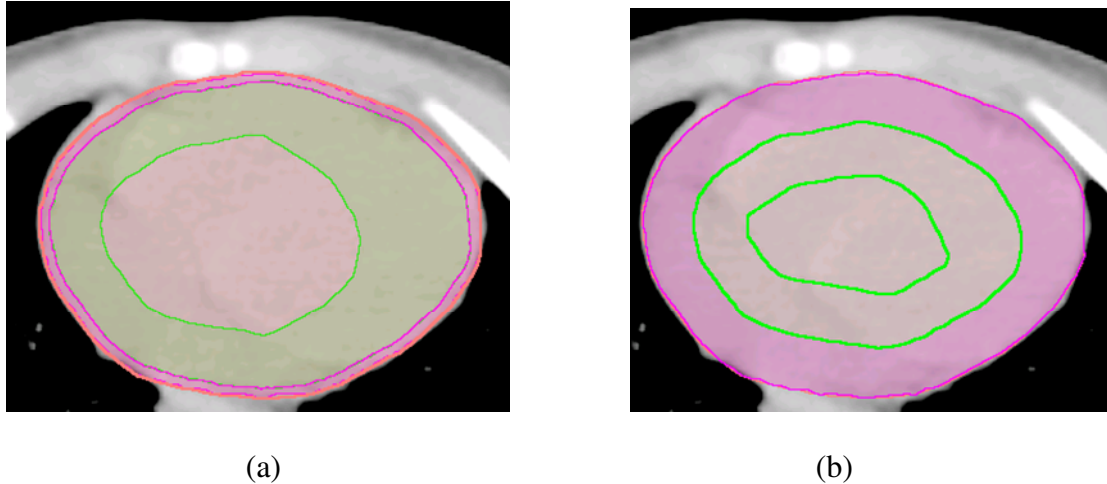


Figure 3-22 Heat sub-structures contouring: (a) baseline contouring (b) revised contouring.

The sensitivity tests were performed to see how sensitive the risk calculations would be to the changes in how the heart was contoured. To accomplish this, the pericardium was redefined as a 1 cm shell (*i.e.*, 5 times thicker than that in baseline calculations) inside the external heart surface, and the myocardium was redefined as a 1 cm shell inside the inner surface of pericardium (Figure 3-22). The *NTCP* calculations were carried out for two patients, and the results are listed in Table 3-19. The predicted *RNTCP* values were much less than 1. This further suggests that proton CSI confers a significantly lower risk of cardiac toxicity compared to photon CSI, regardless of variations in the methods used to contour the heart and its sub-structures.

Table 3-19 Predicted *NTCP* and *RNTCP* values of cardiac toxicity for a 4-year-old boy and a 14-year-old boy based on modified contours.

Patient index	Age at exposure (y)	Structure	<i>RNTCP</i> (Revised cardiac contours)	<i>RNTCP</i> (Baseline)
2	4	Pericardium	1.85E-05	6.34E-05
		Myocardium	4.0×10^{-6}	2.41E-05
16	14	Pericardium	9.4×10^{-4}	3.26×10^{-3}
		Myocardium	1.36E-05	5.45×10^{-2}

4. DISCUSSION

The goals of this work were to estimate the dose to tissues and organs from contemporary craniospinal proton and photon irradiation based on treatment planning system calculations, Monte Carlo simulations, and measurements; to calculate the corresponding predicted risk of radiogenic second cancer and cardiac toxicity using existing dose-risk models; to estimate the uncertainties in the calculated risks, and to test for statistical significance in the difference between the calculated risk of radiation induced late effects. The results show that proton CSI confers lower predicted risks of radiogenic second cancer for the one pediatric patient considered, and lower risks of radiogenic cardiac toxicities for the entire population of pediatric patients considered (n=18), compared to photon CSI. An uncertainty analysis including sensitivity tests reinforced the qualitative findings from the baseline calculations. The major results of this study are summarized in sections 4.1 through 4.3 for the reader's convenience. Sections 4.4 through 4.8 discuss the coherence of this study with existing literature, implications and significance of this work, strengths and limitations of this work and possible future work.

4.1 Outcomes of specific aim one

Specific aim one predicted the ratio of relative risk (*RRR*) and ratio of lifetime risk (*RLAR*) of radiogenic second cancer incidence for one pediatric medulloblastoma patient treated with proton CSI vs. photon CSI using the prevailing standards of care at our institution. The predicted *RRR* for a 4-year-old boy was always less than 1 at 15, 30, 45, 60, 75, 95 years after exposure. The predicted *RRR* values increased with the

time since exposure because competing non-radiogenic risk factors play an increasing role as patient age, and thus the predicted ratio of radiogenic risks after proton vs. photon CSI decrease in importance with time. The lifetime risks of second cancer incidence for this patient were 7.7% and 92% after proton CSI and photon CSI, and $RLAR$ is 0.083. The fact that the RR_{proton} and LAR_{proton} were much lower than the corresponding RR_{photon} and LAR_{photon} (about 10 times lower) strongly suggests that proton CSI would confer a much lower predicted risk of radiogenic second cancer to this pediatric patient compared to photon CSI, and indicates that the same may be true for all pediatric patients undergoing CSI.

4.2 Outcomes of specific aim two

Specific aim two predicted the ratio of normal tissue complication probability ($RNTCP$) of radiogenic cardiac toxicity for a population of pediatric medulloblastoma patients treated with proton CSI vs. photon CSI using prevailing standards of care at our institution. The mean $RNTCP$ values for the whole heart, pericardium and myocardium for the whole population were 1.66×10^{-2} , 3.46×10^{-4} and 3.70×10^{-3} . Statistical tests on the distributions of the risks of radiogenic cardiac toxicity revealed that the predicted risks after proton CSI were statistically significantly lower than those after photon CSI. The $RNTCP$ values did not reveal a significant dependence on the patients' age at exposure and sex. A strong correlation was found between organ dose ratio (proton to photon) and $RNTCP$ values, which confirms the working hypothesis that the lower heart dose delivered from proton CSI is one of the major reasons for its lower risk of predicted cardiac toxicity compared to photon CSI.

4.3 Outcomes of specific aim three

Specific aim three estimated the uncertainty in the calculated *RRR*, *RLAR* and *RNTCP* values (proton vs. photon CSI) for the population of medulloblastoma patients, taking into account dosimetric uncertainties and variations in variables, including the dose-risk model and the mean radiation weighting factor for neutrons ($\overline{w_R}$). Sensitivity tests were carried out by using various scaling factors for $\overline{w_R}$ values, various modifications to dose-risk models for second cancer risk to take into account cell sterilization effects, various *NTCP* model parameters, and variations in the contours that defined the heart.

The predicted *RLAR* values were sensitive to the uncertainties in the $\overline{w_R}$ values. However, the estimated risk of radiogenic second cancer following proton CSI was lower than that for photon CSI as long as the maximum radiation weighting factor was less than 400. On the assumption that the maximum neutron radiation weighting factor is 20, following recommendation in ICRP Publication 92, the calculated risk of radiogenic second cancer following proton CSI was 10 times lower than that following photon CSI. Interestingly, the *RRR* values were more sensitive to the change of $\overline{w_R}$ values for shorter time since exposure than for longer time since exposure because there were smaller competing non-radiogenic risk factors. The *RLAR* values for the thyroid were sensitive to the changes in the risk model related to cell sterilization effects, and an examination of the predicted *RRR* values for a 4-year-old boy revealed an interval of *RRR* results from 0.055 to 0.36 over 9 variations of the risk models.

The *RNTCP* values for cardiac toxicity were sensitive to the uncertainties in the mean radiation weighting factor for neutrons. However, the *RNTCP* values were always much less than one using a wide variety of $\overline{w_R}$ values, e.g., from 0.5 to 10 times of ICRP Publication 92 recommended value, covering the plausible interval of $\overline{w_R}$ values. The *RNTCP* values were very sensitive to m value in Lyman model and to γ value in RS model, which can be explained by the models' inherent properties: The γ value in RS model represents the maximum relative slope of the dose-response curve, and the m value in Lyman model is inversely proportional to the slope of dose-response curve. For these reasons, a change in γ value or m value can make a small change in dose induce a large change in normal tissue complication probability, which makes the difference between different radiation treatment modalities more pronounced. The *RNTCP* values were not sensitive to changes in n values and D_{50} values in Lyman model, nor were they sensitive to s values and D_{50} values in RS model. Based on those findings, combinations of *NTCP* model parameters were chosen to bound the range of possible model parameter sets, and the corresponding predicted *RNTCP* values were always less than 1 (interval from 0 to 0.993). Hence the predicted risks of radiogenic cardiac toxicity following proton CSI were less than that following photon CSI for all 18 patients in the study, regardless of the selection of the *NTCP* model parameters in plausible ranges, which were taken from the literature. A sensitivity test of the contours of the heart sub-structures revealed the calculated *RNTCP* values were still much less than one for all contouring methods that were considered in this work.

4.4 Coherence with existing literature

We compared our results with literature. In a previous study, Newhauser *et al* (2009) estimated the risk of radiogenic second cancer following CSI using photon *versus* proton radiotherapies for CSI of a 3-year-old boy. They reported predicted lifetime risks of second cancer incidence for the boy at 5.1% for passively-scattered proton therapy and 54.8% for conventional photon therapy following 36 Gy CSI. As reported in section 3.2, this study estimated the lifetime risk of second cancer at 7.7% following proton therapy and 92.0% following photon therapy for a 4-year-old boy received 23.4 Gy CSI. If normalized to the same prescribed dose, the lifetime second cancer incidence in our work is about 2.3 times higher than that in their work (Table 4-1).

Table 4-1 Comparison of lifetime risk (prescribed dose 23.4 Gy) of second cancer incidence and ratio of the lifetime risk between proton CSI and conventional photon CSI (CRT) from different studies.

	Lifetime risk (%)		<i>RLAR</i>
	CRT	Proton	(CRT/proton)
Miralbell <i>et al</i> (2002)	35.6	2.4	15
Newhauser <i>et al</i> (2009)	35.6*	3.3	11
This work	92.0	7.7	12

*Value taken from Miralbell *et al* (2002)

Considering stray neutron dose only, Newhauser *et al* (2009) reported 1.5% lifetime risk of second cancer incidence, while we predicted 4.6% lifetime risk of second cancer incidence. If normalized to the same prescribed dose, our result is about

4.7 times higher than their result. There are several possible reasons why our result is higher than theirs:

First, different dose-risk models were used in their and our studies. ICRP Publication 60 (1990), which was published for radiation protection purpose and provided sex-averaged and age (age at exposure or attained age) non-specific risk coefficients, was used in their study. BEIR VII report, which utilized more recent and detailed epidemiological data and contained organ, sex, age specific coefficients, was used in our study. Table 4-2 lists the risk coefficients for lifetime second cancer incidence rate from ICRP Publication 60 (ICRP 1990) (attained age at 76 years) and BEIR VII (NRC, 2006) (attained age at 100 years). From Table 4-2, we can see that the risk coefficients from BEIR VII for the patient we studied (a 4-year-old boy) are generally higher than those from ICRP Publication 60, since a young patient is more prone to have radiogenic second cancer compared to the general population. If we took the sex-averaged risk coefficients from BEIRVII for patient who is 30 years old (the 8th column of Table 4-2), the coefficients are much closer to the risk coefficients from ICRP Publication 60. The other significant difference between those two reports is that BEIR VII report excluded skin cancer from the risk model because the special properties of skin cancer (NRC, 2006). However, the incidence of skin cancer in childhood cancer survivors was large (Meadows *et al* 2009). Based on these observations, if we roughly adjusted the risk values from Newhauser *et al* by age and sex (multiplying the risk coefficient from ICRP 60 by the ratio between 3rd column and 8th column of Table 4-2), the lifetime risk of second cancer incidence would be 106.1 and 9.5 after photon and proton CSI, which are very close to the risk values from this

work. Therefore, after we adjusted the dose-risk coefficient values by age and sex so that the risk models were similar, we had similar values to those of Newhauser *et al* (2009).

Table 4-2 Risk coefficients for lifetime second cancer incidence from ICRP Publication 60 (ICRP 1991) and BEIR VII (NRC, 2006).

Organ	Lifetime risk (%/Sv)						
	ICRP 60	BEIR VII					
		4-year-old male	4-year-old female	4-year- old sex average	30-year- old male	30-year- old female	30-year- old sex average
Stomach	1.22	0.67	0.88	0.78	0.28	0.36	0.32
Colon	1.55	2.95	1.90	2.45	1.25	0.82	1.04
Liver	0.16	0.52	0.24	0.38	0.22	0.10	0.16
Lung	0.90	2.72	6.33	4.53	1.05	2.42	1.74
Breast	0.40	-	9.65	4.83	-	2.53	1.27
Ovary or Prostate	0.14	0.83	0.90	0.87	0.35	0.50	0.43
Bladder	0.60	1.83	2.12	1.98	0.79	0.79	0.79
Thyroid	0.80	0.84	4.62	2.73	0.09	0.41	0.25
Skin	10.0	-	-	-	-	-	-
Leukemia	0.51	1.67	1.27	1.47	0.84	0.63	0.74
Other	0.70	7.62	13.40	10.51	0.20	0.21	0.21

Second, they did not account for the underestimation in out-of-field dose from photon therapy, *i.e.*, they used photon data from Miralbell (2002), which were taken from a TPS. The TPS can underestimate out-of-field photon dose and on average the organ doses from TPS could be about 30% lower than those measured for out-of-field organs (Howell *et al* 2010a).

Third, Newhauser *et al* used a stylized adult phantom, which is less realistic than the patient CT image based voxelized phantom used in this study, in their study to

represent the pediatric patient, and they put spherical dose receptors inside the phantom and used the mean dose in the receptors to represent the mean organ dose. Those affected the neutron doses (Table 4-3).

Good agreement was found between our study and theirs regarding the ratio of lifetime risk for second cancer incidence after proton and photon CSI (Table 4-1). Specifically, they reported 0.097 *versus* 0.083 from this work. Given the differences in methods used for risk calculations, as discussed above, the ratio of risk values are remarkably similar. The possible reason is that although different methods were used in different studies, using the ratio of risk values as a figure of merit cancels some sources of uncertainty, like uncertainties associated with risk models. Thus, the ratio of the risk is an advantageous “figure of merit” for treatment modality comparison research, as long as the methods used are consistent within one comparative study.

More recently, Taddei *et al* (2010c) estimated lifetime risk of second cancer incidence and mortality for a boy and a girl due to stray neutron dose from proton CSI with 23.4 Gy (RBE) prescription. Their risk value for the 10-year-old boy was 8.5% lifetime incidence. Bone marrow and skin were included in their calculation, while this work did not take those two tissues into account. After subtracting second cancer risks from those two tissues, their lifetime risk value for the boy was 5.5%, which agrees well with our lifetime risk value 4.6% due to stray neutrons, although still higher considering the difference in the age of patients being studied. Normally younger patients should have increased risk values because of increased sensitivity and higher dose due to smaller bodies. The most likely reason for their higher risk values is because smaller air gap (2 cm) for spinal fields were used in Taddei *et al* for the 10-

year-old boy, while around 12 cm air gap (Table 2-1) were used in this work for the 4-year-old boy. So the neutron doses from Taddei *et al* were higher than this work (Table 4-3). Table 4-3 lists the stray organ doses in terms of equivalent dose per therapeutic dose (mSv/Gy) from proton CSI from different studies. The neutron doses from Newhauser *et al* (2009) were lower than those from Taddei *et al* (2009) and current study because of different dose recording techniques, and the H_T/D values from Taddei *et al* (2009) were higher than that from current study because they used smaller air gap for spinal fields.

Table 4-3 Comparison of stray organ doses from proton CSI between different studies.

Organs	H_T/D (mSv/Gy)		
	Current study	Taddei (2009)	Newhauser (2009)
Gonads	6.8	4.5	0.8
Colon	8.9	15.4	4.7
Lungs	14.1	28.1	8.0
Stomach	12.4	19.8	5.9
Bladder	7.3	6.7	1.4
Liver	10.6	20.7	5.7
Thyroid	16.4	31.6	12.3
Remainder	10.9	16.1	4.8

A research group at Massachusetts General Hospital estimated stray neutron-induced risk of second cancer for patients received brain fields (Zacharatou Jarlskog and Paganetti 2008) and spinal field (Athar and Paganetti 2009). They reported lifetime risk of second cancer incidence less than 1% due to stray neutron dose in most cases. It is hard to directly compare their results with ours because of the large differences in the treatment technique and dose simulation method. They did not investigate clinically approved CSI plans, but using generic circular proton fields for hypothetical tumors.

Equivalent doses from stray radiation from photon CSI and proton CSI were compared in this study (Figure 3-6), revealing that the stray neutron dose from proton CSI was much lower than the stray photon dose from photon CSI close to the field edge, while the difference became smaller further away from field edge. Proton and photon CSI generated roughly same amount of stray dose at larger distance (beyond 14 cm). Athar *et al* (2010) recently compared out-of-field photon dose from 6 MV IMRT and stray neutron dose from proton therapy in the head and neck and spine region, and their finding was different from ours. They basically divided stray radiation into three geometrical areas: proton therapy offered a lower integral dose in the therapeutic field; the stray neutron dose was a factor 2 higher than stray photon dose within ~ 25 cm from the therapeutic field edge but out of therapeutic field; and proton therapy generated a factor of 2~3 factor lower dose at larger distances to the therapeutic field compared to IMRT. The possible reasons for this discrepancy include: first, different photon treatment techniques were used. We used 6 MV conventional photon CSI while Athar *et al* used 6MV IMRT; second, the field sizes were different. They based their simulations on simplistic 3, 6, and 9 cm diameter fields to treat hypothetical tumors in the head and neck and spine region, while our results were from clinically realistic CSI treatments which extended from the superior aspect of the brain through S2 of the sacrum, with more scatter dose and leakage dose from CSI.

It is also interesting to compare our predicted risk calculations with the CCSS published second cancer incidence data. The cumulative risk of incidence of second malignant neoplasms in childhood cancer survivors was around 2% and 9% at 15 years and 30 years time since diagnosis. The cumulative risk for photon CSI in our study

were 0.5% and 4.4% at 15 years and 30 years time since diagnosis, respectively; and 0.05% and 0.5% for proton CSI at 15 years and 30 years time since diagnosis (Figure 4-1). A possible explanation why the published incidence are higher than ours is the published rates were based on the whole CCSS patient cohort and second cancers from all causes, including patients with various primary childhood cancer diagnosis and patients who received chemotherapy, while our calculated result was based on radiogenic second cancer risks for one patient.

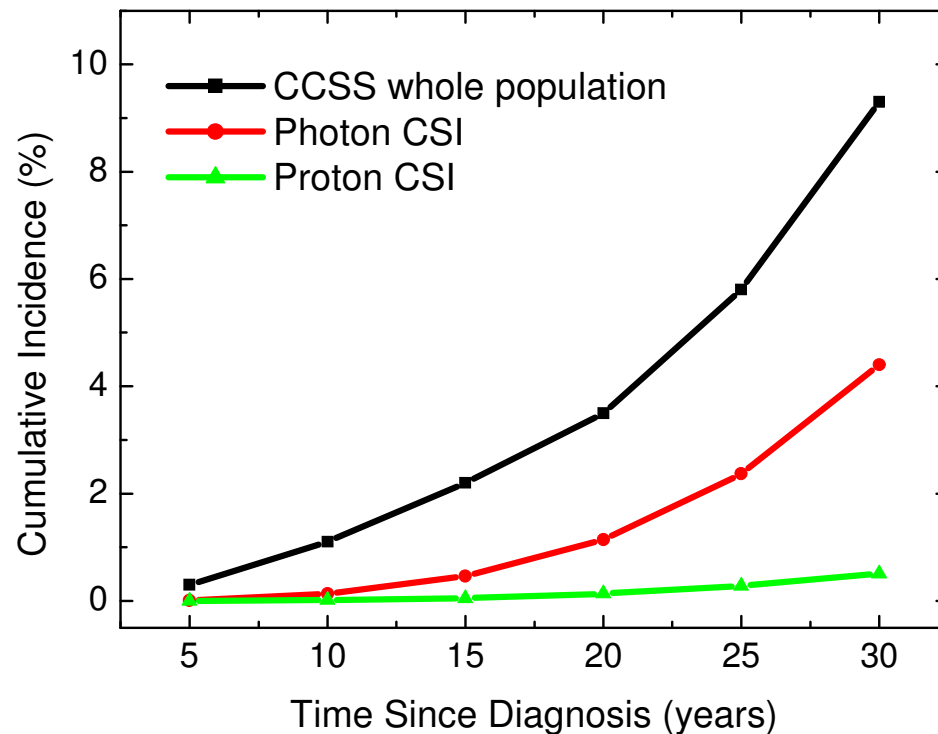


Figure 4-1 Cumulative second cancer incidence from CCSS study (Meadows *et al* 2009, Reprinted with permission. © 2008 American Society of Clinical Oncology) and from this study.

Mu *et al* (2005a) compared different treatment plans, including a conventional photon plan, intensity modulated photon therapy plan, conventional electron plan, intensity modulated electron therapy plan and intensity modulated proton therapy plan for childhood medulloblastoma cases (5 patients). Because they did not include stray radiation dose in their study, the therapeutic absorbed dose to the heart was compared here (Table 4-4). The dosimetric results agree very well between theirs and our work.

Table 4-4 Mean therapeutic absorbed dose to the heart (averaged for different cases, 5 cases in Mu *et al* (2005), and 18 in current work) from photon and proton CSI.

	Mean therapeutic absorbed dose to the heart	
	Photon Gy (s.d.)	Proton Gy(RBE) (s.d.)
Mu <i>et al</i> (2005)	11.9 (0.9)	0.0 (0.0)
This work	10.4 (2.2)	0.2 (0.2)

NTCP calculation results from this study are generally consistent with previous reports of *NTCP* comparisons between photon and proton therapies. Mu *et al* (2005a) reported very low *NTCP* values for late effects using historical *NTCP* model parameters (Burman *et al* 1991) to calculate side effects for five children diagnosed with medulloblastoma, and their explanations for the very low *NTCP* values included: “low total dose; the predictive ability of the *NTCP* models has not been fully tested for late side effects; the dose distribution and clinical data on which the models are based reflect irradiation conditions in the specific patient group, and there are no available *NTCP* parameters based on data sets derived from a pediatric population; and the relevant end-points in a pediatric population might not always be the same as in an

adult population”. We concur with these points, which are also applicable to our study, and they will be discussed later (section 4.7).

4.5 Implications and significance of the findings

Risks of radiogenic late effects associated with modern radiation therapies for pediatric patients are of particular interest because a relatively longer survival time after their treatment and higher degree of radiation sensitivity compared to adults.

This work has several implications for CSI of pediatric patients with modern radiation modalities. In order to develop strategies to minimize radiation complications, one first needs accurate, complete, and personalized radiation dose reconstructions. However, just as dose reconstructions and risk estimations have become more realistic, they are becoming increasingly complex, and a multidisciplinary effort will be advantageous to achieve breakthroughs (Newhauser 2010, Newhauser and Durante 2011). This work suggests the feasibility of utilizing infrastructure and knowledge from medical physics, biology, radiation epidemiology, and statistics toward achieving the goal of improving patients’ quality of life.

An important finding of this work was that proton CSI confers a lower predicted risk of radiogenic second cancer compared to photon CSI for one pediatric patient for follow-up times up to 95 years. The uncertainty analysis demonstrated the *RRR* values were sensitive to mean radiation weighting factor $\overline{w_R}$ for neutrons and dose-risk models. However, the qualitative finding of this study was unchanged, regardless of the changes of $\overline{w_R}$ values in a plausible range and changes of possible dose-risk models considering cell sterilization effects.

Furthermore, this work revealed that proton CSI confers a lower predicted risk of radiogenic cardiac toxicity for the whole heart, pericardium and myocardium compared to photon CSI for a population of pediatric patients. The uncertainty analysis demonstrated that the *RNTCP* values were sensitive to the mean radiation weighting factor $\overline{w_R}$ for neutrons and *NTCP* model parameters. However, the qualitative finding was unchanged regardless of the changes of $\overline{w_R}$ values and *NTCP* model parameters over their respective plausible intervals.

4.6 Strengths of this study

Our study has several strengths. First, we used realistic patient data from clinically deployed treatment planning system and the risk calculations were based on dose distributions from clinically realistic CSI treatment fields. Our in-house Monte Carlo simulation code system allowed us to generate patient-specific voxelized phantoms and accurate stray radiation doses from proton CSI were reconstructed. Previously, the stray doses and associated risks in proton therapy were assessed either in comparatively simplistic stylized computational phantoms or using simplistic circular therapeutic fields (Zacharatou Jarlskog and Paganetti 2008, Athar and Paganetti 2009, Fontenot *et al* 2009, Newhauser *et al* 2009). Although there were several treatment plan comparison papers published before comparing different CSI modalities, the stray radiation were not included in most of them. For the proton part, Monte Carlo simulations were used to obtain stray radiation dose; and for the photon part, the detailed TLD measurements were carried out to obtain stray radiation dose specifically for CSI patients. These advanced dose reconstruction tools provided us with the most

accurate and comprehensive evaluation of radiation doses and risks of any comparative CSI study.

Second, we included both therapeutic and stray radiation dose in our calculations. Most of the previous studies or relevance to this work only included therapeutic dose or only stray neutron dose in proton therapy (Miralbell *et al* 2002, Zacharatou Jarlskog and Paganetti 2008, Athar and Paganetti 2009, Taddei *et al* 2009, Taddei *et al* 2010c). Only one study included both therapeutic and stray radiation dose for CSI (Newhauser *et al* 2009), and the comparison between this study and ours was discussed in section 4.4.

Third, we calculated both second cancer incidence and *NTCP* of cardiac toxicity based on most updated dose-risk model and model parameters, which were rarely done before. The risk models from BEIR VII (2006) report allowed us to estimate risk of second cancer incidence by taking the patient's age at exposure, attained age, and sex into account. The *NTCP* models based on clinical data of cardiac toxicity end points allowed us to estimate risk of cardiac toxicity for each heart sub-structure. It was recommended that clinical outcomes of certain organ are better correlated with *NTCP* parameters derived from the DVH of the same organ (Gagliardi *et al* 2010). Thus the detailed contouring of the heart is a special strength of this study, which provided us DVH information for each heart sub-structure and allowed us to do *NTCP* calculations for each of them.

Fourth, this study used, apparently for the first time, the stray neutron doses for *NTCP* calculations. Historically, the input dose data for *NTCP* model were typically photon dose. Recently, proton dose was incorporated into *NTCP* calculation, and 1.1

relative biologic effectiveness (RBE) was assigned for proton beams (Kaser-Hotz *et al* 2002) or $w_R=2$ was used for proton beams (Mu *et al* 2005a). The neutron dose was not included for two possible reasons: first, the neutron dose equivalent was hard to estimate, especially for proton CSI; second, there are complexities and large uncertainties associated with radiation weight factor for neutrons. In our study, both proton and neutron dose equivalent were included in the total dose and *NTCP* calculations, based on TPS and Monte Carlo simulations. Although the breadth of the range of possible neutron $\overline{w_R}$ values is controversial, the sensitivity test in this study demonstrate that proton therapy confers significantly lower risk of cardiac toxicity than photon therapy, regardless of the uncertainties in neutron $\overline{w_R}$ values.

Finally, the methodology used in this study to calculate the risks of radiogenic second cancer and cardiac toxicity is applicable to other radiogenic late effects and radiation modalities. Our task was and is trying to answer the important question, “How can we reduce the risk of radiogenic late effects like second cancers?” We predicted the risk of developing second cancers and other late effects for pediatric patients’ treatment plans and compared the different radiation treatment modalities. Ultimately, the research methods and results reported here may be translated to routine clinical treatment planning. This will enhance clinicians evidence base, upon which clinical decisions are made, *e.g.*, to utilize proton *vs.* photon CSI.

4.7 Limitations of this study

This study has several limitations. First, only one pediatric patient was used for the estimation of radiogenic second cancer risk because of time and resource

constraints. Future calculations based on more patients may give us more information and provide a more realistic comparison between different modalities.

Second, although the current risk models may not be applicable to organs received high therapeutic dose, a previous study found the final *RRR* values were not sensitive to dose-risk models (Fontenot *et al* 2010a), and the sensitivity test to the thyroid of a 4-year-old boy in this work demonstrated that proton CSI would always confer a lower predicted risk compared to photon CSI.

Third, dose measurements at selected positions within the phantom were used to estimate mean organ stray equivalent dose in photon therapy, while Monte Carlo simulations were used to determine stray equivalent dose in proton therapy. This could introduce systematic uncertainties in to the comparison of dose and risk between these two modalities. However, the TLD measurements were specially designed for CSI. To the best knowledge of the authors', those data are the most accurate and up-to-date stray radiation dose reconstructions for photon CSI.

Fourth, we were unable to compare directly to epidemiological data or apply a risk model that was specifically for children receiving CSI. This was principally because we don't have long-term follow-up data on second cancer or cardiac toxicity for the pediatric patients we studied. *NTCP* models have been used in clinic for plan evaluation and optimization for decades. However, some aspects of these models and their applications remain controversial. The low clinical complication rates and small number of patients involved are the basic difficulties in data collection for determining model parameters to predict normal tissue complications. The general agreement is that the calculated *NTCP* values are highly dependent on the clinical data from which the

model parameters were derived, therefore more data are needed to test the validity of current models (Cox *et al* 1995, Kwa *et al* 1998, Moiseenko *et al* 2000, Schultheiss 2001, Seppenwoolde *et al* 2003). The calculated *NTCP* values are more suitable for a comparative study instead of being absolute predictors (Fuss *et al* 2000, Pierce *et al* 2002). Additionally, the exit dose to heart is low, especially in proton therapy, which may cause high uncertainty in *NTCP* calculations. However, the exhaustive sensitivity tests strengthened our conclusion and gave us enough confidence to claim that proton CSI will deliver lower risk of cardiac toxicity compared to photon CSI.

Fourth, the methods for radiographic identification and delineation of the sub-structures of the heart, *e.g.*, pericardium and myocardium, is not standardized and the uncertainty in heart contouring is not fully understood. Martel *et al* (1998) defined the pericardium volume as a 1 cm thick rind within the contoured heart volume for pericarditis study; Gagliardi *et al* (Gagliardi *et al* 2001) defined the heart with ‘the cranial limit of the heart included the infundibulum of the right ventricle, the right atrium, and the right atrium and auricle and excluded the pulmonary trunk, the ascending aorta and the superior vena cava’, and defined myocardium ‘with the same external contour as the heart. The wall thickness of the left ventricle was assumed to be between 2 and 3 times that of the right ventricle’; Wei *et al* (2008) defined pericardium as 0.5 cm shell extending from the heart contours for pericardial effusion study. In our study, the heart contouring may be simplified, but this kind of simplification is warranted considering the large uncertainties associated with the *NTCP* model itself. Again, the sensitivity tests of varying the heart contouring strengthened our conclusion that proton CSI confers lower risks of cardiac toxicity than photon CSI.

Finally, we only investigated a passively scattered proton CSI and conventional photon CSI in this work, while the other CSI modalities like scanned proton beams and IMRT were not studied. Further study should be carried out for those advanced radiation treatment modalities.

4.8 Future work

Calculating risk of radiogenic second cancer for a population of pediatric patients is a next logical step of this research. Although the same methodology used in this study on one pediatric patient will be used to do the calculations for other patients, it is desirable to have more data of risk values of second cancer. Comparison between different treatment modalities based on those data will be helpful. For example, such data will allow us to determine if our result is statistically significant for a population of patients.

As we mentioned in the limitations of this work, the dose measurements at certain locations were used to estimate photon stray dose in each organ, while the detailed Monte Carlo simulations were used to simulate stray neutron dose in proton therapy. Several groups are developing Monte Carlo photon simulation codes that include a Linac-based photon therapy model and patient specific phantom for photon dose simulations. Such tools will be important for future photon dose reconstructions and risk assessment research.

Proton CSI was compared to conventional photon CSI in this work. In the future, it will be important to know if other treatment modalities like Volumetric Modulated Arc Therapy (VMAT) and Tomotherapy are better choices in certain

situations, considering multiple factors such as treatment time and cost, as well as predicted patients outcomes.

In the future, It will be helpful to have an evidence-based tool with a user-friendly graphical interface to select the best treatment modality for any specific pediatric patient, based on their age at exposure, sex, size, disease site, etc. The current clinical treatment decisions rely heavily on subjective judgment and experience. A more quantitatively, evidence-based radiotherapy modality selection process may help clinicians be more objective in making clinical decisions. In our laboratory, work is underway to automate evidence generation for use in treatment modality decision-making, taking into account various radiogenic late effects and considering various radiation treatment modalities. This work provided prototype component of such system, and our findings strongly suggest that a quantitative evidence-based approach to avoid radiogenic late effects is not only technologically feasible, but it has a large potential to reduce the burden of treatment related health complications experienced by long-term survivors of childhood cancer.

5. CONCLUSION

Proton CSI can significantly reduce the calculated risk of radiogenic second cancer following CSI compared to photon CSI. Baseline calculations of the Ratio of Relative Risk (*RRR*) were always less than 1 after 15, 30, 45, 60, 75, 95 follow-up years for a 4-year-old boy. The Lifetime Attributable Risk (*LAR*) values were 7.7% and 92% after proton CSI and photon CSI, and Ratio of Lifetime Attributable Risk (*RLAR*) was 0.083 for this boy. Sensitivity analysis revealed that quantitative values were sensitive to uncertainties in the risk model and the radiation weighting factor for neutrons. However, the qualitative findings of the study were insensitive to any plausible changes of risk models and mean neutron $\overline{w_R}$ values.

Proton CSI can also significantly reduce the calculated risk of radiogenic cardiac toxicities compared to photon CSI. The mean ratio of normal tissue complication probability (*RNTCP*) values for the whole heart, pericardium and myocardium for the whole population of pediatric patients were 1.66×10^{-2} , 3.46×10^{-4} and 3.70×10^{-3} , respectively. Statistical tests showed that the risks of radiogenic cardiac toxicity from proton CSI were statistically significantly lower than the risks from photon CSI. Sensitivity analysis revealed that *RNTCP* values were sensitive to uncertainties in the *NTCP* model parameters, the mean neutron $\overline{w_R}$ values and heart structure contours. However, the qualitative findings of the study were unchanged with the changes of *NTCP* model parameters, mean neutron $\overline{w_R}$ values and heart contouring in plausible ranges of parameter values.

Bibliography

- Adams M J, Hardenbergh P H, Constone L S and Lipshultz S E 2003 Radiation-associated cardiovascular disease *Crit Rev Oncol Hematol* **45** 55-75
- Aleman B M, van den Belt-Dusebout A W, Klokman W J, Van't Veer M B, Bartelink H and van Leeuwen F E 2003 Long-term cause-specific mortality of patients treated for Hodgkin's disease *J Clin Oncol* **21** 3431-9
- Arjomandy B, Sahoo N, Zhu X R, Zullo J R, Wu R Y, Zhu M, Ding X, Martin C, Ciangaru G and Gillin M T 2009 An overview of the comprehensive proton therapy machine quality assurance procedures implemented at The University of Texas M. D. Anderson Cancer Center Proton Therapy Center-Houston *Med Phys* **36** 2269-82
- Armstrong G T, Liu Q, Yasui Y, Neglia J P, Leisenring W, Robison L L and Mertens A C 2009 Late mortality among 5-year survivors of childhood cancer: a summary from the Childhood Cancer Survivor Study *J Clin Oncol* **27** 2328-38
- Athar B S, Bednarz B, Seco J, Hancox C and Paganetti H 2010 Comparison of out-of-field photon doses in 6 MV IMRT and neutron doses in proton therapy for adult and pediatric patients *Phys Med Biol* **55** 2879-91
- Athar B S and Paganetti H 2009 Neutron equivalent doses and associated lifetime cancer incidence risks for head & neck and spinal proton therapy *Phys Med Biol* **54** 4907-26
- Bednarz B, Athar B and Xu X G 2010 A comparative study on the risk of second primary cancers in out-of-field organs associated with radiotherapy of localized

prostate carcinoma using Monte Carlo-based accelerator and patient models
Med Phys **37** 1987-94

Bednarz B, Hancox C and Xu X G 2009 Calculated organ doses from selected prostate treatment plans using Monte Carlo simulations and an anatomically realistic computational phantom *Phys Med Biol* **54** 5271-86

Bhatia S and Sklar C 2002 Second cancers in survivors of childhood cancer *Nat Rev Cancer* **2** 124-32

Bhatti P, Veiga L H, Ronckers C M, Sigurdson A J, Stovall M, Smith S A, Weathers R, Leisenring W, Mertens A C, Hammond S, Friedman D L, Neglia J P, Meadows A T, Donaldson S S, Sklar C A, Robison L L and Inskip P D 2010 Risk of second primary thyroid cancer after radiotherapy for a childhood cancer in a large cohort study: an update from the childhood cancer survivor study *Radiat Res* **174** 741-52

Blanco A I, Chao K S, El Naqa I, Franklin G E, Zakarian K, Vicic M and Deasy J O 2005 Dose-volume modeling of salivary function in patients with head-and-neck cancer receiving radiotherapy *Int J Radiat Oncol Biol Phys* **62** 1055-69

Brenner D J, Curtis R E, Hall E J and Ron E 2000 Second malignancies in prostate carcinoma patients after radiotherapy compared with surgery *Cancer* **88** 398-406

Brodin N P, Rosenschold P M, Aznar M C, Kiil-Berthelsen A, Vogelius I R, Nilsson P, Lannering B and Bjork-Eriksson T 2011 Radiobiological risk estimates of adverse events and secondary cancer for proton and photon radiation therapy of pediatric medulloblastoma *Acta Oncol* **50** 806-16

- Burman C, Kutcher G J, Emami B and Goitein M 1991 Fitting of normal tissue tolerance data to an analytic function *Int J Radiat Oncol Biol Phys* **21** 123-35
- CBTRUS 2002 Statistical report: Primary brain tumors in the United States, 1995-1999. In: *Central Brain Tumor Registry of the United States*,
- Chapet O, Kong F M, Lee J S, Hayman J A and Ten Haken R K 2005 Normal tissue complication probability modeling for acute esophagitis in patients treated with conformal radiation therapy for non-small cell lung cancer *Radiother Oncol* **77** 176-81
- Choux M, Lena G and Hassoun J 1983 Prognosis and long-term follow-up in patients with medulloblastoma *Clin Neurosurg* **30** 246-77
- Cochran D M, Yock T I, Adams J A and Tarbell N J 2008 Radiation dose to the lens during craniospinal irradiation-an improvement in proton radiotherapy technique *Int J Radiat Oncol Biol Phys* **70** 1336-42
- Cox J D, Stetz J and Pajak T F 1995 Toxicity criteria of the Radiation Therapy Oncology Group (RTOG) and the European Organization for Research and Treatment of Cancer (EORTC) *Int J Radiat Oncol Biol Phys* **31** 1341-6
- David K M, Casey A T, Hayward R D, Harkness W F, Phipps K and Wade A M 1997 Medulloblastoma: is the 5-year survival rate improving? A review of 80 cases from a single institution *J Neurosurg* **86** 13-21
- Dyk J V 1999 *The modern Technology of Radiation Oncology: A compendium for Medical Physicists and Radiation Oncologists*: Wisconsin: Medical Physics Publishing)

Eriksson F, Gagliardi G, Liedberg A, Lax I, Lee C, Levitt S, Lind B and Rutqvist L E

2000 Long-term cardiac mortality following radiation therapy for Hodgkin's disease: analysis with the relative seriality model *Radiother Oncol* **55** 153-62

Fontenot J D, Bloch C, Followill D, Titt U and Newhauser W D 2010 Estimate of the

uncertainties in the relative risk of secondary malignant neoplasms following proton therapy and intensity-modulated photon therapy *Phys Med Biol* **55** 6987-98

Fontenot J D, Lee A K and Newhauser W D 2009 Risk of secondary malignant

neoplasms from proton therapy and intensity-modulated x-ray therapy for early-stage prostate cancer *Int J Radiat Oncol Biol Phys* **74** 616-22

Fontenot J D, Newhauser W D, Bloch C, White R A, Titt U and Starkschall G 2007

Determination of output factors for small proton therapy fields *Med. Phys.* **34** 489-98

Fontenot J D, Newhauser W D and Titt U 2005 Design tools for proton therapy nozzles

based on the double-scattering foil technique *Radiat Prot Dosim* **116** 211-5

Fossati P, Ricardi U and Orecchia R 2009 Pediatric medulloblastoma: toxicity of

current treatment and potential role of protontherapy *Cancer Treat Rev* **35** 79-96

Freeman C R, Taylor R E, Kortmann R D and Carrie C 2002 Radiotherapy for

medulloblastoma in children: a perspective on current international clinical research efforts *Med Pediatr Oncol* **39** 99-108

Fuss M, Poljanc K, Miller D W, Archambeau J O, Slater J M, Slater J D and Hug E B

2000 Normal tissue complication probability (NTCP) calculations as a means to

compare proton and photon plans and evaluation of clinical appropriateness of calculated values *Int J Cancer* **90** 351-8

Gagliardi G, Constine L S, Moiseenko V, Correa C, Pierce L J, Allen A M and Marks L B 2010 Radiation dose-volume effects in the heart *Int J Radiat Oncol Biol Phys* **76** S77-85

Gagliardi G, Lax I and Rutqvist L E 2001 Partial irradiation of the heart *Semin Radiat Oncol* **11** 224-33

Gagliardi G, Lax I, Soderstrom S, Gyenes G and Rutqvist L E 1998 Prediction of excess risk of long-term cardiac mortality after radiotherapy of stage I breast cancer *Radiother Oncol* **46** 63-71

Gurney J G, Kadan-Lottick N S, Packer R J, Neglia J P, Sklar C A, Punyko J A, Stovall M, Yasui Y, Nicholson H S, Wolden S, McNeil D E, Mertens A C and Robison L L 2003 Endocrine and cardiovascular late effects among adult survivors of childhood brain tumors: Childhood Cancer Survivor Study *Cancer* **97** 663-73

Hall E J and Wu C S 2003 Radiation-induced second cancers: the impact of 3D-CRT and IMRT *Int J Radiat Oncol Biol Phys* **56** 83-8

Hendricks J S, McKinney G W, Durkee J W, Finch J P, Fensin M L, James M R, Johns R C, Pelowitz D B, Waters L S and Gallmeier F X 2006 MCNPX, Version 26c. (Los Alamos National Laboratory

Herault J, Iborra N, Serrano B and Chauvel P 2005 Monte Carlo simulation of a protontherapy platform devoted to ocular melanoma *Med Phys* **32** 910-9

Herault J, Iborra N, Serrano B and Chauvel P 2007 Spread-out Bragg peak and monitor units calculation with the Monte Carlo code MCNPX *Med Phys* **34** 680-8

- Hewitt M, Weiner, S L, Simone, J V E 2003 *Childhood Cancer Survivor Ship: Improving care and quality of life* (Washington DC: National Academies Press)
- Hoppe-Hirsch E, Renier D, Lellouch-Tubiana A, Sainte-Rose C, Pierre-Kahn A and Hirsch J F 1990 Medulloblastoma in childhood: progressive intellectual deterioration *Childs Nerv Syst* **6** 60-5
- Howell R M, Scarboro S B, Kry S F and Yaldo D Z 2010a Accuracy of out-of-field dose calculations by a commercial treatment planning system *Phys Med Biol* **55** 6999-7008
- Howell R M, Scarboro S B, Taddei P J, Krishnan S, Kry S F and Newhauser W D 2010b Methodology for determining doses to in-field, out-of-field and partially in-field organs for late effects studies in photon radiotherapy *Phys Med Biol* **55** 7009-23
- Howell R M *et al* 2011 Comparison of therapeutic dose for passively scattered proton and field-in-field photon craniospinal irradiation for medulloblastoma *in preparation*
- ICRP 1990 Recommendations of the International Commission on Radiological Protection. (Oxford: International Commission on Radiological Protection)
- ICRP 2003 Relative biological effectiveness (RBE), quality factor (Q), and radiation weighting factor ($w(R)$). In: *Ann ICRP*, (Oxford: International Commission on Radiological Protection) pp 1-117
- ICRU 1993 Prescribing, recording and reporting photon beam therapy, ICRU report 50. (Bethesda, MD: International Commission on Radiation Units and Measurements)

- Inskip P D and Curtis R E 2007 New malignancies following childhood cancer in the United States, 1973-2002 *Int J Cancer* **121** 2233-40
- Jakacki R I, Goldwein J W, Larsen R L, Barber G and Silber J H 1993 Cardiac dysfunction following spinal irradiation during childhood *J Clin Oncol* **11** 1033-8
- Jemal A, Siegel R, Ward E, Hao Y, Xu J, Murray T and Thun M J 2008 Cancer statistics, 2008 *CA Cancer J Clin* **58** 71-96
- Jemal A, Siegel R, Xu J and Ward E 2010 Cancer statistics, 2010 *CA Cancer J Clin* **60** 277-300
- Kallman P, Agren A and Brahme A 1992 Tumour and normal tissue responses to fractionated non-uniform dose delivery *Int J Radiat Biol* **62** 249-62
- Kaser-Hotz B, Sumova A, Lomax A, Schneider U, Klink B, Fidel J and Blattmann H 2002 A comparison of normal tissue complication probability of brain for proton and photon therapy of canine nasal tumors *Vet Radiol Ultrasound* **43** 480-6
- Kellerer A M, Ruhm W and Walsh L 2006 Indications of the neutron effect contribution in the solid cancer data of the A-bomb survivors *Health Phys* **90** 554-64
- Kiltie A E, Lashford L S and Gattamaneni H R 1997 Survival and late effects in medulloblastoma patients treated with craniospinal irradiation under three years old *Med Pediatr Oncol* **28** 348-54
- Koch N and Newhauser W 2005 Virtual commissioning of a treatment planning system for proton therapy of ocular cancers *Radiat Prot Dosim* **115** 159-63

Koch N, Newhauser W D, Titt U, Gombos D, Coombes K and Starkschall G 2008

Monte Carlo calculations and measurements of absorbed dose per monitor unit for the treatment of uveal melanoma with proton therapy *Phys Med Biol* **53** 1581-94

Kong F M, Pan C, Eisbruch A and Ten Haken R K 2007 Physical models and simpler dosimetric descriptors of radiation late toxicity *Semin Radiat Oncol* **17** 108-20

Krasin M J, Xiong X, Wu S and Merchant T E 2005 The effects of external beam irradiation on the growth of flat bones in children: modeling a dose-volume effect *Int J Radiat Oncol Biol Phys* **62** 1458-63

Kwa S L, Lebesque J V, Theuws J C, Marks L B, Munley M T, Bentel G, Oetzel D, Spahn U, Graham M V, Drzymala R E, Purdy J A, Lichter A S, Martel M K and Ten Haken R K 1998 Radiation pneumonitis as a function of mean lung dose: an analysis of pooled data of 540 patients *Int J Radiat Oncol Biol Phys* **42** 1-9

Lee C T, Bilton S D, Famiglietti R M, Riley B A, Mahajan A, Chang E L, Maor M H, Woo S Y, Cox J D and Smith A R 2005 Treatment planning with protons for pediatric retinoblastoma, medulloblastoma, and pelvic sarcoma: how do protons compare with other conformal techniques? *Int J Radiat Oncol Biol Phys* **63** 362-72

Lin R, Hug E B, Schaefer R A, Miller D W, Slater J M and Slater J D 2000 Conformal proton radiation therapy of the posterior fossa: a study comparing protons with three-dimensional planned photons in limiting dose to auditory structures *Int J Radiat Oncol Biol Phys* **48** 1219-26

- Lipshultz S E and Adams M J 2010 Cardiotoxicity after childhood cancer: beginning with the end in mind *J Clin Oncol* **28** 1276-81
- Little M P 2009 Cancer and non-cancer effects in Japanese atomic bomb survivors *J Radiol Prot* **29** A43-59
- Lyman J T 1985 Complication probability as assessed from dose-volume histograms *Radiat Res Suppl* **8** S13-9
- Martel M K, Sahijdak W M, Ten Haken R K, Kessler M L and Turrisi A T 1998 Fraction size and dose parameters related to the incidence of pericardial effusions *Int J Radiat Oncol Biol Phys* **40** 155-61
- Meadows A T, Friedman D L, Neglia J P, Mertens A C, Donaldson S S, Stovall M, Hammond S, Yasui Y and Inskip P D 2009 Second neoplasms in survivors of childhood cancer: findings from the Childhood Cancer Survivor Study cohort *J Clin Oncol* **27** 2356-62
- Merchant T E, Goloubeva O, Pritchard D L, Gaber M W, Xiong X, Danish R K and Lustig R H 2002 Radiation dose-volume effects on growth hormone secretion *Int J Radiat Oncol Biol Phys* **52** 1264-70
- Merchant T E, Hua C H, Shukla H, Ying X, Nill S and Oelfke U 2008 Proton versus photon radiotherapy for common pediatric brain tumors: comparison of models of dose characteristics and their relationship to cognitive function *Pediatr Blood Cancer* **51** 110-7
- Merchant T E, Kiehna E N, Li C, Shukla H, Sengupta S, Xiong X, Gajjar A and Mulhern R K 2006 Modeling radiation dosimetry to predict cognitive outcomes

in pediatric patients with CNS embryonal tumors including medulloblastoma *Int J Radiat Oncol Biol Phys* **65** 210-21

Mertens A C, Liu Q, Neglia J P, Wasilewski K, Leisenring W, Armstrong G T, Robison L L and Yasui Y 2008 Cause-specific late mortality among 5-year survivors of childhood cancer: the Childhood Cancer Survivor Study *J Natl Cancer Inst* **100** 1368-79

Miralbell R, Lomax A, Bortfeld T, Rouzaud M and Carrie C 1997a Potential role of proton therapy in the treatment of pediatric medulloblastoma/primitive neuroectodermal tumors: reduction of the supratentorial target volume *Int J Radiat Oncol Biol Phys* **38** 477-84

Miralbell R, Lomax A, Cella L and Schneider U 2002 Potential Reduction of the Incidence of Radiation-Induced Second Cancers by using Proton Beams in the Treatment of Pediatric Tumors *Int. J. Radiat Oncol Biol. Phys.* **54** 824-9

Miralbell R, Lomax A and Russo M 1997b Potential role of proton therapy in the treatment of pediatric medulloblastoma/primitive neuro-ectodermal tumors: spinal theca irradiation *Int J Radiat Oncol Biol Phys* **38** 805-11

Moiseenko V, Battista J and Van Dyk J 2000 Normal tissue complication probabilities: dependence on choice of biological model and dose-volume histogram reduction scheme *Int J Radiat Oncol Biol Phys* **46** 983-93

Mowlavi A A, Fornasie M R and de Denaro M 2011 Calculation of energy deposition, photon and neutron production in proton therapy of thyroid gland using MCNPX *Appl Radiat Isot* **69** 122-5

- Moyers M F, Benton E R, Ghebremedhin A and Coutrakon G 2008 Leakage and scatter radiation from a double scattering based proton beamline *Med Phys* **35** 128-44
- Mu X, Bjork-Eriksson T, Nill S, Oelfke U, Johansson K A, Gagliardi G, Johansson L, Karlsson M and Zackrisson D B 2005b Does electron and proton therapy reduce the risk of radiation induced cancer after spinal irradiation for childhood medulloblastoma? A comparative treatment planning study *Acta Oncol* **44** 554-62
- Mulhern R K, Kepner J L, Thomas P R, Armstrong F D, Friedman H S and Kun L E 1998 Neuropsychologic functioning of survivors of childhood medulloblastoma randomized to receive conventional or reduced-dose craniospinal irradiation: a Pediatric Oncology Group study *J Clin Oncol* **16** 1723-8
- Mulrooney D A, Yeazel M W, Kawashima T, Mertens A C, Mitby P, Stovall M, Donaldson S S, Green D M, Sklar C A, Robison L L and Leisenring W M 2009 Cardiac outcomes in a cohort of adult survivors of childhood and adolescent cancer: retrospective analysis of the Childhood Cancer Survivor Study cohort *BMJ* **339** b4606
- Neugut A I 1999 *Multiple Primary Cancers 1999* (Philadelphia: Lippincott Williams & Wilkins)
- Newhauser W 2010 Complexity of advanced radiation therapy necessitates multidisciplinary inquiry into dose reconstruction and risk assessment *Phys Med Biol* **55**

Newhauser W, Fontenot J, Zheng Y, Polf J, Titt U, Koch N, Zhang X and Mohan R

2007a Monte Carlo simulations for configuring and testing an analytical proton dose-calculation algorithm *Phys Med Biol* **52** 4569-84

Newhauser W, Fontenot J, Zheng Y, Polf J, Titt U, Koch N, Zhang X and Mohan R

2007b Monte Carlo simulations for configuring and testing an analytical proton dose-calculation algorithm *Phys Med Biol* **52** 4569-84

Newhauser W, Koch N, Hummel S, Ziegler M and Titt U 2005 Monte Carlo

simulations of a nozzle for the treatment of ocular tumours with high-energy proton beams *Phys Med Biol* **50** 5229-49

Newhauser W D and Durante M 2011 Assessing the risk of second malignancies after modern radiotherapy *Nat Rev Cancer* **11** 438-48

Newhauser W D, Fontenot J D, Mahajan A, Kornguth D, Stovall M, Zheng Y, Taddei P

J, Mirkovic D, Mohan R, Cox J D and Woo S 2009 The risk of developing a second cancer after receiving craniospinal proton irradiation *Phys Med Biol* **54** 2277-91

Newhauser W D, Koch N C, Fontenot J D, Rosenthal S J, D S G, Fitzek M M and

Mohan R 2007c Dosimetric impact of tantalum markers used in the treatment of uveal melanoma with proton beam therapy *Phys Med Biol* **52** 3979-90

Newhauser W D, Zheng Y, Taddei P J, Mirkovic D, Fontenot J D, Giebeler A, Zhang

R, Titt U and Mohan R 2008 Monte Carlo proton radiation therapy planning calculations *T. Am. Nucl. Soc.* 2

NRC 2006 Health Risks from Exposure to Low Levels of Ionizing Radiation: BEIR VII

- Phase 2. (Washington, D.C.: Nation Research Council of the National Academies)

Oeffinger K C, Mertens A C, Sklar C A, Kawashima T, Hudson M M, Meadows A T,

Friedman D L, Marina N, Hobbie W, Kadan-Lottick N S, Schwartz C L,

Leisenring W and Robison L L 2006 Chronic health conditions in adult

survivors of childhood cancer *N Engl J Med* **355** 1572-82

Pierce L J, Butler J B, Martel M K, Normolle D P, Koelling T, Marsh R B, Lichter A S

and Fraass B A 2002 Postmastectomy radiotherapy of the chest wall: dosimetric

comparison of common techniques *Int J Radiat Oncol Biol Phys* **52** 1220-30

Polednak A P and Flannery J T 1995 Brain, other central nervous system, and eye

cancer *Cancer* **75** 330-7

Polf J C and Newhauser W D 2005 Calculations of neutron dose equivalent exposures

from range-modulated proton therapy beams *Phys Med Biol* **50** 3859-73

Polf J C, Newhauser W D and Titt U 2005 Patient neutron dose equivalent exposures

outside of the proton therapy treatment field *Radiat. Prot. Dosim.* **115** 154-8

Robison L L, Mertens A C, Boice J D, Breslow N E, Donaldson S S, Green D M, Li F

P, Meadows A T, Mulvihill J J, Neglia J P, Nesbit M E, Packer R J, Potter J D,

Sklar C A, Smith M A, Stovall M, Strong L C, Yasui Y and Zeltzer L K 2002

Study design and cohort characteristics of the Childhood Cancer Survivor

Study: a multi-institutional collaborative project *Med Pediatr Oncol* **38** 229-39

Ronckers C M, Sigurdson A J, Stovall M, Smith S A, Mertens A C, Liu Y, Hammond

S, Land C E, Neglia J P, Donaldson S S, Meadows A T, Sklar C A, Robison L L

- and Inskip P D 2006a Thyroid cancer in childhood cancer survivors: a detailed evaluation of radiation dose response and its modifiers *Radiat Res* **166** 618-28
- Ronckers E T, Groot W, Steenbakkers M, Ruland E and Ament A 2006b Costs of the 'Hartslag Limburg' community heart health intervention *BMC Public Health* **6** 51
- Schneider U and Kaser-Hotz B 2005 A simple dose-response relationship for modeling secondary cancer incidence after radiotherapy *Z Med Phys* **15** 31-7
- Schneider U, Lomax A and Timmermann B 2008 Second cancers in children treated with modern radiotherapy techniques *Radiother Oncol* **89** 135-40
- Schneider U, Zwahlen D, Ross D and Kaser-Hotz B 2005 Estimation of radiation-induced cancer from three-dimensional dose distributions: Concept of organ equivalent dose *Int J Radiat Oncol Biol Phys* **61** 1510-5
- Schultheiss T E 2001 The controversies and pitfalls in modeling normal tissue radiation injury/damage *Semin Radiat Oncol* **11** 210-4
- Seppenwoolde Y, Lebesque J V, de Jaeger K, Belderbos J S, Boersma L J, Schilstra C, Henning G T, Hayman J A, Martel M K and Ten Haken R K 2003 Comparing different NTCP models that predict the incidence of radiation pneumonitis. Normal tissue complication probability *Int J Radiat Oncol Biol Phys* **55** 724-35
- Sigurdson A J, Ronckers C M, Mertens A C, Stovall M, Smith S A, Liu Y, Berkow R L, Hammond S, Neglia J P, Meadows A T, Sklar C A, Robison L L and Inskip P D 2005 Primary thyroid cancer after a first tumour in childhood (the Childhood Cancer Survivor Study): a nested case-control study *Lancet* **365** 2014-23

- Smith M A, Seibel N L, Altekruse S F, Ries L A, Melbert D L, O'Leary M, Smith F O and Reaman G H 2010 Outcomes for children and adolescents with cancer: challenges for the twenty-first century *J Clin Oncol* **28** 2625-34
- St Clair W H, Adams J A, Bues M, Fullerton B C, La Shell S, Kooy H M, Loeffler J S and Tarbell N J 2004 Advantage of protons compared to conventional X-ray or IMRT in the treatment of a pediatric patient with medulloblastoma *Int J Radiat Oncol Biol Phys* **58** 727-34
- Steel G G 2002 *Basic clinical radiobiology* (New York: Oxford University Press Inc.)
- Stewart J R, Fajardo L F, Gillette S M and Constine L S 1995 Radiation injury to the heart *Int J Radiat Oncol Biol Phys* **31** 1205-11
- Suit H, Goldberg S, Niemierko A, Ancukiewicz M, Hall E, Goitein M, Wong W and Paganetti H 2007 Secondary carcinogenesis in patients treated with radiation: a review of data on radiation-induced cancers in human, non-human primate, canine and rodent subjects *Radiat Res* **167** 12-42
- Taddei P J, Howell R M, Krishnan S, Scarboro S B, Mirkovic D and Newhauser W D 2010a Risk of second malignant neoplasm following proton versus intensity-modulated photon radiotherapies for hepatocellular carcinoma *Phys Med Biol* **55** 7055-65
- Taddei P J, Mahajan A, Mirkovic D, Zhang R, Giebeler A, Kornguth D, Harvey M, Woo S and Newhauser W D 2010b Predicted risks of second malignant neoplasm incidence and mortality due to secondary neutrons in a girl and boy receiving proton craniospinal irradiation *Phys Med Biol* **55** 7067-80

- Taddei P J, Mahajan A, Mirkovic D, Zhang R, Giebeler A, Kornguth D, Harvey M, Woo S and Newhauser W D 2010c Predicted risks of second malignant neoplasm incidence and mortality due to secondary neutrons in a girl and boy receiving proton craniospinal irradiation *Phys Med Biol* **55** 7067-80
- Taddei P J, Mirkovic D, Fontenot J D, Giebeler A, Zheng Y, Kornguth D, Mohan R and Newhauser W D 2009 Stray radiation dose and second cancer risk for a pediatric patient receiving craniospinal irradiation with proton beams *Phys Med Biol* **54** 2259-75
- Tarbell N J, Smith A R, Adams J and Loeffler J S 2000 The challenge of conformal radiotherapy in the curative treatment of medulloblastoma *Int J Radiat Oncol Biol Phys* **46** 265-6
- Tayama R, Fujita Y, Tadokoro M, Fujimaki H, Sakae T and Terunuma T 2006 Measurement of neutron dose distribution for a passive scattering nozzle at the Proton Medical Research Center (PMRC) *Nucl. Instrum. Meth. A* **564** 532-6
- Titt U, Zheng Y, Vassiliev O N and Newhauser W D 2008 Monte Carlo investigation of collimator scatter of proton-therapy beams produced using the passive scattering method *Phys Med Biol* **53** 487-504
- Tubiana M 2009 Can we reduce the incidence of second primary malignancies occurring after radiotherapy? A critical review *Radiother Oncol* **91** 4-15; discussion 1-3
- Wei X, Liu H H, Tucker S L, Wang S, Mohan R, Cox J D, Komaki R and Liao Z 2008 Risk factors for pericardial effusion in inoperable esophageal cancer patients

treated with definitive chemoradiation therapy *Int J Radiat Oncol Biol Phys* **70** 707-14

Yom S S, Frija E K, Mahajan A, Chang E, Klein K, Shiu A, Ohrt J and Woo S 2007 Field-in-field technique with intrafractionally modulated junction shifts for craniospinal irradiation *Int J Radiat Oncol Biol Phys* **69** 1193-8

Yorke E D 2001 Modeling the effects of inhomogeneous dose distributions in normal tissues *Semin Radiat Oncol* **11** 197-209

Yorke E D, Jackson A, Rosenzweig K E, Braban L, Leibel S A and Ling C C 2005 Correlation of dosimetric factors and radiation pneumonitis for non-small-cell lung cancer patients in a recently completed dose escalation study *Int J Radiat Oncol Biol Phys* **63** 672-82

Zacharatou Jarlskog C and Paganetti H 2008 Risk of developing second cancer from neutron dose in proton therapy as function of field characteristics, organ, and patient age *Int J Radiat Oncol Biol Phys* **72** 228-35

Zhang R, Perez-Andujar A, Fontenot J D, Taddei P J and Newhauser W D 2010 An analytic model of neutron ambient dose equivalent and equivalent dose for proton radiotherapy *Phys Med Biol* **55** 6975-85

Zheng Y, Fontenot J, Taddei P, Mirkovic D and Newhauser W 2008 Monte Carlo simulations of neutron spectral fluence, radiation weighting factor and ambient dose equivalent for a passively scattered proton therapy unit *Phys Med Biol* **53** 187-201

Zheng Y, Newhauser W, Fontenot J, Taddei P and Mohan R 2007 Monte Carlo study of neutron dose equivalent during passive scattering proton therapy *Phys Med Biol* **52** 4481-96

Zhang R, Howell R, Giebeler A, Taddei P, Mahajan A, Homann K and Newhauser W 2012 Comparison of risk of radiogenic second cancer between photon and proton craniospinal irradiation for a pediatric medulloblastoma patient *in preparation*

LIST OF PUBLICATIONS DURING PHD PERIOD

- 1) **Rui Zhang**, Rebecca Howell, Annelise Giebeler, Phillip Taddei, Anita Mahajan, Carol Etzel, Wayne Newhauser, “Risk of radiogenic cardiac toxicity for a sample of pediatric medulloblastoma patients”, *in preparation*
- 2) **Rui Zhang**, Rebecca Howell, Annelise Giebeler, Phillip Taddei, Anita Mahajan and Wayne Newhauser *et al*, “Calculation of the risk of cardiac toxicity for a pediatric medulloblastoma patient treated with proton and photon craniospinal irradiation”, *in preparation*
- 3) **Rui Zhang**, Rebecca Howell, Annelise Giebeler, Phillip Taddei, Anita Mahajan, Kenny Homann and Wayne Newhauser, “Comparison of risks of second cancer between photon and proton therapies for a pediatric medulloblastoma patient” *in preparation*
- 4) Laura Rechner, Rebecca Howell, **Rui Zhang**, Carol Etzel, Andrew Lee and Wayne Newhauser, “Risk of radiogenic second cancers following volumetric modulated arc therapy and proton arc therapy for prostate cancer”, *in preparation*
- 5) **Rui Zhang**, Jonas Fontenot, Dragan Mirkovic, John Hendricks, Wayne Newhauser, “High speed Monte Carlo dose reconstruction for proton radiation therapy using lattice versus mesh tallies in MCNPX”, *submitted*
- 6) **Rui Zhang**, Angélica Pérez-Andújar, Jonas Fontenot, Phillip Taddei and Wayne Newhauser, “Analytical model of neutron ambient dose equivalent and equivalent dose for proton radiotherapy”, *Physics in Medicine and Biology*, 55: 6975, 2010
- 7) Phillip J. Taddei, Anita Mahajan, Dragan Mirkovic, **Rui Zhang**, Annelise Giebeler, David Kornguth, Mark C. Harvey, Shiao Woo and Wayne D. Newhauser, “Predicted risk of secondary malignant neoplasm due to secondary neutrons in a girl and boy receiving proton craniospinal irradiation”, *Physics in Medicine and Biology*, 55: 7067, 2010
- 8) Wayne Newhauser, **Rui Zhang**, In reply to Dr. Gottschalk’s comment on Calculation of water equivalent thickness of materials of arbitrary density, elemental composition and thickness in proton beam irradiation, *Physics in Medicine and Biology*, 55: L31-32, 2010
- 9) **Rui Zhang**, Philip J. Taddei, Markus M. Fitzek, and Wayne D. Newhauser, “Water equivalent thickness values of materials used in heavy charged particle beams”, *Physics in Medicine and Biology*, 55: 2481, 2010
- 10) **Rui Zhang**, Wayne Newhauser, “Calculation of water equivalent thickness of materials of arbitrary density, elemental composition and thickness in proton beam irradiation”, *Physics in Medicine and Biology*, 54: 1383, 2009
- 11) Wayne D. Newhauser, Jonas D. Fontenot, Philip J. Taddei, Dragan Mirkovic, Annelise Giebeler, **Rui Zhang**, Anita Mahajan, David Kornguth, Marilyn Stovall, Pablo Yepes, Shiao Woo, and Radhe Mohan, “Contemporary proton therapy systems adequately protect patients from exposure to stray radiation”, *AIP Proc* 1099:450-455, 2009
- 12) Wayne D. Newhauser, Yuanshui Zheng, Philip J. Taddei, Dragan Mirkovic, Jonas D. Fontenot, Annelise Giebeler, **Rui Zhang**, Uwe Titt and Radhe Mohan, “Monte Carlo proton radiation therapy planning calculations”, *Trans of Am Nucl Soc*, Vol 99, 63, 2008

VITA

Rui Zhang enrolled at the University of Science and Technology of China (USTC) in 1997. He won excellent student scholarship every year as an undergraduate student and he completed a Bachelor of Science Degree in Modern Physics in 2001. In that fall, he enrolled at USTC again to pursue a Master Degree in Modern Physics. He completed it in 2004 and won Guahua graduate student scholarship. After that, he came to USA and enrolled at Rice University. Received a second Master Degree in Applied Physics from Rice University in 2007, he enrolled at the University of Texas at Houston Graduate School of Biomedical Sciences (UT-GSBS) to pursue a Doctor of Philosophy degree in Medical Physics. He received Sowell-Huggins Cancer Answer Scholarship and President Research Scholarship from UT-GSBS, UT MD Anderson Cancer Center and UT Health Science Center. One of his publications during PhD period was featured and reported by top ranked Medical Physics journal *Physics in Medicine and Biology*. He and his advisor, Dr. Wayne Newhauser, were also reported by UT MD Anderson Cancer Center “Cancer Frontline” blog for their research in modeling stray neutron dose in proton therapy.